EXPERIMENTAL AND THEORETICAL STUDIES OF ROTOTRANSLATIONAL CORRELATION FUNCTIONS

MYRON EVANS AND GARETH EVANS

Department of Chemistry
University College of Wales
Aberystwyth, Wales

RUSSELL DAVIES

Department of Applied Mathematics
University College of Wales
Aberystwyth, Wales

CONTENTS

Synopsis

This article is concerned with the experimental and theoretical attempts which have recently been made to solve the molecular dynamical problem of how systems of N ($\approx 10^{23}$) interacting molecules evolve in fluids and mesophases such as plastic and liquid crystals. The development in the 1960s of computerized Michelson interferometry has closed the gap between the microwave and mid-infrared region of the electromagnetic spectrum. The region 1 to 300 cm $^{-1}$ is of particular interest to molecular dynamicists since the power absorption coefficient, $\alpha(\omega)$, observed here in liquids as a broad band (the Poley absorption) is the high-frequency adjunct of the dielectric loss, $\varepsilon''(\omega)$, observed in the microwave and lower-frequency regions. As a result of the relation

$$\alpha(\omega) = \frac{\omega\varepsilon''(\omega)}{n(\omega)c}$$

where $n(\omega)$ is the refractive index and c the velocity of light, high-frequency absorptions which are barely visible in measurements of $\varepsilon''(\omega)$ appear in great detail when $\alpha(\omega)$ is

measured because of the frequency multiplication. By observing the absorption and dispersion of a given N-particle system using measurements both on $\varepsilon''(\omega)$ and $\alpha(\omega)$, we can obtain the dipole correlation function, $C_\mu(t)$, and its second derivative, $\ddot{C}_\mu(t)$, which has essentially the same form as the angular velocity correlation function $C_\omega(t)$. Measurements of both $C_\mu(t)$ and $\ddot{C}_\mu(t)$ provide very stringent tests for models of liquid or mesophase dynamics which are apparently successful in other fields, such as depolarized Rayleigh scattering, infrared and Raman broadening, and classical dielectric spectroscopy. One way in which a particular model may be tested is via the orientational autocorrelation function that it generates. We thus define the relation between this function and $C_\mu(t)$, and also the role played by the dynamic internal field in this problem. In addition, since nondipolar molecules display a rotational-type absorption from static to THz frequencies, we discuss the methods used to distinguish between this interaction-induced absorption and the permanent dipolar absorption. We show that both types of bands may be reproduced theoretically within the framework of the Mori continued-fraction representation of the Liouville equation for motions of permanent or induced (temporary) dipoles.

Many, if not all, the dynamical models describing the liquid state may be classified as low-order approximants of the (in general) infinite Mori continued fraction. Since this truncation process necessitates a loss of statistical information, the representation of the intermolecular potential contribution to the system Hamiltonian may be unreliable. On the other hand, higher-order approximants can be used only with the introduction of too many phenomenological parameters. We describe the advantages and disadvantages of various low-order approximant models in different situations.

Having discussed the continued fraction for column vectors of linearly independent dynamical variables, we proceed to discuss its effectiveness in describing the features of experimental static-THz broad-band spectra. First, we attempt to define the role of translation–rotation coupling. This has a direct effect on neutron time-of-flight spectra, but its role in absorption spectra is subtler. The continued fraction may be used for the column vector $\begin{bmatrix} \mathbf{v} \\ \boldsymbol{\omega} \end{bmatrix}$, where $\boldsymbol{\omega}$ is the molecular angular velocity and $\mathbf{v}$ the linear velocity, to show how the correlation matrices $\langle \mathbf{v}(t)\boldsymbol{\omega}^T(0)\rangle$ and $\langle \boldsymbol{\omega}(t)\mathbf{v}^T(0)\rangle$ affect the zero-THz absorption, the Fourier transform of purely orientational correlations. The same approach may be used to determine rototranslational correlation functions which appear in the theory of thermal neutron scattering, *without* assuming the decorrelation of rotation from translation. After dealing with this fundamental question we proceed to evaluate the various models of the Liouville equation, using different experimental approaches to the liquid state.

Approach via Compressed Gas

In this regime we might expect the extended diffusion models to be adequate, but this is clearly not so when measurements on $\alpha(\omega)$ are used. The most characteristic feature of the power absorption is its large shift in peak frequency to higher values as the number density of the absorber is increased. This cannot be followed by any simple variant of J-diffusion or m-diffusion theory, where the angular momentum is randomized at each collision according to a Poisson distribution. These models merely broaden asymmetrically the gas phase $(J \rightarrow J+1)$ distribution. Efforts at evaluating extended diffusion in fields such as NMR relaxation and infrared/Raman broadening indicate that it is not widely known how simple features of the zero-THz absorption may facilitate the assessment of these models. For example, a feature of this type of absorption is that autocorrelation functions should possess Taylor expansions in time t which are even up to t^4, at least. The orientational correlation functions for extended diffusion models, however, expand evenly up to t^2.

Some excellent zero-THz data for the strongly dipolar species CH_2Cl_2 are now available, and these are used to evaluate the following models in addition to extended diffusion.

1. An approximant of the Mori continued fraction resulting from an exponential second memory for the orientational correlation function.
2. The approximant equivalent to the model of itinerant libration. Mathematically, this results from an exponential second memory for the angular velocity autocorrelation function. Physically, the situation is described equally well by the Brownian motion of two interacting dipoles.
3. As liquid densities are attained, the Langevin equation for the inertia-corrected rotational diffusion of the asymmetric top (developed within the last two or three years). This is a zeroth-order approximant, and *even with correction for inertial effects* is unrealistic at THz frequencies. Without the inclusion of inertial effects, the power absorption becomes a plateau at high frequency so that the theoretical zero-THz band is effectively infinitely wide.

Techniques involving Raman/infrared band broadening, light scattering, NMR relaxation, and classical dielectric loss measurements are relatively insensitive to the short-time details of molecular rotational dynamics. Thus data over an extended range of temperature and number density are often needed before departures from inertialess rotational diffusion may be observed with any precision. We develop this point by comparing results for the rotational dynamics of CH_2Cl_2 liquid obtained from the different techniques available. In contrast to the confused and often contradictory deductions drawn from some other fields, the zero-THz profile discriminates much more readily between models, and is thus at the very least a useful source of complementary information. A self-consistent appraisal is attempted within the framework constructed by Mori. This aims at a satisfactory evaluation of such quantities as the mean-square torque and its derivatives, so that some statistical assessment may be made of the potential part of the total N-particle Hamiltonian. At present, features of observed spectra are reflected in model correlation times which are often physically meaningless (e.g., the Debye relaxation time or the time between elastic collisions of extended diffusion) and sometimes directly contradictory.

Approach to the Liquid State via Mesophases (Liquid and Plastic Crystals) and Glasses

These mesophases restrict the degree of rototranslational freedom available in the isotropic fluid. For example, some solid lattices of dipolar molecules with pseudospherical van der Waals contours are rotationally disordered but translationally ordered. Liquid crystals in the smectic, cholesteric, and nematic phases are composed of molecules which are rotationally hindered (about their short axes) but retain a considerable degree of translational freedom. This is especially so in the nematic phase, where, in the absence of external magnetic and electric fields, the director axes meander in space. One of the most far-reaching consequences of zero-THz spectroscopy of these systems is the realization that the whole loss or absorption profile must be regarded as a continuous function of frequency, arising from an ensemble dynamical process which itself evolves continuously in time from the initial $t=0$. In this context we develop some model calculations of the absorption expected in the nematic phase on the basis of restricted rotational freedom. Preliminary calculations suggest that the potential well experienced by a nematogen, for example, in the field of its neighbors, needs to be considerably narrower and steeper than that of isotropic dipolar liquids. The well depth estimated from best fit to the zero-THz data agrees surprisingly well with a rough calculation using a potential of the form

$$V = a\exp(-br) - \frac{c}{r^6}$$

in which the only intermolecular interactions considered are those between the benzene rings of the nematogen.

In supercooled solutions and glasses of some small, dipolar molecules (such as CH_2Cl_2) it is remarkable that the evolution of the rotational dynamics of the dipolar solute extends over as much as 10 to 15 decades of frequency. This is a direct consequence again of the result that for a well-behaved orientational correlation function, low-frequency losses must extend analytically to the THz region, where, as power absorptions, they rise above the Debye plateau and regain transparency typically at 200 to 300 cm^{-1}. Thus any viable model of the rotations in glasses, liquid crystals, and disordered or plastic solids must be capable of linking loss peaks separated in this way. For example, the dielectric loss observed in a glassy solution of CH_2Cl_2 in decalin has been measured recently in the kHz and THz frequency regions at 107 to 148°K. The low-frequency part of the loss curve exhibits a peak which shifts upward about two decades with a 4°K increase in temperature, and at the glass-to-liquid transition temperature

moves almost immediately out of the audiofrequency range to the microwave. The far-infrared (or THz) part of the loss is displaced by 50 to 116 cm^{-1} in the glass as compared with the liquid at 293°K. In addition, therefore, to the well-documented primary and secondary losses in glasses and polymers there exists in general a tertiary process at far-infrared frequencies analogous to the Poley absorption in liquids. Using the itinerant librator model, features described above can be reproduced, and quite satisfactorily so in such specialized cases as fluorobenzene dissolved in a plastic crystal of benzene.

Molecular Dynamics Simulations

Probability density functions are simulated with an atom–atom potential and compared with ones calculated analytically from the itinerant librator model discussed above. The former are non-Gaussian and the latter are Gaussian in nature. Simulations are also used in evaluating translation–rotation functions such as $\langle e^{i\mathbf{q}\cdot\mathbf{r}(t)}P_n(\mathbf{u}(t)\cdot\mathbf{u}(0))\rangle$, useful in the theory of neutron scattering. Here $\mathbf{u}$ is the dipole unit vector, $\mathbf{q}$ the wave vector, and $\mathbf{r}$ the position vector. The use of molecular dynamics is extended to the numerical evaluation of the planar itinerant oscillator system, with the intention of achieving numerically what is analytically intractable.

Finally, simulations are carried out in liquid nitrogen of single-particle and collective correlation functions such as those of the longitudinal and transverse spin density, and current density, which for a structured fluid contains a rotational part. The coupling between transverse spin and current density has also been simulated as the hydrodynamic counterpart of $\langle\omega(t)\mathbf{v}(0)^T\rangle$. The nonvanishing of the matrix possibly explains the zero-frequency splitting observed recently in the depolarized spectrum of scattered light.

I. GENERAL INTRODUCTION. THEORETICAL AND EXPERIMENTAL BACKGROUND

To understand in detail the motions and interactions of about 10^{23} molecules, we would have to follow each trajectory separately over a period of time from the initial $t=0$. In a gas dilute enough so that interactions between each molecule are negligible, this is not an awesome task, since the translation of the center of mass and end-over-end molecular rotation of each molecule are for long periods of time undisturbed. The translation and rotation may safely be described separately. For certain geometries, the Schrödinger equation may be solved to yield the familiar set of rotational absorptions peaking in the far-infrared region[1,2] of the electromagnetic spectrum for some of the commoner dipolar gases. This region, from 1 cm^{-1} (30 GHz) to about 300 cm^{-1}, is often known as the submillimeter or

THz. As the gas is compressed, however, the discrete nature of these absorption lines disappears, until at liquid densities, a broad band is observed peaking with a root-mean-square angular velocity much higher than that of the $J=1$ peak of quantum theory. Figure 1, taken from a paper by Gerschel,[3] illustrates this process along the gas–liquid coexistence curve. After solidification, the broad band may split into a lattice of modes describable in terms of cooperative torsional oscillation of large domains of molecules, with the center-of-mass translation of each strongly hindered.

If we represent the absorption in terms of dielectric loss, the familiar liquid-phase Debye relaxation curve,[4] or a variant thereof, appears, peaking at a frequency much less than that of the gaseous root-mean-square angular velocity. As the density of the liquid increases, the loss peak moves to a lower frequency, while the peak in the power absorption coefficient $\alpha(\omega)$

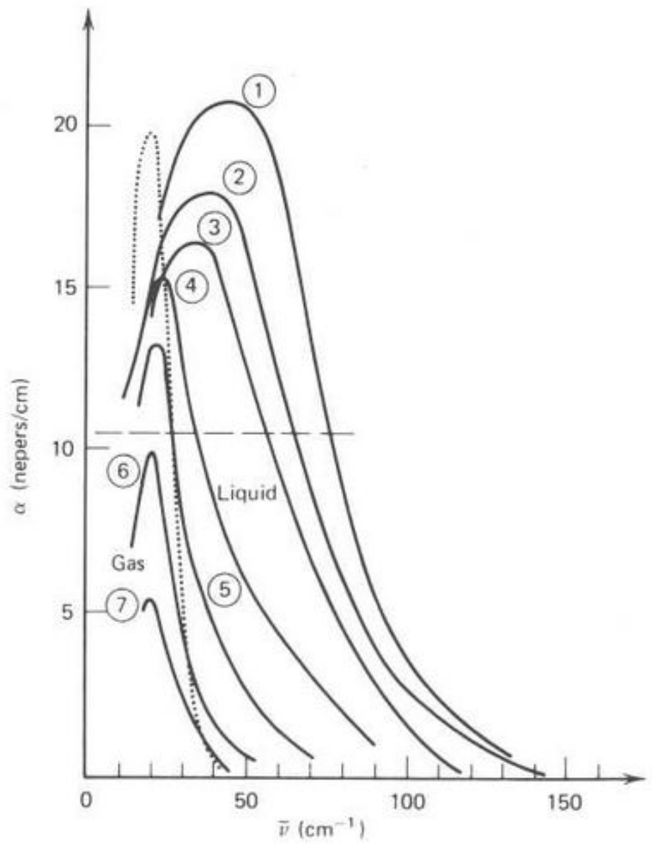

Fig. 1. Far-infrared spectra of $CHCl_3$: (1) to (5) liquid, (6) and (7) gas; d the density in g/cm^3. (1) is 233°K, $d=1.62$; (2) 300°K, $d=1.47$; (3) 353°K, $d=1.36$; (4) 483°K, $d=1.05$; (5) 534°K, $d=0.65$; (6) 543°K, $d=0.38$; (7) 517°K, $d=0.2$; The dotted line represents the free-rotator absorption at 534°K. The dashed line represents the "Debye plateau" at 300°K (see text). [Reproduced by permission from A. Gerschel et al., *Mol. Phys.*, **23**, 317 (1972).]

does just the opposite. Even in fluids of nondipolar molecules such as CCl_4 and benzene, whose end-over-end rotations do not cause infrared or microwave absorptions in the infinitely dilute gas, a liquid-phase broad band appears[5] (Fig. 2). Therefore, the loss and power absorption coefficient may be used as measures of molecular interaction in at least two senses.

1. The gradual inhibition of rotation and interruption of free translation, leading to the inevitable interaction and coupling between these freedoms as the liquid state is approached. Their subsequent decoupling once more in the solid, where center-of-mass translation over long distances is rare and slow.
2. The development of electrostatic and overlap interactions which give rise to temporary, induced dipole moments, and thus to rotational far-infrared absorptions in nondipolar gases[6] such as N_2 and solvents such as CCl_4.

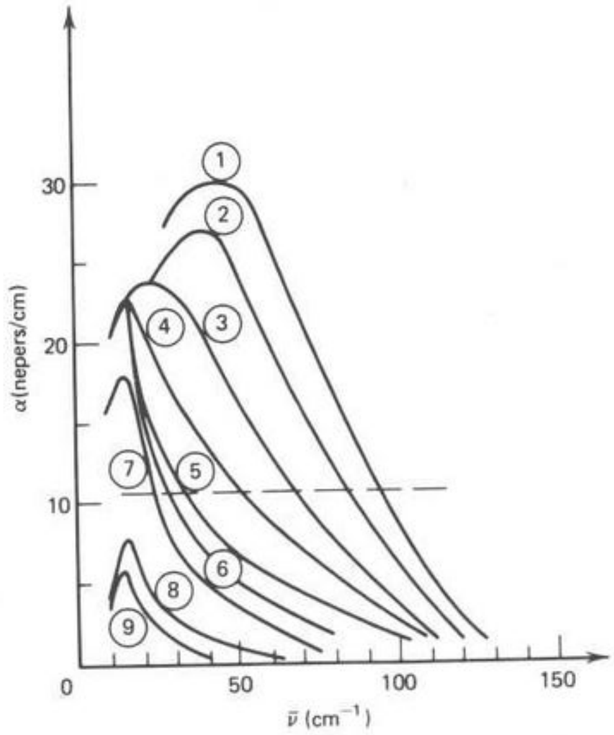

Fig. 2. Far-infrared spectra of C_6H_5F: (1) to (7) liquid, (8) and (9) gas; d the density in g/cm^3. (1) is 239°K, $d=1.08$; (2) 300°K, $d=1.024$; (3) 397°K, $d=0.89$; (4) 459°K, $d=0.79$; (5) 513°K, $d=0.68$; (6) 549°K, $d=0.548$; (7) 559.5°K, $d=0.4$; (8) 559°K, $d=0.3$; (9) 619°K, $d=0.184$. The dashed line is as in Fig. 3. [Reproduced by permission from *Mol. Phys.*, **23**, 317 (1972).]

To interpret these macroscopic observations in terms of molecular motion we must resort to statistical methods since, as pointed out by Hansen and McDonald,[7] the description of each individual molecular trajectory in the fluid, even if possible, is not desirable, on the grounds that a building large enough to house the billions of neatly plotted three-dimensional graphs could not be found. The major problem confronting the liquid-state dynamicist is not one of building a large enough library, but of developing an expansion of the Liouville equation free of numerous phenomenological variables (adjustable for best fit), which gives a consistent description of data from all sources. Such a process should also yield a satisfactory functional for the intermolecular potential energy. A secondary problem, hardly less formidable, is that of treating the "internal field." This means that whenever a solution describing the ensemble dynamical situation is found at the microscopic level, the relation of the displaced field to the measuring field must also be predictable before the macroscopic band shapes can be calculated. A discussion by Scaife[8] is the clearest formulation of this problem in the author's experience. We summarize it here at the outset.

The electrical interaction between the dipole and its surroundings has no influence on the dynamical behavior of the molecule in a nondipolar medium because the field fluctuations in the cavity occupied by the dipole are so rapid as to leave the dipole unaffected. The dipole and the reaction field it sets up in the surroundings are parallel at all times. Thus the experimentalist wishing to study in the zero-THz waveband a dipolar molecule in a dilute nondipolar solvent may use a theory of dipole autocorrelations. When the molecule is surrounded by a dipolar medium of the same molecular type, however, the dipole will be strongly influenced by the fluctuating cavity field. In addition, the dipole itself will polarize its surroundings and thereby produce a further cavity field which will in general not be parallel to the dipole because of the dispersive nature of the medium. A division of the cavity field into a component arising from the surroundings and one generated by the reaction of the surroundings to the preceding motion of the dipole is valid only if saturation effects are neglected. No such division is possible unless the surrounding medium responds in a linear fashion to all applied fields.

If, for the sake of argument, all dynamical memory is neglected, and a Langevin equation accepted for the motion of the dipole, in two dimensions one has the relation

$$I\ddot{\theta}+\xi\dot{\theta}-\mu\mathbf{F}(t)\sin(\psi-\theta)=\lambda(t) \tag{I.1}$$

where I and ξ are constants, $\boldsymbol{\lambda}$ a random force, $\mathbf{F}(t)$ the electric field acting

on the dipole μ, ψ the angle between this field and a particular fixed direction, and θ the angle between this direction and the dipole. The field consists of a fluctuating cavity field $\mathbf{F}_c(t)$ and a reaction field $\mathbf{F}_r(t)$, whose magnitude and direction depends on the motion of the dipole up to time t. Clearly, we cannot calculate the dielectric permittivity $\varepsilon(\omega)$ from a solution of (I.1) since such a solution would require a knowledge of the fields $\mathbf{F}_c(t)$ and $\mathbf{F}_r(t)$, which themselves depend on $\varepsilon(\omega)$. In other words, the most we may hope for analytically is an approximate solution for $\varepsilon(\omega)$ based on some self-consistent technique. Some notable advances in dealing with this dipole–dipole coupling problem have been made by Zwanzig,[9] Bellemans and others[10] and Cole,[11] who consider a lattice of translationally fixed dipoles. Deutch[12] has summarized the situation up to 1976. Coffey[13] has recently extended the work of Budo to show that a distribution of macroscopic relaxation times is to be expected when dipole–dipole coupling effects are present. Scaife[8] points out, however, that there seem to be cases (such as water) where dipole–dipole coupling is very strong but only one macroscopic relaxation time appears. This suggests that, in such cases, the concept of a "microscopic relaxation time" is meaningless, and that we are in fact dealing with a cooperative process involving many molecules.

A. Liouville and Fokker–Planck Equations for the Canonical Ensemble

Setting aside for the moment the vexing question of the internal field, we proceed in this section to describe the fundamental equations of classical mechanics for the N-particle ensemble. These equations must be solved by approximate methods, the purpose of which is to extract a correlation function (or spectrum) with the maximum of realism and the minimum number of adjustable, or phenomenological variables. Our justification for the use of classical rather than quantum mechanics has been given by van Vleck and Weisskopf,[14] who outlined conditions under which rotational quantum lines in the microwave and far infrared give way to broad loss bands in the dense fluid. Some remarks by Lobo, Robinson, and Rodriguez[15] illuminate this question with particular clarity. Suffice it to say that classical theory proves adequate except in such cases as[16] HF and NH_3 dissolved in liquid SF_6, where the fluid state far infrared contours clearly show up the presence of residual, broadened $J\rightarrow J+1$ absorptions (Fig. 3). We shall refer to these specific examples later, and we use as a description some classical perturbations of the quantum delta functions.

Consider, therefore, a linearly independent set $[A_j(t)]$, $j=1,\ldots,n$, of real-valued (implicitly) time-dependent dynamical variables of the given N-particle system. Assume that an ensemble average $\langle\cdot\rangle$ can be defined for the system and that the set of all possible dynamical variables is a real

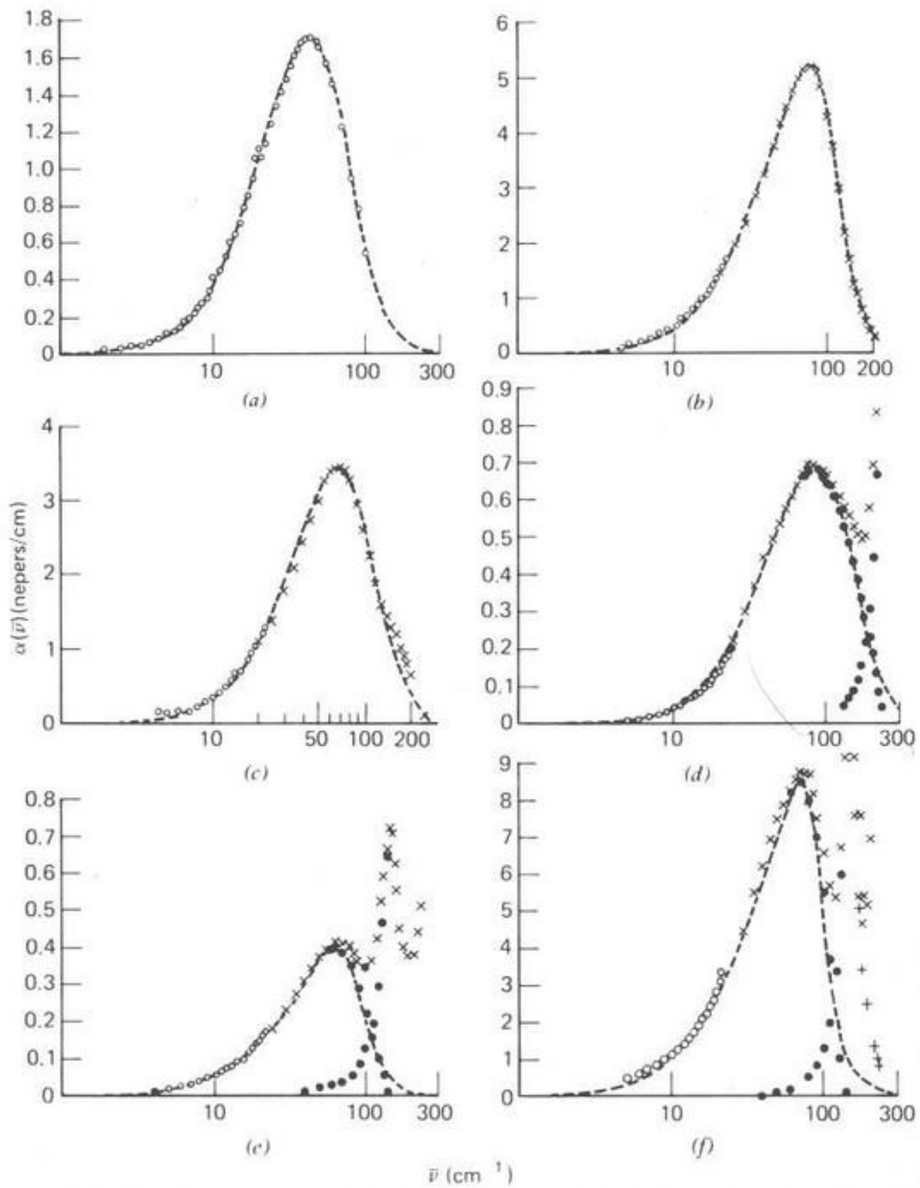

Fig. 3. (*a*) ⊙ Experimental absorption for $CCl_4(l)$ at 296°K. (---), Mori 3 variable theory (Section V); (*b*) (⊙, ×), absorption observed for benzene(*l*) at 296°K; (---), theory; (*c*) (⊙, ×), absorption of $CS_2(l)$ at 296°K; (---), theory; (*d*) (⊙, ×) absorption of cyclohexane at 296°K. The high-frequency proper mode is extrapolated using a model of collision-disturbed vibrators. This technique is also used in (*e*) and (*f*); (---), theory; (*e*) (⊙, ×), absorption of *trans*-decalin at 296°K; (----), theory; (*f*) (⊙, ×), absorption of 1,4-dioxan at 296°K; (----), theory. [Reproduced by permission from *J. Chem. Soc. Faraday Trans. 2*, **72**, 1196 (1976).]

Hilbert space in which the inner product is defined by $(A,B)\equiv\langle AB\rangle$. Without loss of generality we may assume that each particle is a molecular asymmetric top within whose rigid but polarizable framework is embedded a dipole vector $\boldsymbol{\mu}$. The set $[A_j(t)]$ spans an n-dimensional subspace of the Hilbert space. Each variable obeys the classical Liouville equation of motion:

$$\dot{A}_j(t)=\{A_j(t),H\}\equiv i\mathfrak{L}A_j(t) \tag{I.2}$$

where H is the Hamiltonian of the system and $i\mathfrak{L}$ the Liouville operator. The formal solution is

$$A_j(t)=\exp(i\mathfrak{L}t)A_j(0) \tag{I.3}$$

where the propagator $\exp(i\mathfrak{L}t)$ is an orthogonal operator. The time evolution of $A_j(t)$ is therefore a rotation in Liouville space, with

$$\langle A_j(t)A_k(t)\rangle=\langle A_j(0)A_k(0)\rangle \qquad j,k=1,\ldots,n \tag{I.4}$$

From now on we confine the discussion to correlation functions of the form of (I.4), but the general theory is equally applicable to multiparticle correlation functions, and may be used to determine the relation between the two different kinds, as for example in the paper by Kivelson and Madden.[17] This problem is closely linked with that of the internal field.

If $\mathbf{A}(t)$ denotes the $n\times 1$ column vector with elements $A_j(t)$, and $\mathbf{A}^T(t)$ its corresponding row vector, we let $\langle A(t)A^T(t)\rangle$ denote the $n\times n$ matrix with elements $\langle A_j(t)A_k(t)\rangle$. From (I.4) it follows that

$$\langle A(t)A^T(t)\rangle=\langle A(0)A^T(0)\rangle \tag{I.5}$$

Mori[18] shows that $A(t)$ evolves in time according to the equation

$$\dot{\mathbf{A}}(t)=i\Omega_{\mathbf{A}}\mathbf{A}(t)-\int_0^t d\tau\,\phi_{\mathbf{A}}(t-\tau)\mathbf{A}(\tau)+\mathbf{F}_{\mathbf{A}}(t) \tag{I.6}$$

Because of its similarity to Langevin's equation of 1906 for translational Brownian motion,[19] this is sometimes known as a generalized Langevin equation. It is a form of the Liouville equation which proves particularly useful in generating approximate solutions, or models, of the required autocorrelation function. In (I.6) $\Omega_{\mathbf{A}}$ is a resonance frequency operator, the

matrix kernel $\phi_{\mathbf{A}}(t)$ is a memory function (or effective Liouvillian), and $\mathbf{F}_{\mathbf{A}}(t)$ is a generalized random force or torque propagated in a special way from $\mathbf{A}(0)$. These quantities are specified in terms of the projection operators $\hat{P}, \hat{Q}$ defined by

$$\hat{P}\mathbf{G} \equiv \langle GA^T(0)\rangle \langle A(0)A^T(0)\rangle^{-1}\mathbf{A}(0)$$
$$\hat{Q} \equiv \hat{1} - \hat{P}$$

where $\hat{P}$ projects an arbitrary vector $\mathbf{G}$ into the subspace spanned by $\mathbf{A}(0)$, and $\hat{Q}$ projects into the orthogonal complement of this subspace. The appropriate relations are

$$i\Omega_{\mathbf{A}} = \langle \dot{\mathbf{A}}(0)\mathbf{A}^T(0)\rangle \langle \mathbf{A}(0)\mathbf{A}^T(0)\rangle^{-1}$$
$$\mathbf{F}_{\mathbf{A}}(t) = \exp(i\dot{Q}\Omega t)\dot{Q}\dot{\mathbf{A}}(0)$$
$$\phi_{\mathbf{A}}(t) = \langle \mathbf{F}_{\mathbf{A}}(t)\mathbf{F}_{\mathbf{A}}^T(0)\rangle \langle \mathbf{A}(0)\mathbf{A}^T(0)\rangle^{-1} \tag{I.7}$$

The meaning of the generalized force $\mathbf{F}_{\mathbf{A}}(t)$ should not be confused with that of generalized force in classical lagrangian dynamics. In the Mori formalism of (I.6) and (I.7), $\mathbf{F}_{\mathbf{A}}(0)$ is the component of $\dot{\mathbf{A}}(0)$ orthogonal to $\mathbf{A}(0)$, whereas $\mathbf{F}_{\mathbf{A}}(t)$ is propagated from $\mathbf{F}_{\mathbf{A}}(0)$ by the special propagator $\exp(i\dot{Q}\Omega t)$. It is easily shown that

$$\langle \mathbf{F}_{\mathbf{A}}(t)\mathbf{A}^T(0)\rangle = \mathbf{0} \tag{I.8}$$

The simplest physical realizations[20] of (I.6) occur, for example, in the rotational Brownian motion of a spherical top, or a disk about a fixed axis through its center perpendicular to its plane. Equation (I.6) then becomes

$$\frac{D\mathbf{J}}{Dt} + \int_0^t d\tau\, \phi_{\mathbf{J}}(t-\tau)\mathbf{J}(\tau) = \mathbf{F}_{\mathbf{J}}(t) \tag{I.9}$$

where $\mathbf{A} = \mathbf{J}$ is the angular momentum of the rotator, the operator $\Omega_{\mathbf{J}}$ is null, $\phi_{\mathbf{J}}(t)$ is a time-dependent friction tensor, and $\mathbf{F}_{\mathbf{J}}(t)$ is a random driving torque of finite correlation time with mean $\langle \mathbf{F}_{\mathbf{J}}(t)\rangle = 0$. Equation (I.9) is such that the components of each vector are referred to principal body axes, and D/Dt denotes rate of change relative to these axes, so that $DJ_k/Dt = \dot{J}_k$. In the case of the disk there is only one component, referred to the fixed axis. For more complicated geometries nonlinear terms appear in (I.9). Asymmetric-top Brownian angular diffusion has been treated in definitive detail recently by Morita,[21] and McConnell and others[22] for the case where the memory matrix $\phi_{\mathbf{J}}$ consists of delta functions in time. The

more general angular equation

$$\dot{\mathbf{J}}(t) - i\Omega_{\mathbf{J}}\mathbf{J}(t) + \int_0^t d\tau\, \phi_{\mathbf{J}}(t-\tau)\mathbf{J}(\tau) = \mathbf{F}_{\mathbf{J}}(t) \tag{I.10}$$

is formally valid for the asymmetric top, but then the quantities $\Omega_{\mathbf{J}}$, $\phi_{\mathbf{J}}$, and $\mathbf{F}_{\mathbf{J}}$ may not have obvious physical meaning.

All the approximations of (I.6) prior to this have been concerned either with pure translation or pure rotation, the latter being complicated considerably by geometrical factors. Some popular models of the last decade are molded into the Mori framework in Table I (see Section I.B). In the next section we extend the formalism to cover rototranslational movements by deriving suitable approximations for the correlation functions associated with the column vector $\begin{bmatrix} \mathbf{v} \\ \boldsymbol{\omega} \end{bmatrix}$. It turns out that the zero-THz loss in dipolar solutes is markedly dependent upon the degree of rotation–translation coupling. Models devised in terms of pure rotation thus only oversimplify the dynamics considerably.

Reverting to general A, (I.6) can be solved using elementary Laplace transforms, giving

$$\dot{\mathbf{A}}(t) = C_{\mathbf{A}}(t)\mathbf{A}(0) + \int_0^t d\tau\, C_{\mathbf{A}}(t-\tau)\mathbf{F}_{\mathbf{A}}(\tau) \tag{I.11}$$

where $C_{\mathbf{A}}(t)$ is a matrix of normalized correlation functions given by

$$C_{\mathbf{A}}(t) = \mathfrak{L}_a^{-1}\left\{\left[s - i\Omega_{\mathbf{A}} + \tilde{\phi}_{\mathbf{A}}(s)\right]^{-1}\right\}$$
$$= \langle \mathbf{A}(t)\mathbf{A}^T(0)\rangle \langle \mathbf{A}(0)\mathbf{A}^T(0)\rangle^{-1} \tag{I.12}$$

Here $\tilde{\phi}_{\mathbf{A}}(s)$ denotes the Laplace transform of $\phi_{\mathbf{A}}(t)$ and $\mathfrak{L}_a^{-1}$ denotes inverse Laplace transformation.

If the vector $\mathbf{F}_{\mathbf{A}}(t)$ is a multivariate Gaussian process with mean $\langle \mathbf{F}_{\mathbf{A}}(t)\rangle$ and if the initial vector $\mathbf{A}(0)$ at time $t = 0$ is given, it follows from (I.11) that $\mathbf{A}(t)$ at time $t > 0$ is also a multivariate Gaussian process with mean

$$\langle \mathbf{A}(t)\rangle = C_{\mathbf{A}}(t)\mathbf{A}(0) + \int_0^t d\tau\, C_{\mathbf{A}}(t-\tau)\langle \mathbf{F}_{\mathbf{A}}(\tau)\rangle$$

(The Gaussian assumption is fundamental to further progress in this section, but later we present molecular dynamics data for N_2 which clearly shows that it is only approximately valid.)

Restricting ourselves to the special case $\langle \mathbf{F}_{\mathbf{A}}(t)\rangle = 0$ admits the treatment of rotational Brownian motion, for example, and simplifies the algebra

generally. This remains true for rototranslation. Then $\mathbf{A}(t)$ is conditionally distributed with probability density function

$$p(\mathbf{A}(t);t|\mathbf{A}(0)) = (2\pi)^{-(1/2)n}(\det V(t))^{-1/2} \times \exp\Big[-\tfrac{1}{2}(\mathbf{A}(t)-C_{\mathbf{A}}(t)\mathbf{A}(0))^{T}V^{-1}(t)(\mathbf{A}(t)-C_{\mathbf{A}}(t)\mathbf{A}(0))\Big] \tag{I.13}$$

with variance–covariance matrix

$$\begin{aligned} V(t) &= \langle(\mathbf{A}(t)-C_{\mathbf{A}}(t)\mathbf{A}(0))(\mathbf{A}(t)-C_{\mathbf{A}}(t)\mathbf{A}(0))^{T}\rangle \\ &= \langle\mathbf{A}(0)\mathbf{A}^{T}(0)\rangle - C_{\mathbf{A}}(t)\langle\mathbf{A}(0)\mathbf{A}^{T}(0)\rangle C_{\mathbf{A}}^{T}(t) \end{aligned} \tag{I.14}$$

We see from (I.14) that the elements of $V(t)$ can be calculated directly from the elements of the correlation matrix $C_{\mathbf{A}}(t)$, so that if the elements of $C_{\mathbf{A}}(t)$ can be found experimentally or otherwise, the conditional probability density function $p(\mathbf{A}(t);t|\mathbf{A}(0))$ can be calculated.

It is clearly essential to know whether or not the generalized force $\mathbf{F}_{\mathbf{A}}(t)$ is a Gaussian process. This depends both on the nature of $\mathbf{A}(t)$ and on the geometry. For example, if we consider the angular velocity ω of the sphere or disk mentioned above, the corresponding random driving torque $\mathbf{F}_{\omega}(t)$ may be assumed Gaussian (although non-Markovian), so ω is conditionally Gaussian. If, however, we consider the total Euler angle

$$\theta(t) = \int_0^t \omega_1(\tau)\,d\tau$$

it is not obvious whether $F_\theta(t)$ is Gaussian. Here θ is the total angle turned through in time t rather than the angular orientation which is restricted to the range $-\pi \le \theta \le \pi$. In fact, the angular distribution has a wrapped normal distribution which we shall consider later.

One possible way of investigating the Gaussian or non-Gaussian nature of $\mathbf{F}_{\mathbf{A}}(t)$ for a given $\mathbf{A}(t)$ is to expand the operator $\exp(i\hat{Q}\mathfrak{L}t)$ in (I.7). Since $\hat{Q}$ and $\mathfrak{L}$ commute, and $\hat{Q}^m = \hat{Q}$ for $m \ge 1$, we have

$$\mathbf{F}_{\mathbf{A}}(t) = \hat{Q}\dot{\mathbf{A}}(0) + t\hat{Q}i\mathfrak{L}\dot{\mathbf{A}}(0) - \tfrac{1}{2}t^2\hat{Q}\mathfrak{L}^2\dot{\mathbf{A}}(0) + \cdots$$

As a simple illustration we may consider $F_\theta(t)$ for the disk rotating in its plane under a Gaussian restoring torque $\Gamma(t) = -\tau[\theta(t)-\theta(0)]$, where τ is a constant. The Liouville operator is

$$i\mathfrak{L} = I\dot{\theta}\frac{\partial}{\partial\theta} - \tau\theta\frac{\partial}{\partial\dot{\theta}}$$

where I is the moment of inertia of the disk, so that

$$(i\mathfrak{L})^{2m}\dot{\theta} = (-I\tau)^m\dot{\theta}$$
$$(i\mathfrak{L})^{2m+1}\dot{\theta} = I^m(-\tau)^{m+1}\theta$$

Since $\hat{Q}\theta(0) = 0$ and $\hat{Q}\dot{\theta}(0) = \dot{\theta}(0)$, it follows that

$$F_\theta(t) = \dot{\theta}(0)\Big[1 - \frac{1}{2!}I\tau t^2 + \frac{1}{4!}(I\tau)^2t^4 - \cdots\Big] = \dot{\theta}(0)\cos\big[(I\tau)^{1/2}t\big]$$

Similarly, we can show that $F_{\dot\theta}(t) = (\Gamma(0)/I)\cos[(I\tau)^{1/2}t]$, so that $F_{\dot\theta}(t)$ is Gaussian while the nature of $F_\theta(t)$ is determined by that of $\dot{\theta}(0)$.

The conditional probability density functions discussed above are the most informative functions which can be extracted from a statistical treatment of the microscopic ensemble dynamics, more so than the correlation functions, which are integrals over the density functions. We now show that these density functions satisfy a generalized diffusion equation, similar to that of Fokker–Planck.[23] This extends our earlier analogy with the classical theory of Browian motion.

To simplify the analysis, we write $C \equiv C_{\mathbf{A}}(t)$, make the change of variable $\mathbf{B} = C^{-1}\mathbf{A}$, and introduce the probability density function $q(\mathbf{B};t|\mathbf{B}(0)) = p(\mathbf{A};t|\mathbf{A}(0))$. Clearly, $\mathbf{B}(0) = \mathbf{A}(0)$ since $C(0) = 1$. Differentiating q, we find that

$$\frac{\partial q}{\partial t} = -\tfrac{1}{2}\Big[(\det V)^{-1}\frac{d}{dt}(\det V)\Big]q - \tfrac{1}{2}(\mathbf{B}-\mathbf{B}(0))\dot{M}(\mathbf{B}-\mathbf{B}(0))q \tag{I.15}$$

and

$$\frac{\partial q}{\partial \mathbf{B}} = -M(\mathbf{B}-\mathbf{B}(0))q$$

Here $M = C^TV^{-1}C$. Using the identity

$$M^{-1}\dot{M} + \frac{d}{dt}(M^{-1})M = 0$$

we have

$$\frac{\partial}{\partial\mathbf{B}}\cdot\Big[\frac{d}{dt}(M^{-1})\frac{\partial q}{\partial\mathbf{B}}\Big] = \big[\mathrm{tr}(M^{-1}\dot{M}) - (\mathbf{B}-\mathbf{B}(0))\dot{M}(\mathbf{B}-\mathbf{B}(0))\big]q$$

From the identities

$$(\det V)^{-1}\frac{d}{dt}(\det V)=\mathrm{tr}(V^{-1}\dot{V})$$

and

$$\mathrm{tr}(V^{-1}\dot{V})+\mathrm{tr}(M^{-1}\dot{M})=2\,\mathrm{tr}(\dot{C}C^{-1})$$

(I.15) may be rewritten in the form

$$\frac{\partial q}{\partial t}=-\mathrm{tr}(\dot{C}C^{-1})q+\frac{1}{2}\frac{\partial}{\partial \mathbf{B}}\cdot\left[\frac{d}{dt}(M^{-1})\frac{\partial q}{\partial \mathbf{B}}\right] \tag{I.16}$$

Returning to the vector **A**, we find that

$$\frac{\partial q}{\partial t}=\frac{\partial p}{\partial t}+\frac{\partial p}{\partial \mathbf{A}}\cdot\dot{C}C^{-1}\mathbf{A}$$

and

$$\frac{\partial}{\partial \mathbf{B}}\cdot\left[\frac{d}{dt}(M^{-1})\frac{\partial q}{\partial \mathbf{B}}\right]=\frac{\partial}{\partial \mathbf{A}}\cdot\left[C\frac{d}{dt}(M^{-1})C^{T}\frac{\partial p}{\partial \mathbf{A}}\right]$$

which upon substitution into (I.16) finally gives the generalized Fokker–Planck equation

$$\frac{\partial p}{\partial t}=-\frac{\partial}{\partial \mathbf{A}}\cdot(\dot{C}_{\mathbf{A}}C_{\mathbf{A}}^{-1}\mathbf{A}p)+\frac{1}{2}\frac{\partial}{\partial \mathbf{A}}\cdot\left[C_{\mathbf{A}}\frac{d}{dt}(M^{-1})C_{\mathbf{A}}^{T}\frac{\partial p}{\partial \mathbf{A}}\right] \tag{I.17}$$

Equation (I.17) has the associated initial condition

$$p(\mathbf{A};0|\mathbf{A}(0))=\delta(\mathbf{A}-\mathbf{A}(0))$$

where δ denotes the Dirac delta function.

Equation (I.17) is exact for non-Markovian, Gaussian systems. Particular forms of this equation have been discussed by Adelman[24] when the elements of **A** are uncorrelated, and also for phase-space variables of the form $\mathbf{A}=\begin{bmatrix}\mathbf{a}\\ \dot{\mathbf{a}}\end{bmatrix}$. Here we shall be concerned mainly with orientation, angular velocity, and coupled angular and linear velocity. For this purpose we need probability densities of the form $p(\mathbf{A}(t);t|\mathbf{A}(0),\dot{\mathbf{A}}(0))$ as well as those of (I.13). Writing $\dot{\mathbf{A}}$ for **A** in (I.6), we obtain

$$\ddot{\mathbf{A}}(t)=i\Omega_{\dot{\mathbf{A}}}\dot{\mathbf{A}}(t)-\int_0^t d\tau\,\phi_{\dot{\mathbf{A}}}(t-\tau)\dot{\mathbf{A}}(\tau)+\mathbf{F}_{\dot{\mathbf{A}}}(t)$$

which may be solved to give

$$\mathbf{A}(t)=\mathbf{A}(0)+X_{\dot{\mathbf{A}}}(t)\dot{\mathbf{A}}(0)+\int_0^t d\tau\,X_{\dot{\mathbf{A}}}(t-\tau)\mathbf{F}_{\dot{\mathbf{A}}}(\tau)$$

where $X_{\dot{\mathbf{A}}}(t)$ is a cross-correlation matrix given by

$$X_{\dot{\mathbf{A}}}(t)=\mathfrak{L}_a^{-1}\left\{\left[s^2-i\Omega_{\dot{\mathbf{A}}}+s\tilde{\phi}_{\dot{\mathbf{A}}}(s)\right]^{-1}\right\}=\langle\mathbf{A}(t)\dot{\mathbf{A}}^{T}(0)\rangle\langle\dot{\mathbf{A}}(0)\dot{\mathbf{A}}^{T}(0)\rangle^{-1}$$

so that

$$\dot{X}_{\dot{\mathbf{A}}}(t)=C_{\dot{\mathbf{A}}}(t)$$

and

$$X_{\dot{\mathbf{A}}}(t)=\int_0^t C_{\dot{\mathbf{A}}}(\tau)\,d\tau+X_{\dot{\mathbf{A}}}(0) \tag{I.18}$$

$X_{\dot{\mathbf{A}}}(t)$ is also related to $C_A(t)$ by

$$X_{\dot{\mathbf{A}}}(t)=-\dot{C}_{\mathbf{A}}(t)\langle\mathbf{A}(0)\mathbf{A}^{T}(0)\rangle\langle\dot{\mathbf{A}}(0)\dot{\mathbf{A}}^{T}(0)\rangle^{-1}$$

so that

$$C_{\mathbf{A}}(t)=1-\int_0^t d\tau\,X_{\dot{\mathbf{A}}}(\tau)\langle\dot{\mathbf{A}}(0)\dot{\mathbf{A}}^{T}(0)\rangle\langle\mathbf{A}(0)\mathbf{A}^{T}(0)\rangle^{-1}$$

and

$$C_{\dot{\mathbf{A}}}(t)=-\ddot{C}_{\mathbf{A}}(t)\langle\mathbf{A}(0)\mathbf{A}^{T}(0)\rangle\langle\dot{\mathbf{A}}(0)\dot{\mathbf{A}}^{T}(0)\rangle^{-1}$$

The conditional probability density function

$$\begin{aligned}p(\mathbf{A}(t);t|\mathbf{A}(0),\dot{\mathbf{A}}(0))=(2\pi)^{-(1/2)n}(\det W(t))^{-1/2}\\ \times\exp\Big[-\tfrac{1}{2}\big(\mathbf{A}(t)-\mathbf{A}(0)-X_{\dot{\mathbf{A}}}(t)\dot{\mathbf{A}}(0)\big)^{T}W^{-1}(t)\\ \times\big(\mathbf{A}(t)-\mathbf{A}(0)-X_{\dot{\mathbf{A}}}(t)\dot{\mathbf{A}}(0)\big)\Big]\end{aligned} \tag{I.19}$$

is inferred when $\langle\mathbf{F}_{\dot{\mathbf{A}}}(t)\rangle=\mathbf{0}$, with variance–covariance matrix

$$\begin{aligned}W(t)&=\langle\big(\mathbf{A}(t)-\mathbf{A}(0)-X_{\dot{\mathbf{A}}}(t)\dot{\mathbf{A}}(0)\big)\big(\mathbf{A}(t)-\mathbf{A}(0)-X_{\dot{\mathbf{A}}}(t)\dot{\mathbf{A}}(0)\big)^{T}\rangle\\ &=2(1-C_{\mathbf{A}}(t))\langle\mathbf{A}(0)\mathbf{A}^{T}(0)\rangle-X_{\dot{\mathbf{A}}}(t)\langle\dot{\mathbf{A}}(0)\dot{\mathbf{A}}^{T}(0)\rangle X_{\mathbf{A}}^{T}(t)\\ &=2\int_0^t d\tau\,X_{\dot{\mathbf{A}}}(\tau)\langle\dot{\mathbf{A}}(0)\dot{\mathbf{A}}^{T}(0)\rangle-X_{\dot{\mathbf{A}}}(t)\langle\dot{\mathbf{A}}(0)\dot{\mathbf{A}}^{T}(0)\rangle X_{\dot{\mathbf{A}}}(t)\end{aligned} \tag{I.20}$$

Thus $p(\mathbf{A}(t);t|\mathbf{A}(0),\dot{\mathbf{A}}(0))$ is readily calculated from (I.18) to (I.20) from a knowledge of $C_{\dot{\mathbf{A}}}(t)$. This probabilty density also satisfies a generalized Fokker–Planck equation analogous to (I.17).

B. The Mori Continued Fraction

Mori[18] has shown that the Laplace transform, $\tilde{C}_{\mathbf{A}}(s)$, of $C_{\mathbf{A}}(t)$ has a continued-fraction representation, and that the time evolution of the vector $\mathbf{A}(t)$ is determined by the singularities of $\tilde{C}_{\mathbf{A}}(s)$. Tractable approximations

to $C_{\mathbf{A}}(t)$ are thus generated by finite approximants of the continued fraction, and it is this basic idea which is the essential leaven running through this chapter. The derivation of the continued fraction has been discussed in this series by Berne and Harp,[25] so that we quote the result:

$$\tilde{C}_{\mathbf{A}}(s) = \mathfrak{Q}_a[\langle \mathbf{A}(t)\mathbf{A}^T(0)\rangle\langle \mathbf{A}(0)\mathbf{A}^T(0)\rangle^{-1}]$$
$$= \cfrac{1}{s - i\Omega_0 + \cfrac{1}{s - i\Omega_1 + \cfrac{1}{\cdots \cfrac{1}{s - i\Omega_{n-1} + \tilde{C}_{\mathbf{A},n}(s)\phi_{\mathbf{A},n}(0)}\cdot\phi_{\mathbf{A},n-1}(0)}\cdot\phi_{\mathbf{A},2}(0)}\cdot\phi_{\mathbf{A},1}(0)} \tag{I.21}$$

Here

$$i\Omega_j \equiv \langle \dot{\mathbf{f}}_j \mathbf{f}_j^T\rangle\langle \mathbf{f}_j \mathbf{f}_j^T\rangle^{-1}$$

and

$$\phi_{\mathbf{A},j}(0) = \langle \mathbf{f}_j \mathbf{f}_j^T\rangle\langle \mathbf{f}_{j-1} \mathbf{f}_{j-1}^T\rangle^{-1}$$

where the $\mathbf{f}$ vectors are given by

$$\mathbf{f}_0 = \mathbf{A} \qquad \hat{P}_0 = \hat{P}$$
$$\mathbf{f}_j = \left[\hat{1} - \sum_{k=0}^{j-1} \hat{P}_k\right] i\mathfrak{Q}\mathbf{f}_{j-1} \qquad j \geq 1 \tag{I.22}$$
$$\dot{\mathbf{f}}_j = \left[\hat{1} - \sum_{k=0}^{j-1} \hat{P}_k\right] i\mathfrak{Q}\mathbf{f}_j \qquad j \geq 1 \tag{I.23}$$

where $\hat{P}_k$ projects into the subspace spanned by $\mathbf{f}_k(0)$. From (I.22) and (I.23) we find

$$\mathbf{f}_0 = \mathbf{A}$$
$$\mathbf{f}_1 = \dot{\mathbf{A}} - [\langle \dot{\mathbf{A}}\mathbf{A}^T\rangle\langle \mathbf{A}\mathbf{A}^T\rangle^{-1}]\mathbf{A}$$
$$\mathbf{f}_2 = \ddot{\mathbf{A}} - [\langle \dot{\mathbf{A}}\mathbf{A}^T\rangle\langle \mathbf{A}\mathbf{A}^T\rangle^{-1} + \langle \ddot{\mathbf{A}}\mathbf{f}_1^T\rangle\langle \mathbf{f}_1\mathbf{f}_1^T\rangle^{-1}$$
$$- \langle \dot{\mathbf{A}}\mathbf{A}^T\rangle\langle \dot{\mathbf{A}}\mathbf{f}_1^T\rangle\langle \mathbf{A}\mathbf{A}^T\rangle^{-1}\langle \mathbf{f}_1\mathbf{f}_1^T\rangle^{-1}]\dot{\mathbf{A}}$$
$$- [\langle \ddot{\mathbf{A}}\mathbf{A}^T\rangle\langle \mathbf{A}\mathbf{A}^T\rangle^{-1} - \langle \dot{\mathbf{A}}\mathbf{A}^T\rangle^2\langle \mathbf{A}\mathbf{A}^T\rangle^{-2}$$
$$- \langle \dot{\mathbf{A}}\mathbf{A}^T\rangle\langle \ddot{\mathbf{A}}\mathbf{f}_1^T\rangle\langle \mathbf{A}\mathbf{A}^T\rangle^{-1}\langle \mathbf{f}_1\mathbf{f}_1^T\rangle^{-1}$$
$$+ \langle \dot{\mathbf{A}}\mathbf{A}^T\rangle^2\langle \dot{\mathbf{A}}\mathbf{f}_1^T\rangle\langle \mathbf{A}\mathbf{A}^T\rangle^{-2}\langle \mathbf{f}_1\mathbf{f}_1^T\rangle^{-1}]\mathbf{A}$$

where $\dot{\mathbf{A}} = i\mathfrak{Q}\mathbf{A}$. Thus $\phi_{\mathbf{A},j}$ and Ω_j are related to the moments of the frequency distribution function of $C_{\mathbf{A}}(t)$. For example, when $\mathbf{A}$ is a scalar,

$$\langle \omega^n\rangle \equiv \int_{-\infty}^{\infty} \omega^n P(\omega)\, d\omega = i^{-n}\left[\frac{d^n}{dt^n} C_A(t)\right]_{t=0} \tag{I.24}$$

where $$P(\omega) \equiv \frac{1}{\pi}\mathrm{Re}[\tilde{C}_A(i\omega)] = \frac{1}{2\pi}\int_{-\infty}^{\infty} C_A(t)\exp(-i\omega t)\, dt$$

As $n \to \infty$ (I.21) leads to an infinite continued fraction, with the time evolution of $C_{\mathbf{A}}(t)$ determined by the singularities of this fraction in the complex s-plane.

Many molecular models of fluid dynamics in the literature are approximants of this expansion. Indeed, for reasons of consistency, it is difficult to see a model approximating the Liouville equation which does not fit into the expansion represented by (I.21). Table I shows a selection of these, where $\mathbf{A}$ is the angular momentum $\mathbf{J}$ or the dipole orientation $\mathbf{u}$. The real power of the continued fraction is its general validity for classifying not only molecular but also hydrodynamical and ferromagnetic phenomena within the same theoretical framework. The generalized hydrodynamics developed in the last few years[7,26,27] has proved useful in explaining the observations made by polarized and depolarized light scattering, and the results of computer simulation. The special brand of mode–mode coupling[12,28] used has been slow in influencing molecular theories, but we suggest later in this section how molecular rototranslation may be described.

Mori in his original paper discusses how, if we truncate the continued fraction at a particular memory matrix $\tilde{C}_{\mathbf{A},n}(s)$, it is often possible (Table I) to introduce one of the following approximations or any of their combinations: (1) long-time approximation, (2) a perturbation procedure, (3) a high- or low-temperature approximation, and (4) a short-time approximation.

1. *Long-Time Approximation*

Consider a scalar A and denote the first spectral moment by $\Omega_0 = \langle \omega\rangle$. When $A(t)\exp(-i\Omega_0 t)$ is a slowly varying function of time in a certain time scale Δt, the function $\tilde{C}^{(0)}_{A,n}(s) \equiv \tilde{C}_{A,n}(s + i\Omega_0)$ will be insensitive to s in a small region around the origin in the complex s-plane (i.e., at low frequencies). We can then neglect the s-dependence of $\tilde{C}_{A,n}(s)$, thus truncating the continued fraction with

$$\tilde{C}^{(0)}_{A,n}(s) \simeq \xi_{A,n} \equiv \int_0^{\infty} C_{A,n}(t)\exp(-i\Omega_0 t)\, dt \tag{I.25}$$

TABLE I
Some Dynamical Models in Mori's Formalism[a]

Memory function	Model	Comments
$\phi_1^{(u)}(t) = D\delta(t)$, where D is a diffusion coefficient, δ the Dirac delta function	Debye, rotational diffusion[37] of the inertialess spherical top with embedded dipole	Used extensively to describe dielectric experiments, but leads to a plateau in $\alpha(\omega)$, the power absorption coefficient at frequencies high with respect to the Debye relaxation time. $C_u(t) = e^{-t/\tau_0}$.
$\phi_1^{(u)}(t) = \phi_1^{(u)}(0)e^{-\gamma_1 t}$ before ensemble averaging	Gordon m diffusion[16,34] linear molecule; space reorientation	Instantaneous collisions perturb the angular momentum vector (J) in direction but not in magnitude. Power spectrum diverges logarithmically around $\omega = 0$. Binary collision model. Mean-square torque singular at every impact. Does not follow the observed THz frequency shifts in ω_{max}.
$\phi_1^{(u)}(t) = \phi_{FR}^{(u)}(t)e^{-\gamma\|t\|}$ where $\phi_{FR}(t)$ is the free-rotor ensemble memory function	Gordon J diffusion.[16,34] Linear molecule; space reorientation	As for M diffusion, J randomized both in direction and magnitude onto a Poisson distribution. A slow return to spectral transparency at high THz frequencies of the far infrared. Does not follow changes in ω_{max}.
$\phi_1^{(u)}(t) = \phi_1^{(u)}(0)\exp(-\gamma t)\cos\omega_0 t$	Damped planar libration[38,39]	$\delta(\omega)$ falls off asymptotically at high frequencies as ω^{-2}, as for J diffusion. ω_0 is the libration frequency, synonymous with ω_{max}, the far-infrared peak frequency. $C_u(t)$ a sum of three exponentials, as for the itinerant planar librator.
$\phi_1^{(u)}(t) = \phi_1^{(u)}(0)\exp(-\gamma t)$	Maximum information entropy.[25]:space orrientation of CO	$\gamma = (\pi/4)^{1/2}\phi_1(0)\int_0^\infty \psi(t)\,dt; \psi(t) = \langle \omega_\perp(0)\cdot \omega_\perp(t)\rangle$where $\omega_\perp$ is perpendicular to **u**. THz spectrum too sharp compared with experimental data unless γ is varied for best fit.
$\phi_2^{(u)}(t) = {}^{FR}\phi_2^{(u)}(t)\psi(t)$	Desplanques	$\psi(t)$ as above. In general, the theoretical spectrum $\alpha(\omega)$ is too sharp in the far infrared.
$\phi_2^{(u)}(t) = \beta\phi_{2FR}^{(u)}(t)\exp(-\|t\|/\tau)$	Bliot and Constant[40,41]	$\phi_{2FR}^{(u)}(t)$ is the second memory of the free rotor. β and τ are stochastic variables, the former being proportional to the mean-square torque. Too sharp in the far infrared for broad bands. $C_u(t)$ even up to t^4 of its Taylor series.
$\phi_2^{(u)}(t) = \phi_2^{(u)}(0)\exp(-\gamma t)$	First used by Barojas, Levesque, and Quentrec in a simulation[42] of liquid nitrogen	Used extensively[43] by Evans for semiempirical analyses of a wide range of zero-THz data. Used by Drawid and Halley[44] for Heisenberg paramagnetism (see text).

TABLE I (*Continued*)

Memory function	Model	Comments
$\phi_1^{(J)}(t)=\phi_1^{(J)}(0)\delta(t)$	Asymmetric top, Langevin equation for rotational Brownian diffusion[21,22] in space	Produces a high-frequency return to transparency but no THz resonance (or Poley absorption—see text).
$\phi_2^{(\omega)}(t)=\phi_2^{(\omega)}(0)\exp(-\gamma t)$	This approximant produces $\tilde{C}_\omega(s)$ formally identical with that of planar itinerant libration[29]	Here $\omega\equiv\dot{\theta}$ is the angular velocity of a disk librating in a plane, (I.30).
Eqs. (I.50)–(I.53)	A zeroth-order approximant of the system of Damle and others[29] for neutron scattering	Leads to $\tilde{C}_\omega(s)$ formally identical with that from (I.31). A physical system identical with that of (I.30). A finite friction, however, exists between ring and annulus. May be interpreted also in terms of dipole–dipole coupling, (I.54).
Modeling performed on the memory function of **J** by Lindenberg and Cukier[45]		Generalized stochastic model for molecular rotational motion in condensed media, encompassing all previous stochastic models of rotational relaxation as specialized cases. Close in spirit to the approach of Kivelson and Keyes.[46]

[a] $\phi_n(t)$ is the nth memory of the dipole unit vector (**u**) or angular momentum (**J**).

It may be shown that

$$\tilde{C}_A(s+i\Omega_0)\simeq g_{n-1}(s)/g_n(s) \tag{I.26}$$

where $g_j(s)$ is a jth-degree polynomial defined by

$$g_j(s)=\left[s+i(\Omega_0-\Omega_{n-j})\right]g_{j-1}(s)+\phi_{A,n-j+1}(0)g_{j-2}(s) \quad j\geq 2 \tag{I.27}$$

$$g_0(s)=1, \qquad g_1(s)=s+i(\Omega_0-\Omega_{n-1})+\lambda_{n-1} \tag{I.28}$$

with

$$\lambda_{j-1}\equiv\phi_{A,j}(0)\xi_j=\phi_{A,j}(0)/\left[i(\Omega_0-\Omega_j)+\lambda_j\right]$$

The singularities of (I.26) are given by the zeros of $g_n(s)$. Denoting these zeros by $s_\alpha=i(\beta_\alpha-\Omega_0)-\gamma_\alpha, \alpha=1,\ldots,n$, and taking the inverse Laplace transform of (I.26), we have

$$C_A(t)\simeq\sum_{\alpha=1}^{n}R_\alpha\exp\left[(i\beta_\alpha-\gamma_\alpha)t\right] \tag{I.29}$$

where R_α is the residue of the ratio $g_{n-1}(s)/g_n(s)$ at the pole s_α.

The approximation in (I.25) corresponds to the description of $A(t)\exp(-i\Omega_0 t)$ in the time scale Δt distinctly larger than the decay time τ_n of $C_{A,n}(t)$. Mori calls this the nth-order long-time approximation around $s=i\Omega_0$. Equation (I.25) is valid if all the n poles are located in the left-half s-plane inside a semicircle center $s=i\Omega_0$, and radius $1/\tau_n$. These poles represent slow processes, and the higher-frequency components which correspond to the remaining singularities of $C_A(t)$ are represented by the nth-order random force $f_n(t)$, whose correlation time is much smaller than the relaxation time of the slow processes.

Rotational Motions: The Planar Itinerant Librator. Let A be the rate at which an angle θ is swept out by a dipole rotating in a plane. It is easily shown that the operators $i\Omega_0$, $i\Omega_1$, and $i\Omega_2$ vanish identically. Introducing the third-order long-time approximation around $s=0$, we have

$$\tilde{C}_{\dot{\theta}}(s)=\frac{s^2+\lambda_2 s+\phi_{\dot{\theta},2}(0)}{s^3+\lambda_2 s^2+\left[\phi_{\dot{\theta},1}(0)+\phi_{\dot{\theta},2}(0)\right]s+\phi_{\dot{\theta},1}(0)\lambda_2} \tag{I.30}$$

This expression for $\tilde{C}_{\dot{\theta}}(s)$ may be identified with a simple model[29] of the angular Brownian motion of a dipole immersed in a bath of interacting particles. We shall return to the experimental evaluation of this later—it has been used extensively[30] to describe the zero-THz absorptions in fluids and glasses. The quantities λ_2, $\phi_{\dot{\theta},1}(0)$, and $\phi_{\dot{\theta},2}(0)$ may be given solid physical meanings in terms of the disk/annulus system illustrated in Fig. 4. It is assumed in the rotational dynamics leading to (I.30) that a librating central molecule together with its cage of neighbors may be represented by an

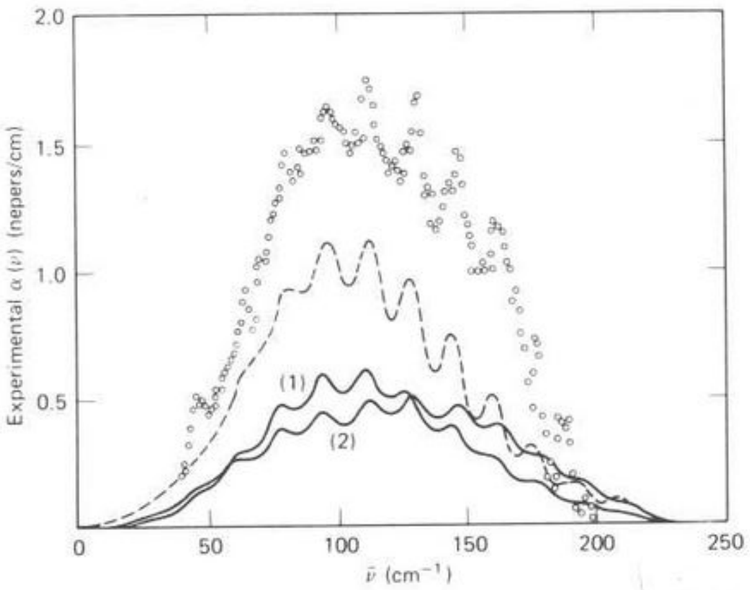

Fig. 4. Experimental absorption of HBr/SF_6 liquid mixture at 296°K. (---), Frenkel/Wegdam formalism (see text); ordinate scale unnormalized. (—), (1) truncated Mori formalism of Bliot and Constant, $\beta_2=1$; (2) $\beta_2=1.2$. Both curves (1) and (2) are unnormalized to the experimental data on the ordinate scale. [Reproduced by permission from *Chem. Phys. Lett.*, **42**, 331 (1976).]

annulus which is free to rotate about a central axis, perpendicular to its plane. Concentric and coplanar with the annulus is a disk which is free to rotate about the same central axis. (The words "disk" and "annulus" are used only as a convenient scematic description of the model; the theory will apply to a body of arbitrary shape provided that it is constrained to rotate in two dimensions.) The disk carries a dipole μ lying along one of its diameters, the orientation of the dipole is specified by an angle $\theta(t)$ relative to a fixed direction, and the position of a point on the rim of the annulus is specified by an angle $\psi(t)$ relative to the same fixed direction. The mechanical interaction between the central molecule and its neighbors is a restoring torque acting on the dipole, which is proportional to the angular displacement $\theta(t)-\psi(t)$ of the dipole in space. Furthermore, if it is stipulated that on the average each cage containing a molecule behaves in the same way, so that we may study the behavior of a single cage containing a dipole and examine how the dipole orientation changes when the measuring field is switched off, then the equations of motion are[13]

$$\begin{aligned} I_1\ddot{\psi}(t)+I_1\beta_1\dot{\psi}(t)-I_2\gamma^2[\theta(t)-\psi(t)]&=I_1\dot{W}_1(t)\\ I_2\ddot{\theta}(t)+I_2\beta_2\dot{\theta}(t)+I_2\gamma^2[\theta(t)-\psi(t)]&=I_2\dot{W}_2(t)\\ \beta_1=\xi_1/I_1 \qquad \beta_2&=\xi_2/I_2 \end{aligned} \tag{I.31}$$

Here I_1 is the moment of inertia of the annulus; I_2 that of the disk; $\xi_1\dot{\psi}(t)$ and $\xi_2\dot{\theta}(t)$ are the frictional couples acting on the annulus and disk, respectively, arising from the thermal motion of the surroundings; $\dot{W}_1$ and $\dot{W}_2$ are Wiener processes representing random couples acting on the annulus and disk; and γ is the natural angular frequency of oscillation when the annulus is held stationary.

In the case $\beta_2=0$ (no friction between annulus and disk), the angular velocity correlation function $\langle\dot{\theta}(t)\dot{\theta}(0)\rangle$ is given by the inverse Laplace transform of (I.30) with

$$\lambda_2=\beta_1 \qquad \phi_{\dot{\theta},1}(0)=\gamma^2 \qquad \phi_{\dot{\theta},2}(0)=\left(\frac{I_2}{I_1}\right)\phi_{\dot{\theta},1}(0) \tag{I.32}$$

Writing $J=I\dot{\theta}$ for the angular momentum of the disk librating and diffusing in its plane, then from (I.17) we have

$$\frac{\partial p}{\partial t}=\tilde{\beta}(t)\left[\frac{\partial}{\partial J}(Jp)+kTI_2\frac{\partial^2 p}{\partial J^2}\right] \tag{I.33}$$

where the probability density function is

$$p(J;t|J(0))=\left[2\pi kTI_2(1-C_J^2(t))\right]^{-1/2}\exp\left[-\frac{(J-C_J(t)J(0))^2}{2kTI_2(1-C_J^2(t))}\right] \tag{I.34}$$

and

$$\begin{aligned} C_J(t)&=\langle J(t)J(0)\rangle/(kTI_2)\\ \tilde{\beta}(t)&=-\dot{C}_J(t)/C_J(t) \end{aligned} \tag{I.35}$$

with

$$p(J;0|J(0))=\delta(J-J(0))$$

The probability density functions calculated from (I.33) to (I.35) exhibit widely different decays for each pair of $\phi_1(0),\phi_2(0)$ values (dropping the subcript J), and are directly interpretable in terms of the structure and dynamics of the molecular fluid they represent. We consider two cases in order of increasing ratio $\phi_2(0)/\phi_1(0)$; the parameters used to calculate $C_J(t)$ are given in Table II. In each case we adopt the normalization $(2kT/I_2)=1$, and take $J(0)=0$. In Figs. 5*a* and 6*a* the probability densities are displayed at various times ranging from near the origin to ~2 psec. In

TABLE II
Parameters Used to Calculate $C_J(t)$ of (I.30)

Fig.	T(°K)	$\beta_1(2kT/I_2)^{1/2}$	$\phi_1(0)(2kT/I_2)$	$\phi_2(0)(2kT/I_2)$	$10^{-12}(2kT/I_2)^{1/2}$
5,7	296	4.0	1.0	8.0	2.25
6,8	340	2.0	0.78	200.0	1.44

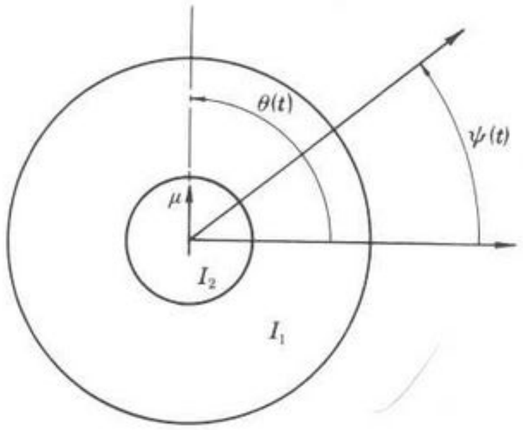

Fig. 5. Schematic of the disk–annulus representation of (I.30). [Reproduced by permission from *Proc. R. Soc. Lond.*, **356**, 269 (1977).]

Figs. 6*b* and 7*b* the decay of the peak height is shown as a function of time. The curve in Fig. 6*b* decays smoothly; the torque is not subject to abrupt changes on the average (i.e., the torque derivative is not large compared with the torque itself). The model fluid as a whole is not one where the angular momentum for individual dipoles is restricted to favored values for any significant period of time, since $p(J;t|J(0))$ broadens out rapidly to the equilibrium distribution. Collisions take place with a low mean transfer of momentum.

On the other hand, the probability density function associated with a ratio $\phi_2(0)/\phi_1(0) \gg 1$ reveals over 2 psec quite different features (Fig. 7). In this case the disk is very heavy and the torque derivative is large compared with the torque itself. This means abrupt changes in the root-mean-square torque which acts on the annulus. The oscillations in p imply that periodically it becomes increasingly probable to find a mean angular momentum which corresponds physically to a torsional motion at the bottom of an energetically favorable potential well. Here a molecule is encaged along a well-defined axis for relatively long times, since at each successive peak maximum in p the distribution width is narrow. Hard energetic collisions are needed to affect the motion of the heavy disk.

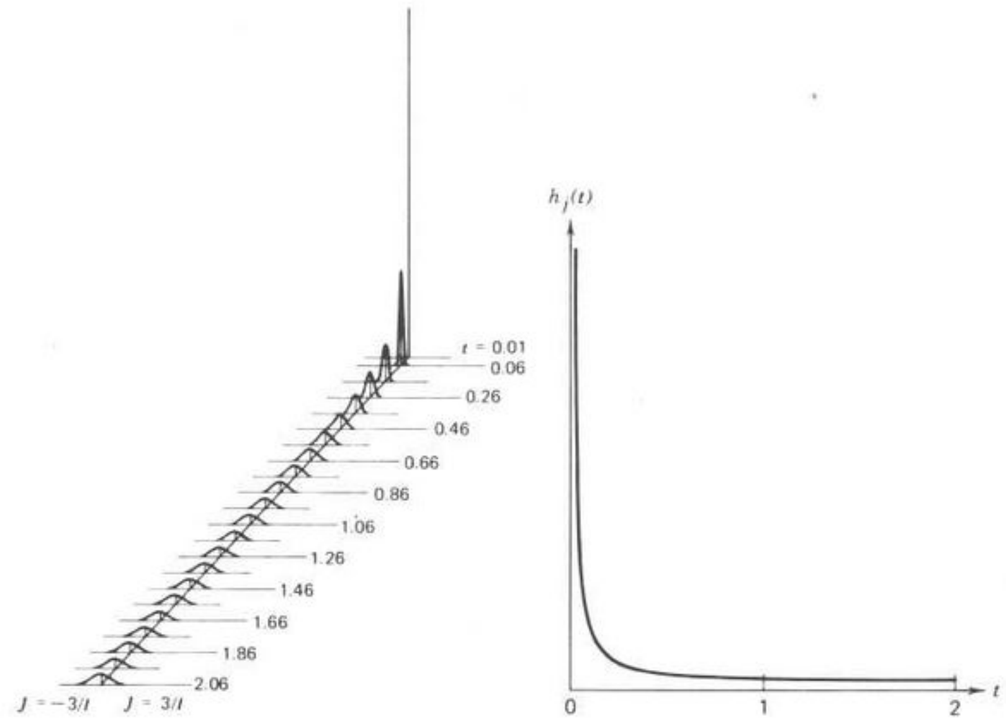

Fig. 6. (*a*) $p(J;t/J(o))$ for β_1, $\phi_1(o)$ and $\phi_2(o)$ as in Table II. p is plotted on the vertical axis, J on the horizontal axes (from $-3/I$ to $3/I$), and time t on the diagonal axis. (*b*) Plot of pdf peak height vs. time (psec). [Reproduced by permission from *Mol. Phys.*, **35**, 864 (1978).]

$C_J(t)$ may also be used to calculate $p(\theta(t);t|\theta(0),\dot{\theta}(0))$ which describes the torsional oscillation of the dipole $\boldsymbol{\mu}$ in an itinerant librator of (I.30). If $\theta(t)$ is the total angle turned through in time t, then from (I.19) and (I.20)

$$p(\theta(t);t|\theta(0),\dot{\theta}(0)) = \left[\frac{2\pi kT}{I_2}\left(2\int_0^t X_J(\tau)\,d\tau - X_J^2(t)\right)\right]^{-1/2} \times \exp\left[-\frac{\left(\theta(t)-\theta(0)-X_J(t)\dot{\theta}(0)\right)^2}{\left(\frac{2kT}{I_2}\right)\left(2\int_0^t X_J(\tau)\,d\tau - X_J^2(t)\right)}\right] \tag{I.36}$$

where

$$X_J(\tau) = \int_0^t C_J(\tau)\,d\tau$$

In practice, however, we wish $\theta(t)$ to represent the angular orientation at time t. The probability density function for *restricted* to the range $(-\pi,\pi)$ is that of a wrapped normal distribution which may be approximated by the von Mises distribution:

$$p(\theta(t);t|\theta(0),\dot{\theta}(0)) \simeq \left[2\pi I_0(\alpha(t))\right]^{-1} \exp\left[\alpha(t)\cos\left(\theta(t)-\theta(0)-X_J(t)\dot{\theta}(0)\right)\right] \tag{I.37}$$

The function $\alpha(t)$ can be found at any specific time t by solving the equation

$$\frac{I_1(\alpha(t))}{I_0(\alpha(t))} = \exp\left[-\frac{kT}{I}\left(\int_0^t X_J(\tau)\,d\tau - \tfrac{1}{2}X_J^2(t)\right)\right]$$

numerically. Here $I_0(\cdot)$ and $I_1(\cdot)$ are the modified Bessel functions of zeroth and first order, respectively. As illustrated in Figs. 6*a* and 7*a*, the functions $p(\theta;t|\theta(0),\dot{\theta}(0))$ are symmetric about $\theta(0)$, and eventually die

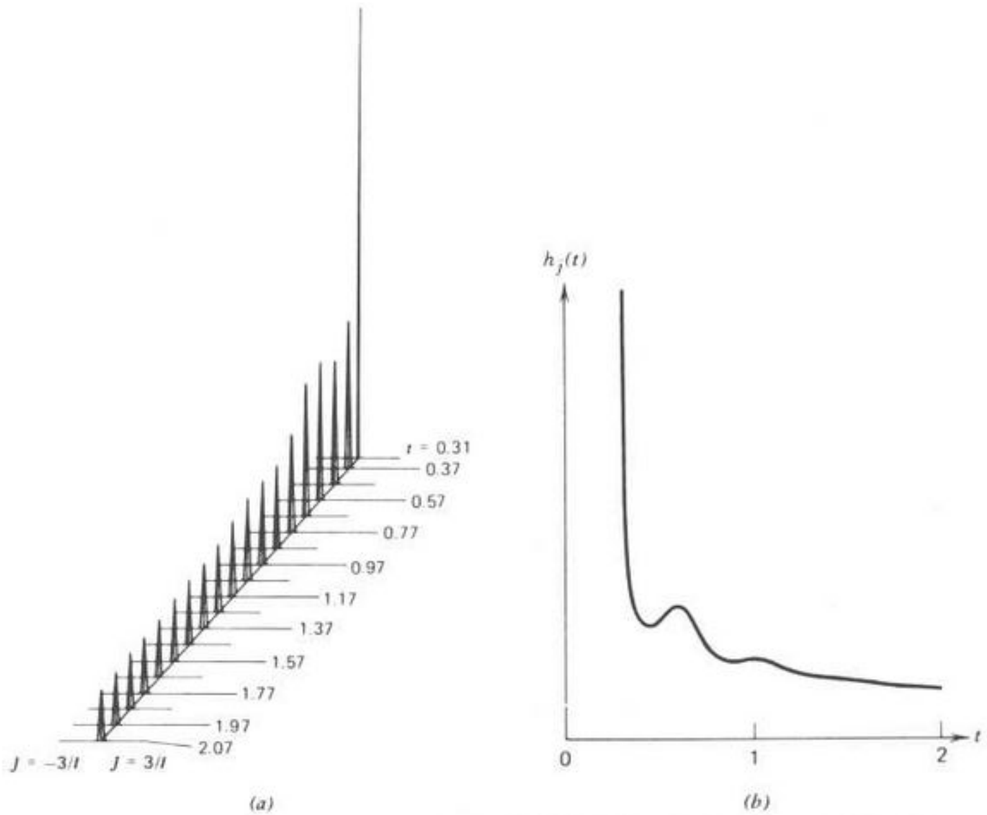

Fig. 7. Key as in Fig. 6; parameters and pdf's defined in the text and Table II.

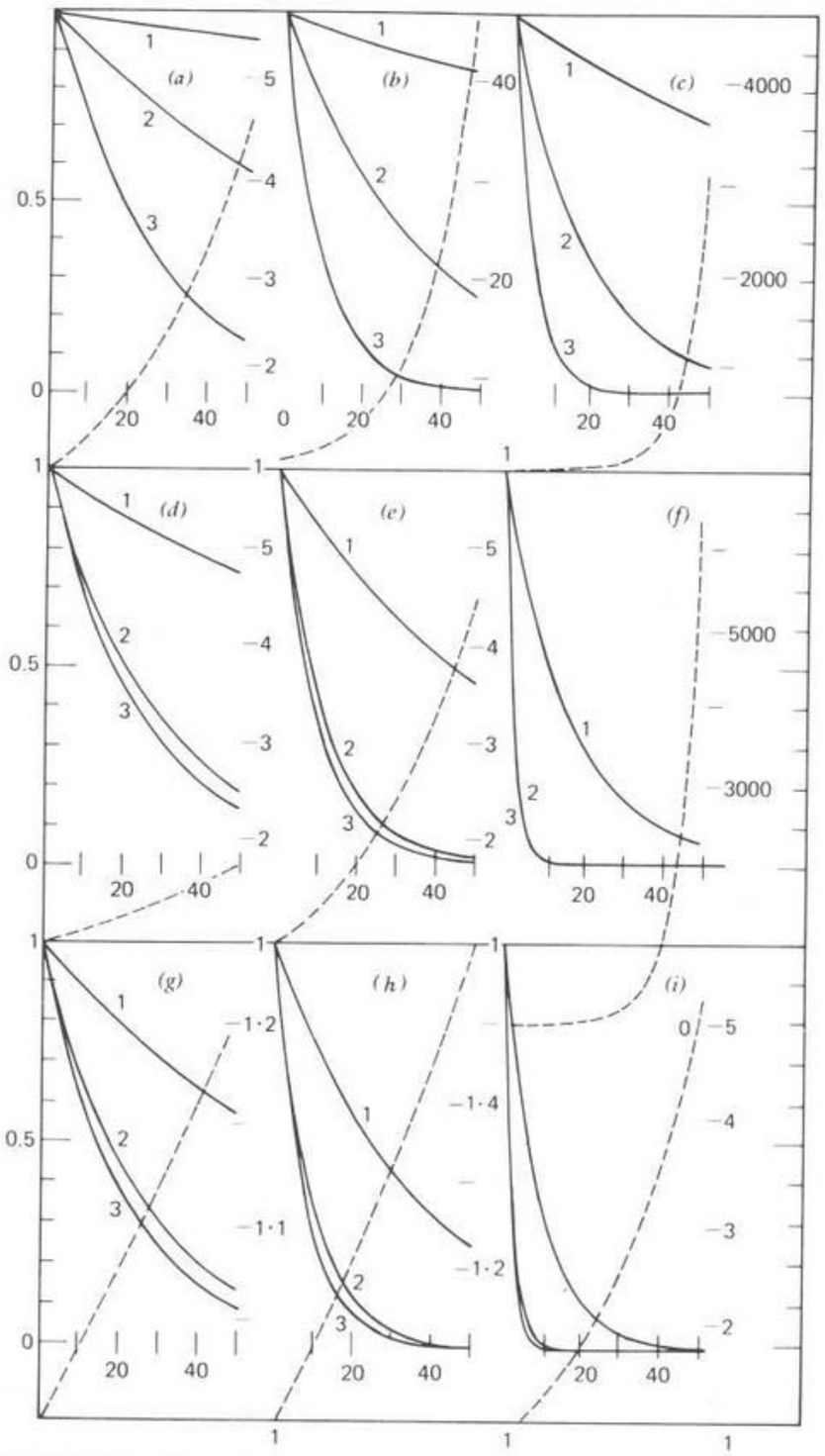

Fig. 8. (1) $C_0(\boldsymbol{Q},t)$; (2) $C_1(\boldsymbol{Q},t)$; (3) $C_1(o;t)$; (----), the ratio $C_1(\boldsymbol{Q},t)/C_1^{(u)}(\boldsymbol{Q},t)$ for $Q=1$, $\kappa=0.4$. (*a*) $\lambda=0.1$, $\beta_\omega=50$; (*b*) $\lambda=0.1$, $\beta_\omega=20$; (*c*) $\lambda=0.1$, $\beta_\omega=10$; (*d*) $\lambda=0.5$, $\beta_\omega=50$; (*e*) $\lambda=0.5$, $\beta_\omega=20$; (*f*) $\lambda=0.5$, $\beta_\omega=5$; (*g*) $\lambda=1.0$, $\beta_\omega=50$; (*h*) $\lambda=1.0$, $\beta_\omega=20$; (*i*) $\lambda=1.0$, $\beta_\omega=5$. λ is the roughness parameter, κ the mass-distribution parameter of Berne and Montgomery. The parameters above are in reduced units specified by these authors. [Reproduced by permission from *Faraday Discuss. Chem. Soc.*, **66** (1978).]

down to a flat distribution as $t\to\infty$. The similarity in shape to Gaussian distributions disappears as time increases. The equation of the decay curve of peak height (Figs. 6*b* and 7*b*) is

$$h_\theta(t)=\frac{\exp[\alpha(t)]}{2\pi I_0(\alpha(t))}$$

as opposed to

$$h_J(t)=\left[2\pi kTI_2\left(1-C_J^2(t)\right)\right]^{-1/2}$$

for the angular momentum J. Whereas for angular momentum there is an onset of oscillation in $h_J(t)$, the decay of $h_\theta(t)$ is free of them, except perhaps for the most rapid torque rate of change. Roughly speaking, this is because the oscillations are integrated out in forming $X_J(t)$. In the underdamped regime, however, where $\phi_2(0)<\phi_1(0)$, both $h_J(t)$ and $h_\theta(t)$ will decay in a highly oscillatory fashion.

The probability density function $p(\theta(t);t|\theta(0),\dot\theta(0))$ is the planar reorientational counterpart of the translational van Hove function[31] $G_s(\mathbf{r};t|\mathbf{0})$, where r is center-of-mass displacement. G_s may be obtained from atomic fluids by scattering thermal neutrons incoherently and inelastically. In molecular fluids, however, translation-rotation coupling is of great practical and theoretical importance,[32] and the self-part of the observable van Hove function is in general the joint probability density function $G_s(\mathbf{r},\Omega;t|\mathbf{0},\Omega(0))$. (For planar reorientation Ω is replaced by the scalar θ.) Moreover, tractable expressions for the self van Hove function have been developed in the first Born approximation, when coupling between rotation and translation is ignored. In the next section we show how this coupling may be included in joint probability density functions.

Rotation–Translation Coupling—Itinerant Libration. In this section we first deal with the coupled autocorrelation functions of immediate interest to neutron scattering. Second, within the context of (I.30), we discuss the influence of molecular center-of-mass translation upon the momentum autocorrelation $\langle J(t)J(0)\rangle$ and hence on the zero-THz loss profile, related directly to the Fourier transform of $\langle\cos\theta(t)\cos\theta(0)\rangle$. The zero-THz power absorption coefficient is the Fourier transform[30] of

$$\left\langle\frac{d}{dt}(\cos\theta(t))\left(\frac{d}{dt}(\cos\theta(t))\right)_{t=0}\right\rangle$$

when the influence of the internal field is not considered.

The first kind of autocorrelation function is, for general space rototranslation,[32]

$$C_k(\mathbf{q};t)=\langle P_k(\boldsymbol{\mu}(t)\cdot\boldsymbol{\mu}(0))\exp[i\mathbf{q}\cdot\Delta\mathbf{r}(t)]\rangle \tag{I.38}$$

where k is a positive integer, $P_k(x)$ the Legendre polynomial of degree k, $\mathbf{q}$ the scattering wave vector, and $\Delta\mathbf{r}(t)=\mathbf{r}(t)-\mathbf{r}(0)$ the displacement in time t. The $C_k(\mathbf{q};t)$ in neutron scattering theory are approximated by

$$C_k^{(u)}(\mathbf{q};t)=\langle P_k(\boldsymbol{\mu}(t)\cdot(\boldsymbol{\mu}(0))\rangle\langle\exp[i\mathbf{q}\cdot\Delta\mathbf{r}(t)]\rangle \tag{I.39}$$

Berne and Montgomery[32] have lately shown, however, that the maximum deviation between $C_k(\mathbf{q};t)$ and $C_k^{(u)}(\mathbf{q};t)$ occurs for wave numbers commonly found in thermal neutron scattering, and it was pointed out that the effect of the coupling would increase for structured molecules as opposed to the rough spheres which they considered analytically. In this work, Berne and Montgomery adopt the Chandler[33] binary collision approximation (Table I)—an earlier approximant of (I.21) than that resulting in (I.30). When translational effects are ignored, this approximant becomes the Gordon J-diffusion model for spherical tops.[34] Furthermore, they adopt (1) a second-order expansion for the Laplace transform of the free-particle rotation–translation correlation function, and (2) a partial curtailment to first order of (1) in obtaining $C_k(\mathbf{q};s)$, the Laplace transform of $C_k(\mathbf{q};t)$. If, however, we dispense with approximation (2) and keep to second order, we obtain

$$\tilde C_k(\mathbf{Q};s)=\frac{s^2+2\beta_k(Q)s+\left[\beta_k^2(Q)-k(k+1)-Q^2\right]}{s^3+2\beta_k(Q)s^2+\beta_k^2(Q)s+\beta_k(Q)\left[k(k+1)+Q^2\right]} \tag{I.40}$$

Here $\mathbf{Q}$ denotes the dimensionless wave vector and

$$\beta_k(Q)=\beta_w\left[\frac{k(k+1)+\left\{\dfrac{(1+\lambda)K+1}{\lambda}\right\}Q^2}{k(k+1)+Q^2}\right] \tag{I.41}$$

where λ is a slip coefficient, K a loading parameter, and the dimensionless angular velocity relaxation rate of the rough sphere fluid. Equation (I.40) is similar in structure to (I.30), and its inverse Laplace transform may be recovered analytically. In Fig. 9 we see that for $Q=1$, (1) the ratio $C_1(\mathbf{Q};t)/C_1^{(u)}(\mathbf{Q};t)$ always increases (from unity) with time; (2) for fixed λ, the ratio increases more rapidly the smaller the value of β_w; and (3) the

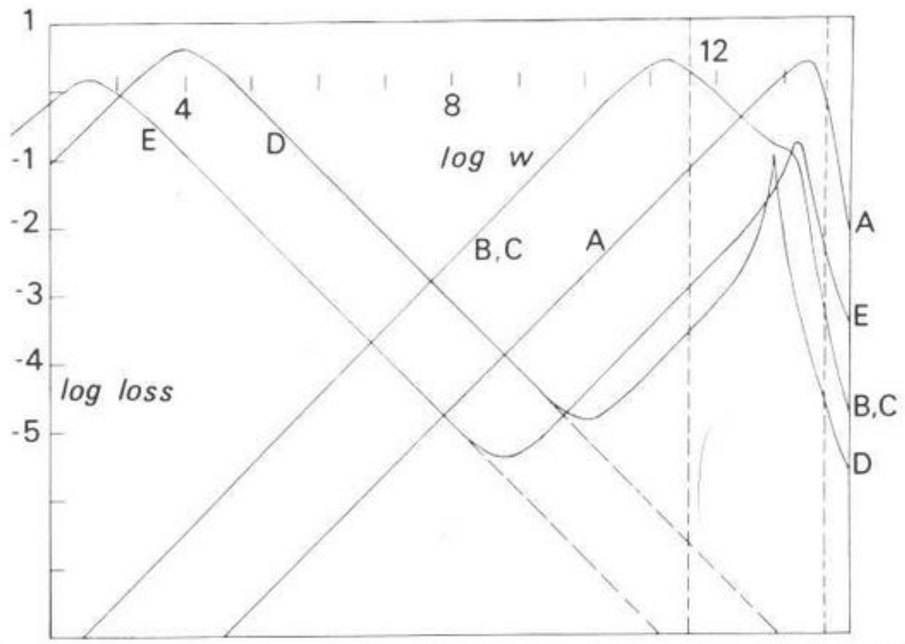

Fig. 9. Log-log plot (schematic) of loss against angular frequency expected from various classes of dipolar compounds, as simulated by (I.31). (*A*) Water free from hydrogen bonding (in dilute solution); gaslike rototranslation in the liquid state. The Debye and Poley portions of the loss are indistinguishable. (*B*), (*C*) Liquids such as benzonitrile and plastic crystals such as $(CH_3)_3Cl$, where the Poley absorption is clearly resolved on the high-frequency side of the Debye curve. (*D*) Mesophase, such as the nematic of 4-cyano-4′*n*-heptyl biphenyl. The Poley absorption is considerably sharper than in cases (*B*) and (*C*) and well separated on the frequency scale. (*E*) Glasses, such as those of CH_2Cl_2 in decalin (see text). Here the β process is shown at low frequency together with the high frequency far-infrared adjunct.

ratio is greatest for small λ. Thus for given $\mathbf{Q}$ the coupling effect is small when β_ω is large and collisions are rough. It is greatest when slipping conditions are invoked in a dilute fluid where the angular velocity relaxes fairly slowly.

For structured molecules, rather than consider $C_1(\mathbf{q};t)$, we discuss an alternative and simpler means of investigating the interplay between spin angular velocity and linear velocity. For a diatomic, for example, one may consider the total velocity autocorrelation function for an atom. If $\boldsymbol{\mu}$ is the interatomic displacement vector, then the total velocity $\mathbf{v}_a$ of an atom is

$$\mathbf{v}_a = \mathbf{v} + \tfrac{1}{2}\boldsymbol{\omega}\times\boldsymbol{\mu} \tag{I.42}$$

where $\mathbf{v}$ denotes the center-of-mass velocity and $\boldsymbol{\omega}$ the spin angular velocity about the center of mass. Thus the autocorrelation function of $\mathbf{v}_a$ contains information on both linear and angular velocities. The relation between the

autocorrelations of $\mathbf{v}_a$ and $\mathbf{v}$ can easily be found if $\boldsymbol{\omega}$ is constrained to lie in a fixed direction, as in the planar itinerant librator, so that $\dot{\theta}(t)=\omega(t)$. For (I.42) we have

$$\langle \mathbf{v}_a(t)\cdot\mathbf{v}_a(0)\rangle = \langle \mathbf{v}(t)\cdot\mathbf{v}(0)\rangle + \langle \mathbf{v}(t)\cdot\boldsymbol{\omega}(0)\mathbf{x}\boldsymbol{\mu}(0)\rangle + \tfrac{1}{4}\langle \boldsymbol{\mu}(t)\cdot\boldsymbol{\mu}(0)\boldsymbol{\omega}(t)\cdot\boldsymbol{\omega}(0)\rangle \tag{I.43}$$

since

$$\langle \boldsymbol{\omega}(t)\mathbf{x}\boldsymbol{\mu}(t)\cdot\mathbf{v}(0)\rangle = \langle \mathbf{v}(t)\cdot\boldsymbol{\omega}(0)\mathbf{x}\boldsymbol{\mu}(0)\rangle$$

The central term in the right-hand side of (I.43) describes the effect of rotation–translation coupling and would vanish in a decoupled approximation; the third term describes the coupling between reorientation and spin angular velocity, which vanishes only in the limit $t\to\infty$. Although it is easily shown that

$$\langle \boldsymbol{\mu}(t)\cdot\boldsymbol{\mu}(0)\boldsymbol{\omega}(t)\cdot\boldsymbol{\omega}(0)\rangle = \frac{d^2}{dt^2}\langle \boldsymbol{\mu}(t)\cdot\boldsymbol{\mu}(0)\rangle$$

this relation hides the dependence of the third term on the joint conditional probability density function $p(\omega(t),\theta(t);t|\omega(0),\theta(0))$, which describes a cylindrical distribution of importance in its own right. We demonstrate its use by calculating $\langle \boldsymbol{\mu}(t)\cdot\boldsymbol{\mu}(0)\boldsymbol{\omega}(t)\cdot\boldsymbol{\omega}(0)\rangle$ explicitly.

Since $\boldsymbol{\mu}(t)\cdot\boldsymbol{\mu}(0)=\mu^2\cos(\theta(t)-\theta(0))$, the required correlation function is defined by

$$\begin{aligned}&\langle \boldsymbol{\mu}(t)\cdot\boldsymbol{\mu}(0)\boldsymbol{\omega}(t)\cdot\boldsymbol{\omega}(0)\rangle \\ &= \mu^2\int_{-\infty}^{\infty}\int_{-\infty}^{\infty}\int_{-\pi}^{\pi}\int_{-\pi}^{\pi}\omega\omega_0\cos(\theta-\theta_0)p(\omega,\theta;t|\omega_0,\theta_0)p(\omega_0,\theta_0)\,d\omega\,d\omega_0\,d\theta\,d\theta_0\end{aligned} \tag{I.44}$$

where $\omega(0)=\omega_0$, $\theta(0)=\theta_0$, and $p(\omega_0,\theta_0)$ is the joint density for the initial distribution of ω and θ at time $t=0$. Since ω and θ are statistically independent variables, and the initial distribution of ω may be assumed Maxwellian, we may write

$$p(\omega_0,\theta_0) = \left(\frac{2\pi k}{I_2}\right)^{1/2}\exp\left[-\frac{\omega_0^2}{(2kT/I_2)}\right]p(\theta_0)$$

where the initial distribution $p(\theta_0)$ satisfies

$$\int_{-\pi}^{\pi}p(\theta_0)\,d\theta_0 = 1$$

but otherwise need not be specified for the purpose of the present calculation. Since $\theta(t)$ is restricted to the range $-\pi \leq \theta \leq \pi$, the cylindrical distribution has a marginal distribution for ω which is normal, and a marginal distribution for θ which is wrapped normal. It may be specified by generalizing a well-known result in the theory of wrapped distributions.[35] If x is a normally distributed random variable with mean $\langle x \rangle$ and variance $\sigma_x^2 = \langle (x - \langle x \rangle)^2 \rangle$, the corresponding wrapped variate $\tilde{x} = x (\mathrm{mod}\, 2\pi)$ has a density

$$p(\tilde{x}) = \frac{1}{2\pi}\left[1 + 2\sum_{n=1}^{\alpha}\{\cos(n\langle x\rangle)\cos(n\tilde{x}) + \sin(n\langle x\rangle)\sin(n\tilde{x})\}\right]\exp\left(-\tfrac{1}{2}n^2\sigma_x^2\right)$$

Extending this result to the case of two normal variables, only one of which is wrapped, we obtain the expression

$$p(\omega,\theta;t|\omega_0,\theta_0) = \frac{1}{(2\pi)^2}\int_{-\infty}^{\infty}\Bigg[\exp\left(is\langle\omega\rangle - \tfrac{1}{2}s^2\sigma_\omega^2 - is\omega\right) + 2\sum_{N=1}^{\infty}\{\cos(s\langle\omega\rangle + n\langle\theta\rangle)\cos(s\omega + n\theta) + \sin(s\langle\omega\rangle + n\langle\theta\rangle)\sin(s\omega + n\theta)\} \times \exp\left\{-\tfrac{1}{2}\left(s^2\sigma_\omega^2 + 2ns\,\mathrm{cov} + n^2\sigma_\theta^2\right)\right\}\Bigg]ds \quad \text{(I.45)}$$

where the covariance term is defined by

$$\mathrm{cov} = \langle(\omega - \langle\omega\rangle)(\theta - \langle\theta\rangle)\rangle$$

In terms of the normalized correlation functions $C_\omega(t)$ and $X_\omega(t) = \int_0^t C_\omega(\tau)\,d\tau$, we have

$$\begin{aligned}
\langle\omega\rangle &= C_\omega(t)\omega_0 \\
\langle\theta\rangle &= \theta_0 + X_\omega(t)\omega_0 \\
\sigma_\omega^2 &= \frac{kT}{I_2}\left(1 - C_\omega^2(t)\right) \\
\sigma_\theta^2 &= \frac{kT}{I_2}\left(2\int_0^t X_\omega(\tau)\,d\tau - X_\omega^2(t)\right) \\
\mathrm{cov} &= \frac{kT}{I_2}X_\omega(t)(1 - C_\omega(t)) \qquad \text{(I.46)}
\end{aligned}$$

Equation (I.44) may be integrated using (I.45) and (I.46) and some standard integrals to give

$$\langle\boldsymbol{\mu}(t)\cdot\boldsymbol{\mu}(0)\boldsymbol{\omega}(t)\cdot\boldsymbol{\omega}(0)\rangle = \mu^2\frac{kT}{I_2}\left[C_\omega(t) - \frac{kT}{I_2}X_\omega^2(t)\right]\exp\left[-\frac{kT}{I_2}\int_0^t X_\omega(\tau)\,d\tau\right] \qquad \text{(I.47)}$$

But from (I.36) it may be shown that

$$\begin{aligned}
\langle\boldsymbol{\mu}(t)\cdot\boldsymbol{\mu}(0)\rangle &\equiv \mu^2\int_{-\pi}^{\pi}\int_{-\pi}^{\pi}\int_{-\infty}^{\infty}\cos(\theta - \theta_0)p(\theta;t|\theta_0,\omega_0)p(\theta_0,\omega_0)\,d\theta\,d\theta_0\,d\omega_0 \\
&= \mu^2\exp\left[-\frac{kT}{I_2}\int_0^t X_\omega(\tau)\,d\tau\right] \qquad \text{(I.48)}
\end{aligned}$$

and hence that

$$\langle\boldsymbol{\mu}(t)\cdot\boldsymbol{\mu}(0)\boldsymbol{\omega}(t)\cdot\boldsymbol{\omega}(0)\rangle = \langle\boldsymbol{\mu}(t)\cdot\boldsymbol{\mu}(0)\rangle\left[\langle\boldsymbol{\omega}(t)\cdot\boldsymbol{\omega}(0)\rangle - \left(\frac{kT}{I_2}X_\omega(t)\right)^2\right] \qquad \text{(I.49)}$$

Thus the full decoupled approximation to (I.43) reads

$$\langle\mathbf{v}_a(t)\cdot\mathbf{v}_a(0)\rangle = \langle\mathbf{v}(t)\cdot\mathbf{v}(0)\rangle + \langle\boldsymbol{\mu}(t)\cdot\boldsymbol{\mu}(0)\rangle\left[\langle\boldsymbol{\omega}(t)\cdot\boldsymbol{\omega}(0)\rangle - \left(\frac{kT}{I_2}X_\omega(t)\right)^2\right]$$

Notice also that analogously with (I.38) and (I.39), for space reorientation of the diatomic we have

$$\langle\boldsymbol{\mu}(t)\cdot\boldsymbol{\mu}(0)\boldsymbol{\omega}(t)\cdot\boldsymbol{\omega}(0)\rangle \neq \langle\boldsymbol{\mu}(t)\cdot\boldsymbol{\mu}(0)\rangle\langle\boldsymbol{\omega}(t)\cdot\boldsymbol{\omega}(0)\rangle \qquad t > 0$$

A more direct study of rotation–translation coupling may be attempted by considering the correlation matrix for the vector $\begin{bmatrix}\mathbf{v}\\ \boldsymbol{\omega}\end{bmatrix}$ under the assumption that the matrices $\langle\mathbf{v}(t)\boldsymbol{\omega}^T(0)\rangle$ and $\langle\boldsymbol{\omega}(t)\mathbf{v}^T(0)\rangle$ are not null when $t > 0$. Within a memory formalism we therefore propose that past rotations influence future translations and past translations influence future rotations. Instantaneously at time t, of course, the statistical correlation between $\mathbf{v}(t), \boldsymbol{\omega}(t)$, and any of their time derivatives must vanish. As shown below, it is a simple matter to generalize the Mori continued-fraction approximant corresponding to planar itinerant libration, with the introduction of only one further phenomenological parameter specifying the off-diagonal elements of the third memory matrix of $\begin{bmatrix}\mathbf{v}\\ \boldsymbol{\omega}\end{bmatrix}$. [It should be noted that in planar motion the matrix elements of $\langle\mathbf{v}(t)\boldsymbol{\omega}^T(0)\rangle$ do not all

vanish, even though the scalar correlation $\langle \mathbf{v}(t)\cdot\boldsymbol{\omega}(0)\rangle$ does.] It is seen that the new "coupling" parameter also appears in the transforms of $\langle \mathbf{v}(t)\mathbf{v}^T(0)\rangle$ and $\langle \boldsymbol{\omega}(t)\boldsymbol{\omega}^T(0)\rangle$, which emphasizes the inadequacy of a decoupled approximation, even when studying autocorrelations.

Since the components of $\mathbf{v}$ are mutually statistically uncorrelated, the elements of the correlation matrix of $\begin{bmatrix} \mathbf{v} \\ \boldsymbol{\omega} \end{bmatrix}$ are typified by those of the 2×2 matrix

$$C(t)=\begin{bmatrix} \dfrac{\langle v(t)v(0)\rangle}{\langle v^2(0)\rangle} & \dfrac{\langle v(t)\omega(0)\rangle}{\langle \omega^2(0)\rangle} \\ \dfrac{\langle \omega(t)v(0)\rangle}{\langle v^2(0)\rangle} & \dfrac{\langle \omega(t)\omega(0)\rangle}{\langle \omega^2(0)\rangle} \end{bmatrix} \tag{I.50}$$

where v and ω are scalar components. Interpreting (I.21) in matrix form, the Laplace transform of $C(t)$ is

$$\begin{aligned} \tilde{C}(s)&=\left[s+\tilde{C}_1(s)\phi_1(0)\right]^{-1} \\ &=\left[s+\left\{s+\tilde{C}_2(s)\phi_2(0)\right\}^{-1}\phi_1(0)\right]^{-1} \end{aligned} \tag{I.51}$$

where $\tilde{\phi}_1(s)=\tilde{C}_1(s)\phi_1(0)$ and $\tilde{\phi}_2(s)=\tilde{C}_2(s)\phi_2(0)$

are the transforms of the first and second memory matrices, and the $\phi_j(0)$ are defined by

$$\phi_j(0)=\langle \mathbf{f}_j\mathbf{f}_j^T\rangle\langle \mathbf{f}_{j-1}\mathbf{f}_{j-1}^T\rangle^{-1} \qquad j=1,2$$

with

$$\mathbf{f}_0=\begin{bmatrix} v(0) \\ \omega(0) \end{bmatrix} \qquad \mathbf{f}_1=\begin{bmatrix} \dot{v}(0) \\ \dot{\omega}(0) \end{bmatrix} \qquad \mathbf{f}_2=\begin{bmatrix} \ddot{v}(0)+\dfrac{\langle \dot{v}^2(0)\rangle}{\langle v^2(0)\rangle}v(0) \\ \ddot{\omega}(0)+\dfrac{\langle \dot{\omega}^2(0)\rangle}{\langle \omega^2(0)\rangle}\omega(0) \end{bmatrix}$$

We find that

$$\phi_j(0)=\begin{pmatrix} \phi_{tj} & 0 \\ 0 & \phi_{rj} \end{pmatrix}$$

where

$$\phi_{t1}=\frac{\langle \dot{v}^2(0)\rangle}{\langle v^2(0)\rangle} \qquad \phi_{r1}=\frac{\langle \dot{\omega}^2(0)\rangle}{\langle \omega^2(0)\rangle}$$

and

$$\phi_{t2}=\frac{\langle \ddot{v}^2(0)\rangle}{\langle \dot{v}^2(0)\rangle}-\frac{\langle \dot{v}^2(0)\rangle}{\langle v^2(0)\rangle} \qquad \phi_{r2}=\frac{\langle \ddot{\omega}^2(0)\rangle}{\langle \dot{\omega}^2(0)\rangle}-\frac{\langle \dot{\omega}^2(0)\rangle}{\langle \omega^2(0)\rangle}$$

These terms are identical with the corresponding terms in the (decoupled) planar itinerant librator model. To attempt a description of rototranslational coupling consider, first, the first-order approximant in (I.51) defined by

$$\tilde{C}_1(s)\phi_1(0)=\begin{pmatrix} \lambda_t & \lambda_{tr} \\ \lambda_{rt} & \lambda_r \end{pmatrix}$$

where the λ's may be interpreted as frictional parameters. It follows that

$$\begin{aligned} \tilde{C}(s)&=\begin{pmatrix} s+\lambda_t & \lambda_{tr} \\ \lambda_{rt} & s+\lambda_r \end{pmatrix}^{-1} \\ &=\frac{1}{\Delta(s)}\begin{pmatrix} s+\lambda_r & -\lambda_{tr} \\ -\lambda_{rt} & s+\lambda_t \end{pmatrix} \end{aligned}$$

where

$$\Delta(s)=(s+\lambda_t)(s+\lambda_r)-\lambda_{tr}\lambda_{rt}$$

Writing $b=2(\lambda_t+\lambda_r)$, $c=\lambda_t\lambda_r-\lambda_{tr}\lambda_{rt}$, we find

$$\langle v(t)v(0)\rangle$$

$$=\begin{cases} \langle v^2(0)\rangle\exp(-bt)\left[\cos(c-b^2)^{1/2}t+\dfrac{\lambda_r-b}{(c-b^2)^{1/2}}\sin(c-b^2)^{1/2}t\right] & c>b^2 \\ \langle v^2(0)\rangle\exp(-bt)\left[\cosh(b^2-c)^{1/2}t+\dfrac{\lambda_r-b}{(b^2-c)^{1/2}}\sinh(b^2-c)^{1/2}t\right] & c<b^2 \end{cases}$$

$$\langle \omega(t)v(0)\rangle$$

$$=\begin{cases} -\dfrac{\langle \omega^2(0)\rangle\lambda_{tr}}{(c-b^2)^{1/2}}\exp(-bt)\sin(c-b^2)^{1/2}t & c>b^2 \\ -\dfrac{\langle \omega^2(0)\rangle\lambda_{tr}}{(b^2-c)^{1/2}}\exp(-bt)\sinh(b^2-c)^{1/2}t & b^2<c \end{cases}$$

with similar expressions for $\langle\omega(t)\omega(0)\rangle$ and $\langle\omega(t)v(0)\rangle$. Since $\langle v(t)\omega(0)\rangle = \langle\omega(t)v(0)\rangle$, it follows that

$$\lambda_{tr}\langle\omega^2(0)\rangle = \lambda_{rt}\langle v^2(0)\rangle$$

and hence only three of the four parameters $\lambda_t, \lambda_r, \lambda_{tr}, \lambda_{rt}$ are independent. It can be seen that the translational autocorrelation function $\langle v(t)v(0)\rangle$ involves not only the translational parameter λ_t, but also the rotational parameter λ_r linked via the coupling parameter λ_{tr}; and similarly for the rotational autocorrelation. When $\lambda_{tr}=0$, the dependence reduces to one parameter and the cross-correlation $\langle v(t)\omega(0)\rangle$ vanishes identically. Moreover, when $\lambda_{tr}\neq 0$, the cross-correlation $\langle v(0)\omega(0)\rangle$ vanishes, as it should.

To obtain the generalized model for planar itinerant libration we simply define the third memory matrix by

$$\tilde{C}_3(s)\phi_3(0) = \begin{pmatrix} \lambda_t & \lambda_{tr} \\ \lambda_{rt} & \lambda_r \end{pmatrix}$$

and hence find

$$\tilde{C}(s) = \frac{1}{\Delta_2(s)} \begin{bmatrix} s + \left[s + (s+\lambda_r)\dfrac{\phi_{t2}}{\Delta(s)} \right] \dfrac{\phi_{r1}}{\Delta_1(s)} & -\dfrac{\lambda_{tr}\phi_{r2}\phi_{r1}}{\Delta(s)\Delta_1(s)} \\ -\dfrac{\lambda_{rt}\phi_{t2}\phi_{t1}}{\Delta(s)\Delta_1(s)} & s + \left[s + (s+\lambda_t)\dfrac{\phi_{r2}}{\Delta(s)} \right] \dfrac{\phi_{t1}}{\Delta_1(s)} \end{bmatrix}$$

where

$$\Delta_1(s) = \left[s + (s+\lambda_t)\frac{\phi_{r2}}{\Delta(s)} \right] \left[s + (s+\lambda_r)\frac{\phi_{t2}}{\Delta(s)} \right] - \frac{\lambda_{tr}\lambda_{rt}\phi_{t2}\phi_{r2}}{\Delta^2(s)}$$

and

$$\Delta_2(s) = \left\{ s + \left[s + (s+\lambda_t)\frac{\phi_{r2}}{\Delta(s)} \right] \frac{\phi_{t1}}{\Delta_1(s)} \right\} \times \left\{ s + \left[s + (s+\lambda_r)\frac{\phi_{t2}}{\Delta(s)} \right] \frac{\phi_{r1}}{\Delta_1(s)} \right\} - \frac{\lambda_{tr}\lambda_{rt}\phi_{t2}\phi_{t1}\phi_{r2}\phi_{r1}}{\Delta^2(s)\Delta_1^2(s)}.$$

We now have:

$$\lambda_{tr}\phi_{r2}\phi_{r1} = \lambda_{rt}\phi_{t2}\phi_{t1}$$

and thus all correlation functions involve the seven independent phenomenological parameters ϕ_{t1}, ϕ_{t2}, ϕ_{r1}, ϕ_{r2}, λ_t, λ_r, and λ_{tr}. When the coupling parameter $\lambda_{tr}=0$, the determinants $\Delta(s)$, $\Delta_1(s)$, and $\Delta_2(s)$ reduce to simple factors, the autocorrelation functions become dependent on only three parameters (in each case), and the cross-correlations vanish identically.

It is the authors' belief that *all* continued-fraction-approximant models should contain coupling parameters such as λ_{tr}, except of course for cases where the correlation matrices can be shown to vanish at all times for reasons of symmetry.

Further Applications of the Long-time Approximation. Consider the case in (I.31), where β_2 is finite. The dynamical system is then described by (I.6) with

$$A(t) = \begin{bmatrix} \dot{\theta}(t) \\ \dot{\psi}(t) \end{bmatrix}$$

$$\phi_A = \begin{bmatrix} \beta_2\delta(t)+\gamma^2 & -\gamma^2 \\ -(I_2\gamma/I_1)^2 & \beta_1\delta(t)+(I_2\gamma/I_1)^2 \end{bmatrix} \tag{I.52}$$

$$F_A = \begin{bmatrix} \dot{W}_2 \\ \dot{W}_1 \end{bmatrix} \qquad [\text{with a null resonance operator}]$$

Equation (I.30) becomes

$$C_{\dot{\theta}}(s) = \frac{kT}{I_2} \frac{s^2+\beta_1 s+(I_2\gamma/I_1)^2}{s^3+s^2(\beta_1+\beta_2)+\left(\beta_1\beta_2+\gamma^2\left(1+(I_2/I_1)^2\right)\right)s+\gamma^2\left(\beta_1+\beta_2(I_2/I_1)^2\right)} \tag{I.53}$$

In Fig. 9 we plot some zero-THz dielectric loss profiles obtained from (I.53) for various friction coefficients β_1 and β_2 and force constant. The effect of β_2 is to broaden the γ resonance, and with $\beta_1 \gg \beta_2$ it is interesting to note the loss profile may extend over many decades of frequency. This might be typical of the situation in glasses, disordered solids, or liquid crystals, where a cage of nearest-neighboring molecules under collective reorientation would do so, if at all, only very slowly compared with the libration of the inner molecule, taking place at THz frequencies. The version of

the long-time approximation embodied in (I.50) to (I.53) may then be used to link together loss peaks separated on the frequency scale by many decades. In these solids therefore, whatever the precise validity of (I.53) it is needless to emphasize that any study of rotational motions of the permanent dipole in the condensed phase should not end at frequencies lower than those of the far infrared. Conversely, data above 10 cm^{-1} should not be analyzed without taking into account the low-frequency loss. In the extreme of charge carrier hopping in semiconductors or chalcogenide glasses,[36] the peak of the loss is often at too low a frequency to measure; nevertheless, the librational movement of molecular frameworks in between the occasional hopping of charges will produce a quasiharmonic Poley type of absorption (a resonance around the frequency γ) at THz frequencies. This is to be expected on the grounds of (I.53), which is of course an approximation of the Liouville equation, neglecting all cooperative movements embodied in the resonance operator $\Omega_{\mathbf{A}}$ of (I.6).

It is remarkable that to (I.53) may be ascribed another interpretation in terms of the Brownian motion of two interacting dipoles as in Fig. (I.10). The following conditions are imposed.

1. The potential between the dipoles has the form

$$V(\theta-\psi)=\tfrac{1}{2}I_2\gamma^2(\theta-\psi)^2 \tag{I.54}$$

2. The measuring field is applied in the same plane of rotation of the dipoles μ_1 and μ_2 which rotate about an axis about the common center perpendicular to the plane containing $\boldsymbol{\mu}_1$ and $\boldsymbol{\mu}_2$. β_1 and β_2 are the opposing friction coefficients arising from the surroundings. This interpretation of (I.53) is restrictive in the sense that it still applies to planar motions, but by varying the terms in the column vector **A** and memory matrix $\phi_{\mathbf{A}}$ the model is capable of further improvement. Developments may be made to account for more realistic potentials than that of (I.54), and of space reorientation. In the present context γ is a measure of the dipole–dipole coupling strength.

The two physical processes embodied in Figs. 5 and 10 may be distinguished experimentally by noticing that in the itinerant oscillator we might expect $I_1>I_2$ by geometrical considerations, but in the dipole interaction model $I_1=I_2$ for a neat fluid. Further, in a dilute solution of dipolar molecules in nondipolar solvents, where a theory of autocorrelations is valid, dipole–dipole coupling is considerably weakened, whereas the THz resonance remains. It seems unlikely that a theory of dipole–dipole resonance can account for the persistent resonance band. The problem of kinematics vs. electrostatics in the context of (I.54) reduces to one of de-

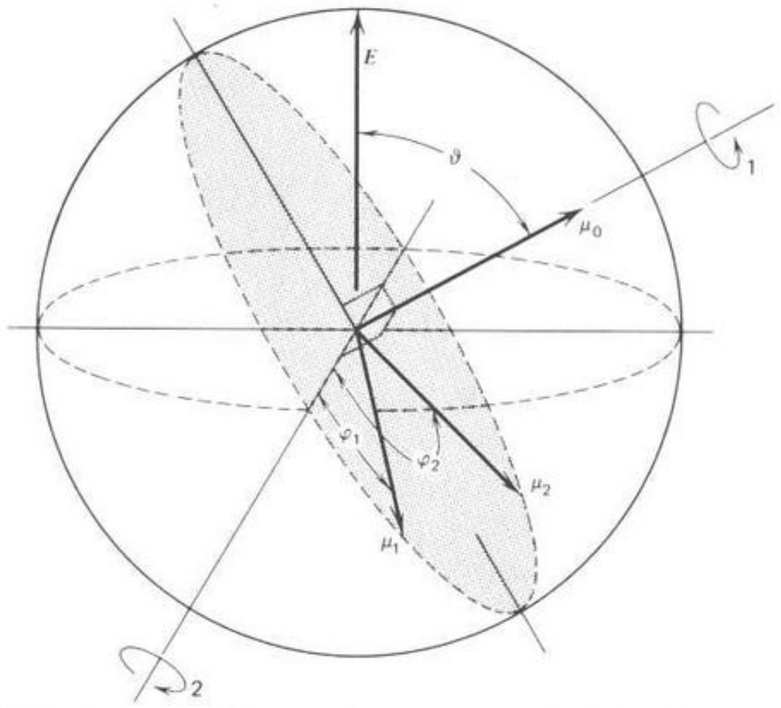

Fig. 10. Dipole–dipole interaction as an interpretation of (I.53) (where θ of Fig. I.5 is zero) and $(\phi_2-\phi_1)\equiv(\theta-\psi)$ in the notation of (I.31). [Reproduced by permission from *Mol. Phys.*, (1979), **37**, 473]

termining, experimentally, whether $I_1=I_2$ is in closer agreement with the data than $I_1>I_2$. This is resolved in Section II.C.

C. Collective Variables

The effect of a finite resonance operator on the theoretical zero-THz loss profile has removed, like rotation/translation coupling, some of the restrictions of the simple Langevin equation. The resonance operator $i\Omega_A$ remains finite in the following instances:

1. The coupling between even and odd variables is finite.
2. When time-reversal symmetry is destroyed by an external pertubation such as a magnetic field.

The role of the resonance operator $i\Omega_A$ may be described most clearly by making the separation

$$\frac{d}{dt}A(t)\equiv F(t)=F_1(A(s),t\geq s\geq t_0)+F_2(t,t_0) \tag{I.55}$$

where the Langevin equation is now

$$\frac{d}{dt}A(t)=i\Omega_A-\beta A(t)+f(t) \tag{I.56}$$

Here $A(t)$ denotes a normal coordinate, Ω is the angular frequency of a monochromatic sound wave or spin wave, and $f(t)$ represents a random force, which is a stochastic rather than mechanical quantity, as usual. Here $f(t)$ is a random part of $F(t)$, thus depending on the thermodynamic state of the system. F_1 is a functional of $A(s)$ depending also on the past history of $A(t)$, and F_2 represents the terms which depend explicitly on the other degrees of freedom. Expanding F in terms of $A(s), t\geq s\geq t_0$, the linear term obtained has a generalized form of the systematic part of the equation

$$\frac{d}{dt}A(t)=\int_{t_0}^{t}\theta(t-s)A(s)\,ds+f(t) \tag{I.57}$$

and the sum of the nonlinear terms of F uniquely defines the quantity $f(t)$. The collective description of many-particle systems by much fewer variables than the number of degrees of freedom is possible if and only if the fluctuations due to $f(t)$ are negligible.

Extracting the linear term in (I.55) is equivalent to projecting $A(t)$ into the subspace of Hilbert space spanned by A in (I.6). This may be envisaged geometrically as projecting $A(t)$ onto the A-axis. The projection of a column vector G onto this axis is then $\hat{P}G=\langle\mathbf{G}\mathbf{A}^T\rangle\langle\mathbf{A}\mathbf{A}^T\rangle^{-1}\mathbf{A}$. The operation in (I.55) is then equivalent for a column vector $\mathbf{A}$ of splitting $i\Omega\mathbf{A}$ into its projection and vertical components:

$$\dot{\mathbf{A}}=\langle\dot{\mathbf{A}}\mathbf{A}^T\rangle\langle\mathbf{A}\mathbf{A}^T\rangle^{-1}+(1-\hat{P})\dot{\mathbf{A}}\equiv i\Omega_{\mathbf{A}}+(1-\hat{P})\mathbf{A} \tag{I.58}$$

The matrix $i\Omega_A$ therefore has eigenvalues which determine the temperature-dependent eigenfrequencies of collective oscillations. Very pronounced effects on the power spectrum (e.g., the Rytov splitting of Rayleigh scattering) are describable in terms of these oscillations. The effect of an external magnetic field of time-reversal symmetry has been discussed in detail by Berne and Harp[25] in this series, so we restrict our discussion to the main points of interest.

Consider a Hilbert space of dynamical variables whose invariant parts are set to zero. Denote the inner product of two variables F and G by $\langle FG\rangle$. F and G are, for example, linear combinations of the Hermitian functions of particle coordinates ($\mathbf{r}_j$) and momenta ($\mathbf{p}_j$), and of spins $\mathbf{s}_j$

which are even or odd with respect to time reversal

$$(\mathbf{r}_j\rightarrow\mathbf{r}_j;\mathbf{p}_j\rightarrow-\mathbf{p}_j;\mathbf{s}_j\rightarrow-\mathbf{s}_j)$$

Collective, or hydrodynamic variables such as mass density or momentum density are such quantities (see Section III.D.1). Denoting the system Hamiltonian by H_0 and the external magnetic field by $\mathbf{H}$, we have

$$H_0(\mathbf{H})\rightarrow H_0(-\mathbf{H}) \tag{I.59}$$

$$\langle F(t)G(0)\rangle_{\mathbf{H}}=\varepsilon_F\varepsilon_G\langle F(-t)G(0)\rangle_{-\mathbf{H}} \tag{I.60}$$

Where ε_F and ε_G are 1 or -1, according as whether F or G is even or odd. $-\mathbf{H}$ indicates the reversal of the external magnetic field. Now consider a column vector $\mathbf{A}$ of such variables as F and G. In the absence of the magnetic field, the linear or odd variables are orthogonal:

$$\langle FG\rangle=0 \qquad \text{if } \varepsilon_F\varepsilon_G=-1 \tag{I.61}$$

This is not so in the external perturbation, and the coupling between even and odd variables gives rise to collective oscillations. Denoting the signatures of A_j by ε_j, the determinant of $\langle\mathbf{A}\mathbf{A}^T\rangle$ is invariant under time reversal and the cofactor of the (i,j) element changes its sign by $\varepsilon_i\varepsilon_j$. The (i,j) element of the inverse matrix of $\langle A_iA_j\rangle$ is transformed accordingly. Therefore, the projection operator is invariant under time reversal:

$$[\hat{P}G(t)]_{\mathbf{H}}\rightarrow\varepsilon_G[\hat{P}G(-t)]_{-\mathbf{H}} \tag{I.62}$$

Now arrange the set $\mathbf{A}$ such that the first m variables are even and the rest are odd. Denote the even and odd parts by A_e and A_o. Then

$$\Omega_{\mathbf{A}}(t)_{\mathbf{H}}=\begin{bmatrix}-\Omega_{ee} & \Omega_{eo}\\ \Omega_{oe} & -\Omega_{oo}\end{bmatrix}_{-\mathbf{H}} \tag{I.63}$$

where Ω_{ee} is the submatrix of Ω consisting of the elements of the first m rows and columns and Ω_{eo} that of the first m rows and last $(n-m)$ columns. Ω_{oe} and Ω_{oo} are defined similarly.

Another type of symmetry relation is that between the Fourier transform components. Denote those of the local densities of physical quantities by F_k and G_k. Since there is no inhomogenous field applied, we have, from the translational invariance,

$$\langle F_k(t)G_q(0)\rangle=0 \qquad \text{if} \qquad \mathbf{k}\neq\mathbf{q}$$

This is characteristic of linear phenomena. If one assumes inversion symmetry

$$\langle F(\mathbf{r})G(\mathbf{0})\rangle = \langle F(-\mathbf{r})G(\mathbf{0})\rangle$$
$$\langle F_k(t)G_k(0)\rangle = \langle F_k(t)G_{-k}(0)\rangle \tag{I.64}$$

In the absence of a magnetic field or similar type of external application, these symmetry relations are simplified. $\langle \mathbf{A}(t)\mathbf{A}^T(0)\rangle$ is split into two disjoint submatrices and the projection takes the form

$$\hat{P}G = \langle GA_e\rangle\langle A_eA_e\rangle^{-1}A_{es} + \langle GA_o\rangle\langle A_oA_o\rangle^{-1}A_o \tag{I.65}$$

The diagonal elements of (I.63) then vanish.

1. *Relation between Multi- and Single-Particle Correlation Functions*

Since the collective oscillations in a fluid are significant spectroscopically a theorem is needed to explain the relation between many- and single-particle correlation functions, (i.e., to provide a macro–micro correlation). Assume therefore that the collective elements $A(p,q;t)$ of the column vector $\mathbf{A}$ may be defined as sums over monomolecular elements $\alpha(p,q;t)$:

$$A(p,q;t) = \sum_{i=1}^{N} \alpha_i(p,q;t) \tag{I.66}$$

where N is the number of molecules in the system. For example, the multimolecular or macroscopic dipole moment would be defined by

$$\mathbf{M}(p,q;t) = \sum_{i=1}^{N} \boldsymbol{\mu}_i(p,q;t) \tag{I.67}$$

and the dielectric tensor by

$$\varepsilon(p,q;t) = \sum_{i=1}^{N} \varepsilon_i(p,q;t) \tag{I.68}$$

$\boldsymbol{A}$ evolves in time according to (I.6). The continued fraction may then be employed as an approximate solution. Alternatively, we may use the language of Kivelson and Keyes, where the correlation function of the dielectric tensor is proportional to that of a primary variable which is slowly varying, and its time evolution is calculated by means of a pair of coupled

transport equations in which the primary variable is coupled to a secondary variable. This is a rapidly varying quantity dependent on intermolecular forces. Equation (I.30), for instance, may be derived in this fashion by using three orientational variables interrelated by three coupled transform equations. The macro–micro correlation theorems discussed by Kivelson and co-workers[17,46,47] are useful in that they demonstrate that collective correlation matrices of the form

$$J(t) = \langle \mathbf{A}(t)\mathbf{A}^T(0)\rangle\langle \mathbf{A}(0)\mathbf{A}^T(0)\rangle^{-1} \tag{I.69}$$

must have the same general mathematical structure as the corresponding matrix of autocorrelation functions.

The macro–micro correlation theorems are most useful in those systems where superimposed correlations due to, for example, dipole–dipole interaction are not overwhelmingly important. The theorems assert that the theory of autocorrelations used in the following sections may be utilized when dealing with spectral band shapes dependent on correlations between many particles. Multimolecular correlations may always be built up from autocorrelations—an expression of the domino theory. It is interesting to note in concluding this section that hydrodynamic interactions between well-separated solute particles in a fluid medium may persist via a mechanism of translation/rotation mixing. The rotation of a dipole sets up a velocity perturbation which imposes a torque on another. Wolynes and Deutch[48] have considered a many-particle coupled translation/rotation model in which the coupled Brownian diffusion of solute particles is described using anisotropic potentials in a continuum solvent, the motion of which is described hydrodynamically. There is a long-range dynamical orientation correlation between solute particles which again (see Section I) manifests itself in the appearance of off-diagonal coupled diffusion constants in the N-particle translation/rotation Langevin equation describing the system. If we follow this paper and consider a collection of N Brownian solute molecules labeled with position coordinates $\mathbf{X}_i, i=1,\ldots,N$, and orientation coordinated $\Omega_i, i=1,\ldots,N$, then for infinitesimally small step Brownian motion (delta memories), the configurational probability density function $P([X,\Omega]=[0])$ is locally conserved and therefore satisfies the Fokker–Planck equation

$$\partial P/\partial t = -\sum_i \left[\nabla_{x_i}\cdot\mathbf{J}_{x_i} + \mathbf{L}(i)\cdot\mathbf{J}_{\Omega_i}\right] \tag{I.70}$$

where $\mathbf{J}_{x_i}$ and $\mathbf{J}_{\Omega_i}$ are the probability current densities along the positional and orientational coordinates of the ith particle. $\mathbf{L}(i)$ is the operator $\mathbf{u}\mathbf{x}\nabla_{\mathbf{u}_i}$,

where $\mathbf{u}_i$ is a unit vector fixed in the molecule. For Brownian particles the probability current densities are linearly related to the deviation of the configurational probability density from its equilibrium value

$$J_{xi} = -\sum_j \left[D_{ij}^{xx}(Q)\cdot\left(\nabla_{\mathbf{x}_j} P + \beta \nabla_{\mathbf{x}_j} U\right) + D_{ij}^{x\Omega}(Q)\cdot\left(\mathbf{L}_j P + \beta P \mathbf{L}_j U\right)\right] \tag{I.71}$$

$$J_{\Omega i} = -\sum_j \left[D_{ij}^{\Omega x}(Q)\cdot\left(\nabla_{\mathbf{x}j} P + \beta \nabla_{\mathbf{x}j} U\right) + D_{ij}^{\Omega\Omega}(Q)\cdot\left(\mathbf{L}_j P + \beta P \mathbf{L}_j U\right)\right] \tag{I.72}$$

where $U(Q)$ is the potential of mean force of the system. The equilibrium probability distribution $P_{eq}(Q)$ is related to $U(Q)$ according to

$$P_{eq}(Q) = \text{const}\exp\left[-\beta U(Q)\right] \tag{I.73}$$

The potential of mean force will be affected by any collective fluctuation. The diffusion tensors $D(3\times 3)$ are functions of the Brownian particles' configuration. If it is assumed that the the time scales of momentum and configuration change may be separated in a dense fluid, then the D tensors are integrals over the time autocorrelation matrices defined by the tensor product:

$$D_{ij}^{xx}(Q) = \int_0^\infty \langle \mathbf{v}_i(0)\mathbf{v}_j(t)\rangle_Q \, dt \tag{I.74a}$$

$$D_{ij}^{x\Omega}(Q) = \int_0^\infty \langle \mathbf{v}_i(0)\boldsymbol{\omega}_j(t)_Q \, dt \tag{I.74b}$$

$$D_{ij}^{\Omega x}(Q) = \int_0^\infty \langle \boldsymbol{\omega}_i(0)\mathbf{v}_j(t)\rangle_Q \, dt \tag{I.74c}$$

$$D_{ij}^{\Omega\Omega}(Q) = \int_0^\infty \langle \boldsymbol{\omega}_i(0)\boldsymbol{\omega}_j(t)\rangle_Q \, dt \tag{I.74d}$$

A more acceptable theory for high-frequency spectroscopy would involve memory terms and a Fokker–Planck equation of the form of (I.7). However, using delta memories the Langevin equations for rotation–translation again take the form

$$M_i \dot{\mathbf{v}}_i = -\sum_j \left[\xi_{ij}^{xx}\cdot\mathbf{v}_j + \xi_{ij}^{x\Omega}\cdot\boldsymbol{\omega}_j\right] + \mathbf{F}_i(t) \tag{I.75}$$

$$I_i \dot{\boldsymbol{\omega}}_i = -\sum_j \left[\xi_{ij}^{\Omega x}\cdot\mathbf{v}_j + \xi_{ij}^{\Omega\Omega}\cdot\boldsymbol{\omega}_j\right] + \mathbf{T}_i(t) \tag{I.76}$$

The friction tensors ξ originate hydrodynamically as follows. The translation or rotation of a Brownian particle causes a flow in the surrounding solvent. The moving solvent then exerts a flow of force and torque on the other particles. The outcome of this is that the $\underline{D}$ tensors are directly related to Oseen's tensors, which are the Green's functions for the steady state, linearized, incompressible-fluid, Navier–Stokes equations. Thus

$$D_{ij}^{xx} = kT\left[(\xi_0^{xx})^{-1}\delta_{ij} + (1-\delta_{ij})T_{ij}^{xx}\right] \tag{I.77}$$

$$D_{ij}^{\Omega x} = kT(1-\delta_{ij})T_{ij}^{x\Omega} \tag{I.78}$$

$$D_{ij}^{\Omega x} = kT(1-\delta_{ij})T_{ij}^{\Omega x} \tag{I.79}$$

$$D_{ij}^{\Omega\Omega} = kT\left[(\xi_0^{\Omega\Omega})^{-1}\delta_{ij} + (1-\delta_{ij})T_{ij}^{\Omega\Omega}\right] \tag{I.80}$$

Here ζ_{ij} is the Kronecker delta. The "rotation–rotation" Oseen tensor $T^{\Omega\Omega}$ is simple in form and takes a formally identical interparticle distance dependence as that between the interaction of dipoles. The long-range translation–rotation and rotation–translation tensors $D^{x\Omega}$ and $D^{\Omega x}$ take a more involved form.

D. Experimental Methods for Rotational Correlation Functions

In this section we shall describe the technique of Fourier transform spectroscopy which we use to obtain power absorption coefficients and refractive indices in the THz region of the electromagnetic spectrum (2 to $300\,\text{cm}^{-1}$). The subject of submillimeter spectroscopy is developing explosively and "definitive" articles and books[1,2] are rapidly outdated. Here we shall summarize our own methods and attempt to put them in perspective. The tables published by Berne and Harp and by Williams[51] are especially useful in describing the various correlation functions amenable to experimental measurement. The advantage of zero- TH_z spectroscopy (far infrared and dielectric spectroscopy considered in unison) is that the evolution of the measurable autocorrelation function (that of the rotational velocity[52]) mirrors in great detail the initial decay of the orientational autocorrelation functions that are also observed in depolarized Rayleigh scattering. Experimentally, dielectric spectroscopy in isolation produces an exponential correlation function that is easily reproducible theoretically by a great number of models which are seemingly quite different in dynamical origin. The absurd situation then arises that the classical Debye model of rotational diffusion (infinitesimally small changes of angular momentum taking place infinitely fast in an inertialess sphere) produces the same type of loss curve as a model of 180° hopping from potential wells. Both models

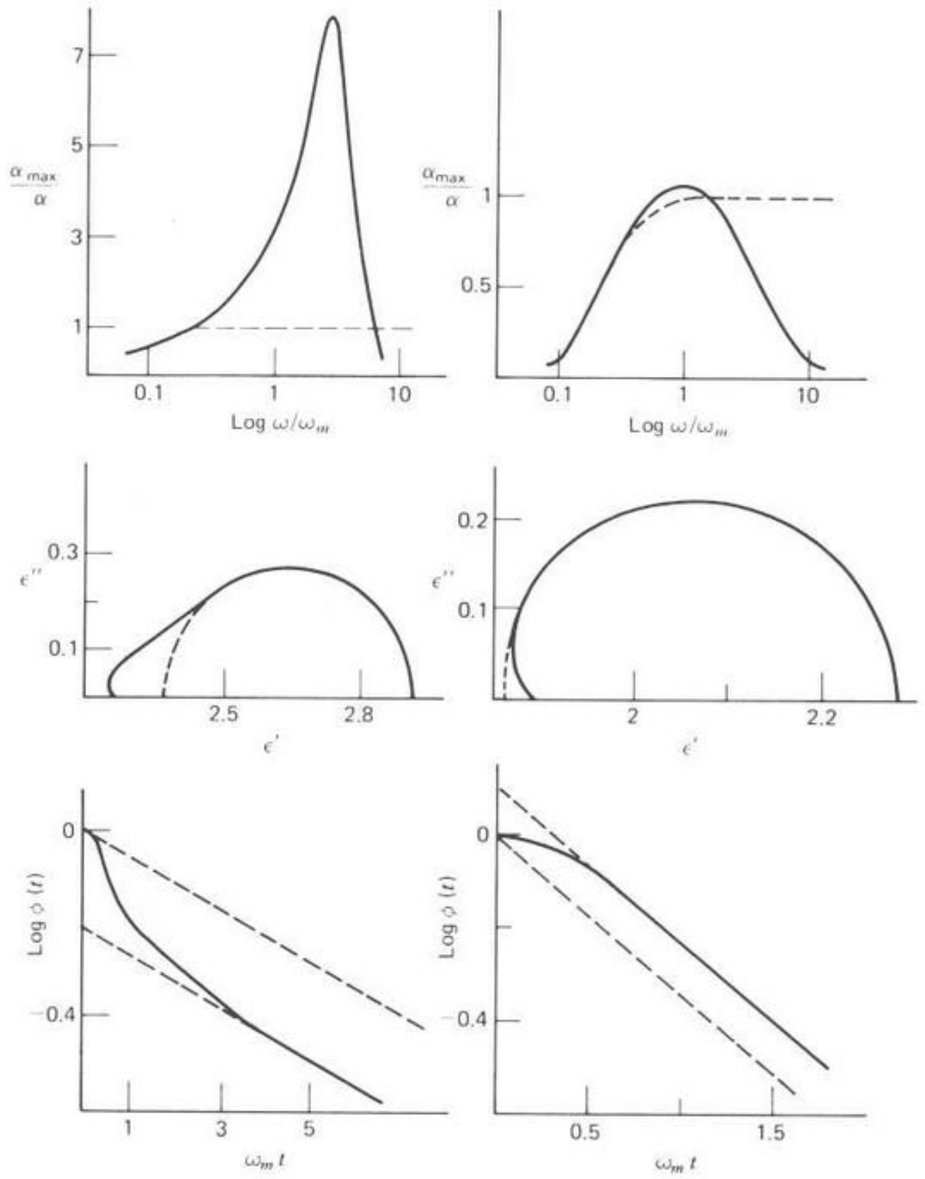

Fig. 11. Comparison with experiment of the Debye equations at high frequency in two extreme cases where the Poley absorption is pronounced (left column, a solution of CH_3CN in CCl_4 5% mole fraction), and small (right column, 20% mole fraction $(CH_3)_3CCl$ in hexane at 298°K). The dotted curve is the theoretical absorption according to the Debye model of rotational diffusion. (Reproduced by permission from P. Desplanques, Thèse d'Etat, Lille, 1973, p. 45.)

are clearly unacceptable when considered in relation to infrared power absorption coefficients in liquids (Fig. 11, from a thesis by Desplanques), since both produce an unrealistic plateau absorption.

The unique advantage of making both loss measurements [those on $\varepsilon''(\omega)$] and power absorption measurements on the same sample arises from the fundamental relations

$$\alpha(\omega) = \frac{2\sqrt{2}\ \pi\varepsilon''(\bar{\nu})\bar{\nu}}{\left(\left(\varepsilon'(\bar{\nu})^2+\varepsilon''(\bar{\nu})^2\right)^{1/2}+\varepsilon'(\bar{\nu})\right)^{1/2}}$$
$$= 2\pi\bar{\nu}\varepsilon''(\bar{\nu})/n(\bar{\nu}) \tag{I.81}$$

Here $\bar{\nu}$ is the wave number (in cm^{-1}), related to the angular frequency (ω) by $\omega = 2\pi\bar{\nu}c$. $\varepsilon'(\bar{\nu})$ is the frequency-dependent dielectric permittivity, and $n(\bar{\nu})$ the refractive index. Measurements on $\varepsilon''(\bar{\nu})$ and $\varepsilon'(\bar{\nu})$ yield accurately the long-time behavior of the multiparticle orientational correlation functions of the dipole vector $\boldsymbol{\mu}$, and measurements on $\alpha(\bar{\nu})$ and $n(\bar{\nu})$ do the same for its second derivative at short times. In contrast, measurements of depolarized Rayleigh scattering yield the equivalent of $\varepsilon''(\bar{\nu})/\bar{\nu}$, so that the high-frequency wing information is often lost as instrumental noise. Notice that $\alpha(\bar{\nu})$ is approximately $\bar{\nu}\varepsilon''(\bar{\nu})$, so that high-frequency information is "enlarged" by the frequency multiplication. To illustrate this, in Fig. 12 we present the zero-THz absorption profile for CH_2Cl_2 at 298 K in terms of $\varepsilon''(\bar{\nu})$ and $\alpha(\bar{\nu})$, along with some dynamical models of the autocorrelation functions. All of these succeed in matching $\varepsilon''(\bar{\nu})$, but none very well $\alpha(\bar{\nu})$. Alternatively, in the time domain, the Fourier transform of the Lorentzian $\varepsilon''(\omega)/\omega$ gives the multiparticle orientational correlation function (if we set aside the internal field modification), which for the $\varepsilon''(\omega)$ curve of Fig. 13 would be nearly a featureless exponential decay. In contrast, the direct Fourier transform of $\alpha(\omega)$ yields $-\ddot{C}_m(t)$, which is oscillatory, as illustrated in Figs. 14 to 19. Brot has indicated[52] that a further advantage of making $\alpha(\omega)$ measurements is that the many-particle different versions of internal field correction turn out to be almost identical numerically and have little affect on the shape of $-\ddot{C}_m(t)$ when normalized at the origin. Despite the kinematic complications pointed out by van Kanynenburg and Steele,[55] $-\ddot{C}_m(t)$ is numerically often identical[30] to the angular velocity correlation function. In the absence of memory effects this is a single exponential, so that Figs. 14 to 19 are clearly indicitive of the need for more realistic approximants of (I.6) when **A** refers to angular velocity.

By consideration of $\mathbf{A} = \begin{bmatrix} \mathbf{v} \\ \boldsymbol{\omega} \end{bmatrix}$ in the context of (I.6) we have shown that rototranslation influences $\alpha(\omega)$ through the relations between $\langle \mathbf{v}(t)\cdot\mathbf{v}(0)\rangle$,

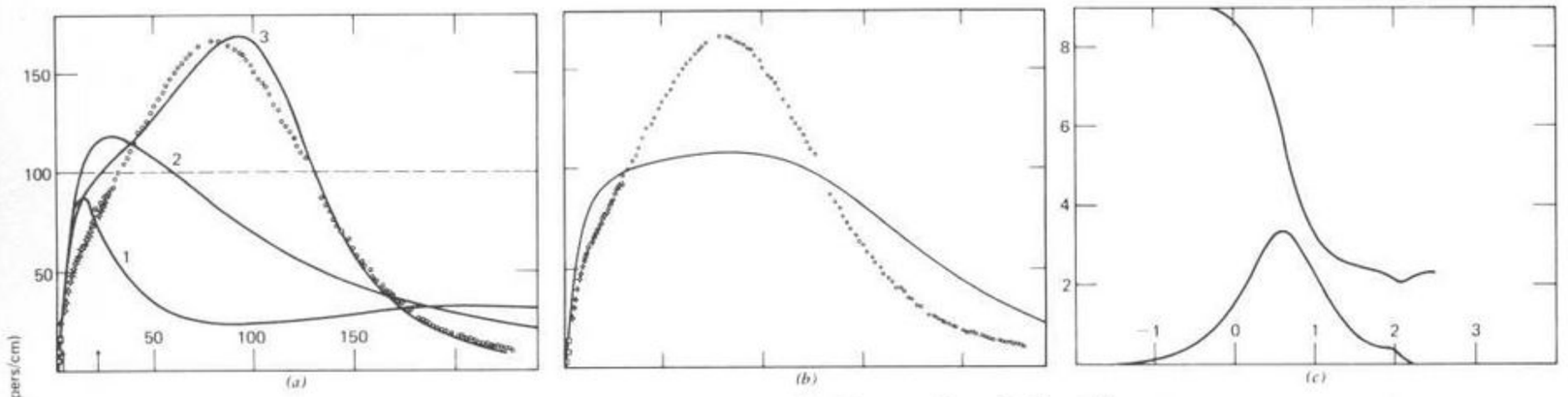

Fig. 12*a*. Absorption of CH_2Cl_2 (liquid) in the far infrared compared with some dynamical models. (*a*) (1) Asymmetric top, Langevin equation; (2) Chandler binary collision approximation; (3) Mori theory, iterating on γ and $K_1(o)$ for least-mean-squares best fit. (*b*) Mori theory, γ, $K_0(0)$ and $K_1(o)$ fixed. (*c*) Microwave loss and dispersion, *all* models give a good fit.

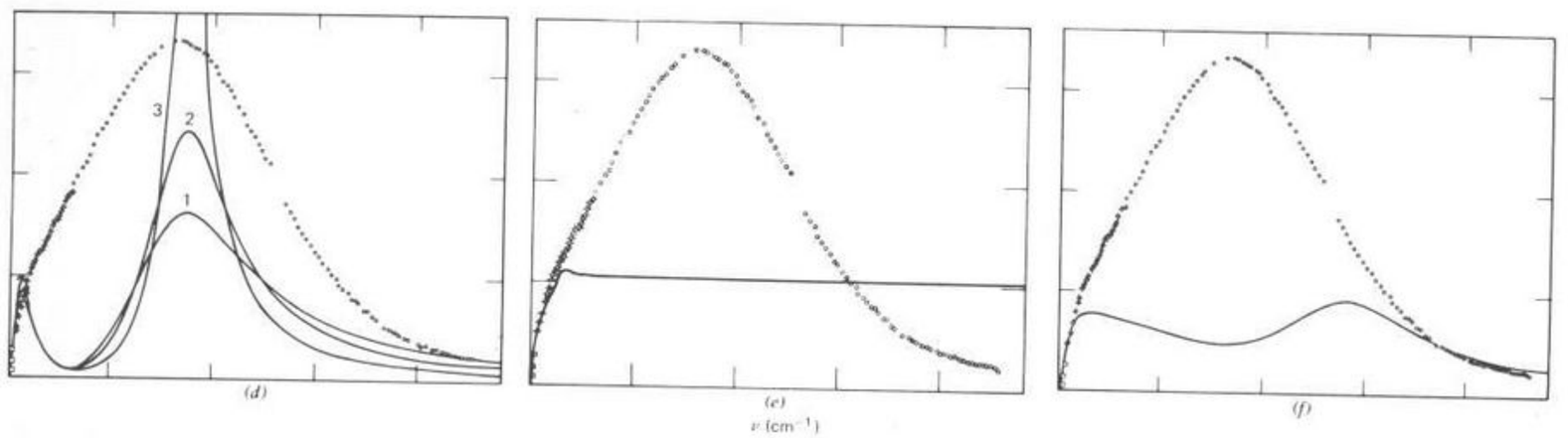

(*d*) (1), (2), (3), itinerant librator, decreasing β_2. (*e*) and (*f*) illustrate the disasters which sometimes result by allowing too much freedom of choice of parameters in a model when least-mean-squares fitting. In this case the itinerant librator (see original text for more details). Even in (*e*) and (*f*) the microwave data are fitted very well. Ordinates: $\alpha(\bar{\nu})$ (nepers/cm); abscissas: $\bar{\nu}$ (cm^{-1}). [Reproduced by permission from *J. Chem. Soc. Faraday Trans. 2*, 1978, **74**, 2143.]

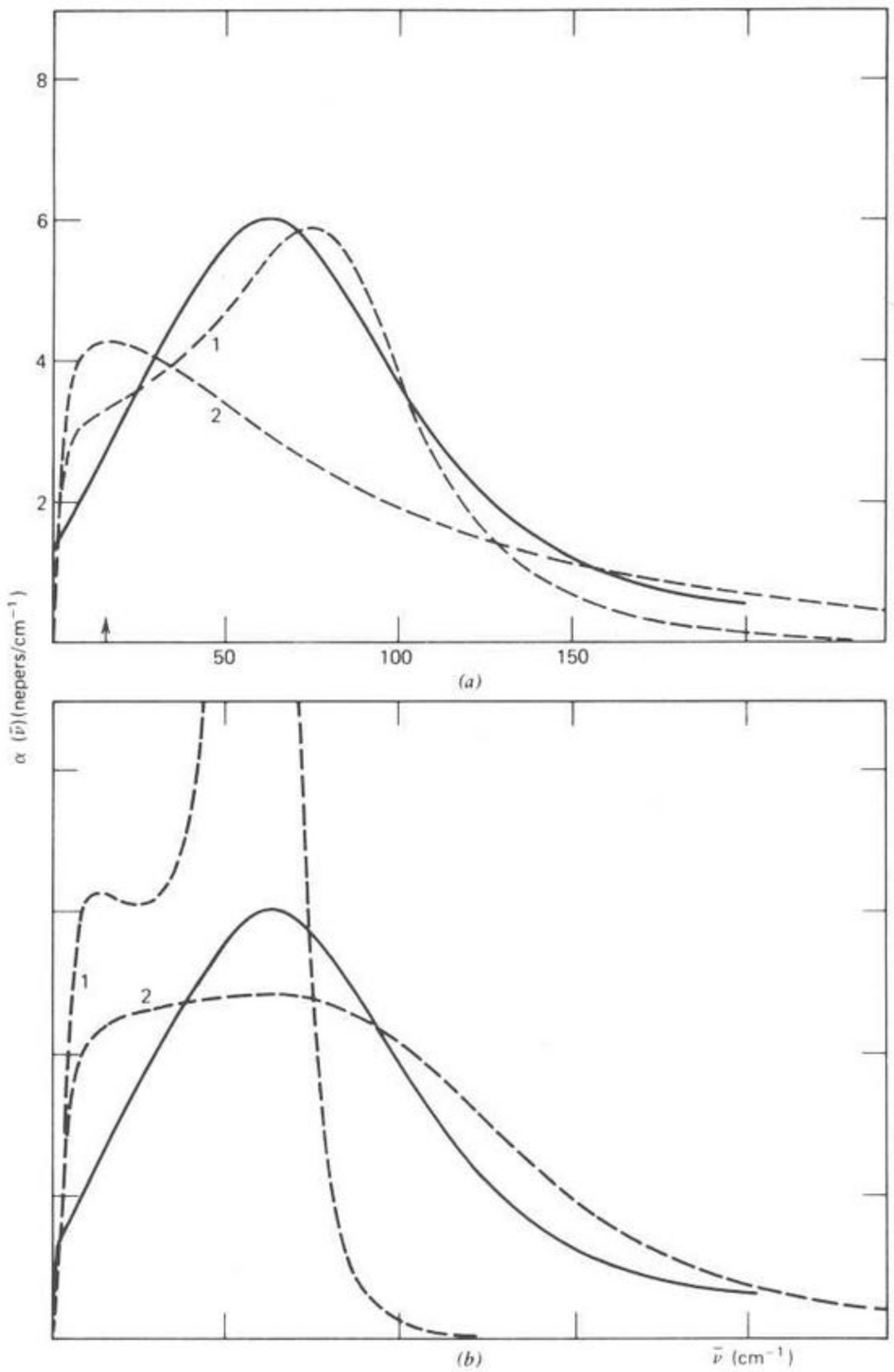

Fig. 12*b*. Absorption of CH_3CN/CCl_4 (1% solution) in the far infrared. (*a*) (—), Experimental; (1) *J* diffusion; (2) Mori theory iterating on γ and $K_1(o)$ for least-mean-squares best fit. (*b*) (—), Experimental; (1) the continued fraction representation iterating with $K_1(t) = K_1(o)\exp(-\pi/2\sqrt{K_1(o)})$; (2) iterating with $K_2(t) = K_2(o)\exp[-(\pi/2)\sqrt{K_2(o)}]$. (*c*) (—), Experimental; (1), (2), itinerant librator, increasing β_2. (*d*) (—), Experimental; (----), itinerant librator iterating on both β_1 and β_2. Ordinates: $\alpha(\bar{\nu})$ (nepers/cm); abscissas: $\bar{\nu}$ (cm^{-1}).

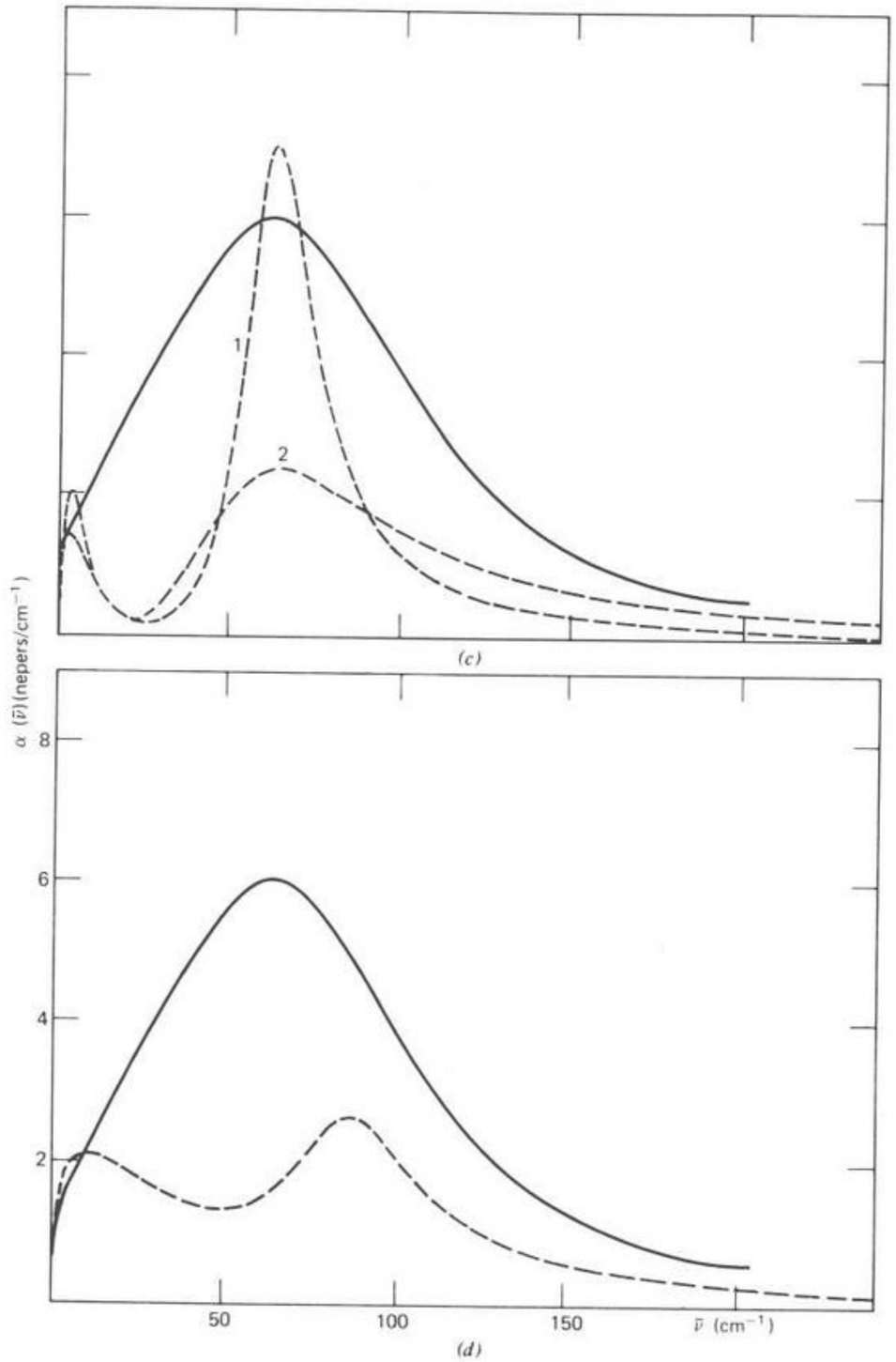

Fig. 12*b*. Continued

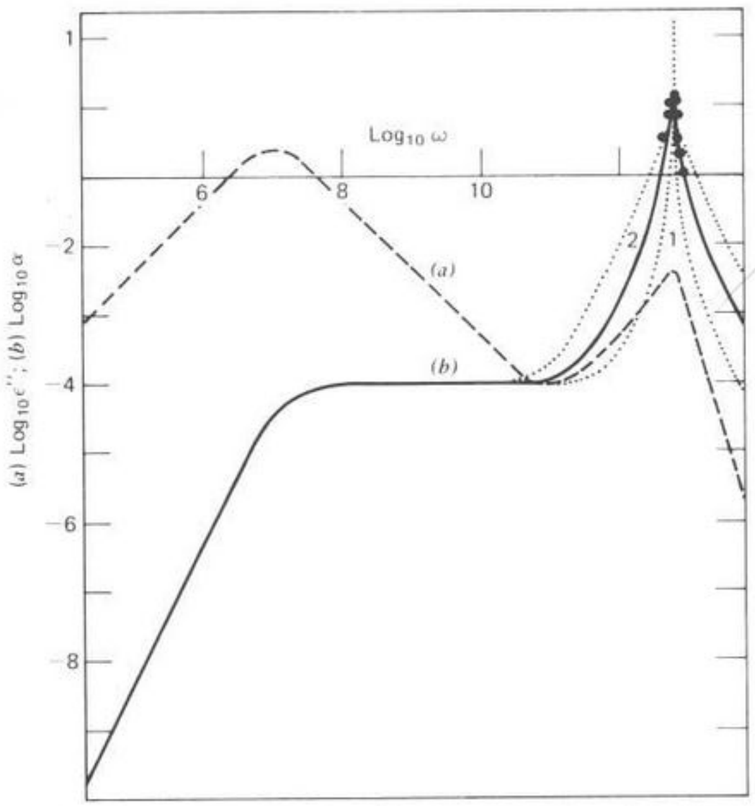

Fig. 13. Log-log plot (schematic) of (1) $\alpha(\omega)$, (2) $\epsilon''(\omega)$, and (3) $\epsilon''(\omega)/\omega$ (proportional to the Rayleigh wing). (●), Denote data in the far infrared for CH_2Cl_2/decalin glass.

$\langle \omega(t) \cdot \omega(0) \rangle$, $\langle \mathbf{v}(t) \cdot \omega(0) \rangle$, and $\langle \omega(t) \cdot \mathbf{v}(0) \rangle$. The macro-micro correlation theorem then ensures that the same effects will be present for the multiparticle correlation functions. However, the advantages of measuring $\epsilon''(\omega)$ and $\alpha(\omega)$ in liquids as opposed to incoherent neutron scattering is that with the former we measure only resultant orientations of dipole vectors, due to rototranslation, whereas with the latter the time-of-flight spectrum reflects all aspects of the molecular rototranslations, due to the large momentum transfer, and is far too richly informative to be interpretable.

We shall, for historical reasons, refer to the broad far-infrared band rising above the Debye plateau in Fig. 11 as the Poley absorption.[56] In dipolar liquids this is essentially the zero-THz profile expressed in terms of $\alpha(\omega)$ (in nepers/cm). Although the total rotational absorption cross-section per molecule (A_0/N) should remain constant through various changes of material state, it is extraneously and intrinsically affected by the mechanisms outlined below.

1. The observed A_0/N sometimes differs by an internal field factor from that which is estimated theoretically. The correction is frequency-dependent, but the function $\alpha(\omega)$ is not distorted to any troublesome degree.

2. The available sum rules for A_0/N derived by Gordon[34] and by Brot[52] take no account of electrodynamic contributions. These may be thought of in terms of multipole–multipole effects, particularly the dipole–dipole effects described by Kirkwood. Neither is any account taken of long-range hydrodynamical effects as described already. The sum rule refers strictly to autocorrelations of single molecules. Large differences are known between the experimental and theoretical estimates of the absorption cross-section for many dipolar liquids. They cannot be attributed solely to collision induced absorptions of temporary dipole moments (Section D) which originate in the effect on any given dipole of the combined electrodynamic fields of all its neighbors at an instant t. These fluctuate in direction and magnitude with time but have a finite average value measurable by a broad submillimeter absorption[5] consisting of molecules with no permanent dipole moment, such as CCl_4. This induced absorption contains information on the intermolecular potential energy and may be used to study molecular motions and interactions in nondipolar gases, liquids, and plastic crystals.

Therefore, we adopt the criterion that to measure the extent of cross-correlations and induced absorption, it is necessary to use in dilute solution a strongly dipolar species such as CH_2Cl_2. Figure 20 then shows that a shift in the wavenumber of maximum absorption ($\bar{\nu}_{max}$) to low frequencies with dilution is a marked characteristic of the spectrum. Even at infinite dilution a large difference remains, however, between $\bar{\nu}_{max}$ and the root-mean-square angular velocity (ω_J) of the infinitely dilute gas. This is the most useful feature of the spectrum and the one which theoretical models find difficult to reproduce. It strongly discriminates against the use of gas-phase models (M and J diffusion) in the liquid. These, in their simplest form, produce profiles centered always at ω_J.

The constancy of (A_0/N) with dilution of CH_2Cl_2 in CCl_4 is evidence for the fact that the Poley absorption in this case is hardly affected by collision-induced absorption (proportional to a power of N). The extent of the induced absorption may be measured roughly from the fact that in CCl_4, $\alpha(\bar{\nu})$ peaks at 1.5 nepers/cm, whereas in CH_2Cl_2 it reaches 160 nepers/cm. In dilute solution, induced absorption will still be present because of the interaction between CH_2Cl_2 and CCl_4 molecules. The types of information available from the zero-THz profile are summarized in Table III.

1. *Some Instrumental Details*[57]

The Michelson Interferometer. A Fourier transform spectrometer (N.P.L./Grubb-Parsons "cube") (Fig. 21) is used for submillimeter spectroscopy because in such an instrument a simultaneous observation of all the elements of the spectrum (multiplex record) is kept, which has the

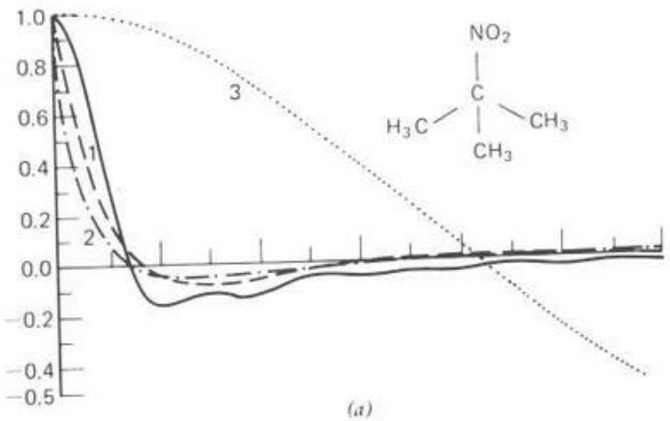

(a)

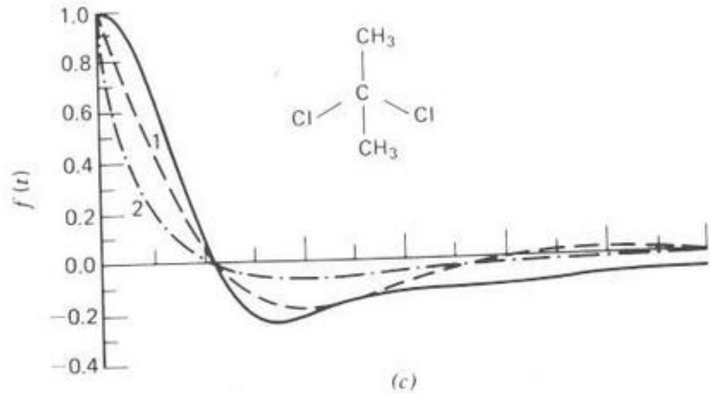

(c)

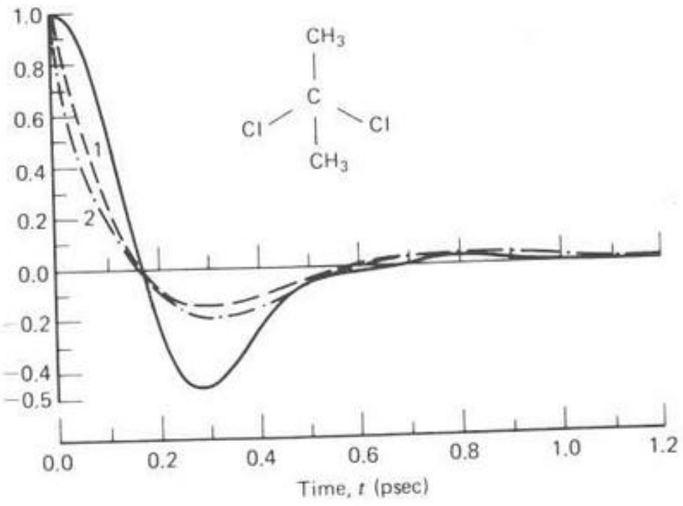

(e)

Fig. 14. (—), Experimental value of $-\ddot{C}_M(t)$ from a direct Fourier transform of the far infrared $\alpha(\omega)$, normalized to unity at the origin. (---), (1) and (2) are models (see text) typifying the need for a realistic description at short times (least-mean-squares fitting). (· · · · ·), (3) Free-rotor function equivalent to $-\ddot{C}_M(t)$. (*a*) Rotator phase, 294°K; (*b*) rotator phase, 273°K, and (·---·---·), 219°K; (*c*) liquid at 295°K; (*d*) liquid at 241°K; (*e*) rotator phase at 235°K; (*f*) rotator phase at 192°K. Abscissa: time, *t* (psec). [Reproduced by permission from *J. Chem. Soc. Faraday Trans. 2*, **71**, 2051 (1975).]

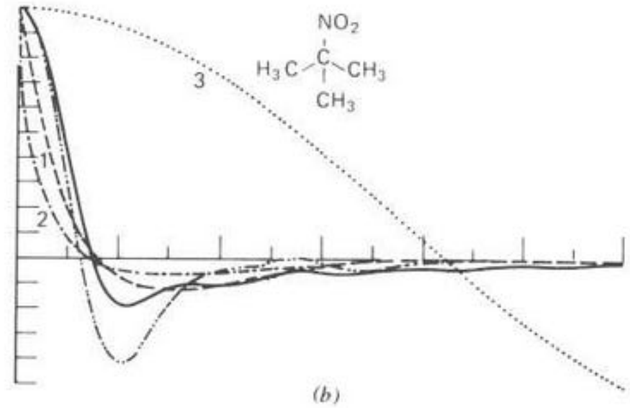

(b)

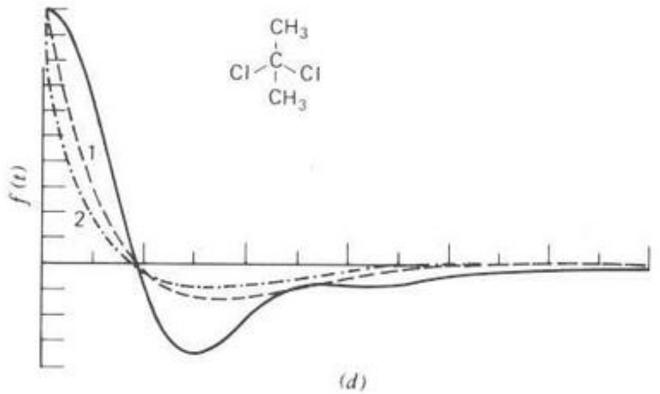

(d)

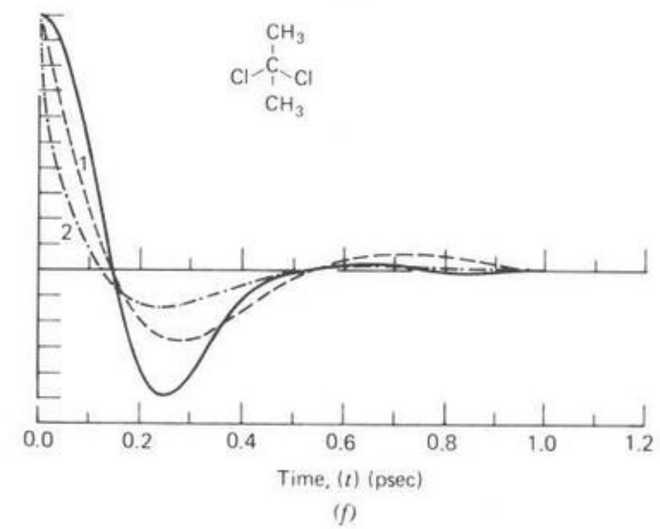

(f)

Fig. 14. Continued

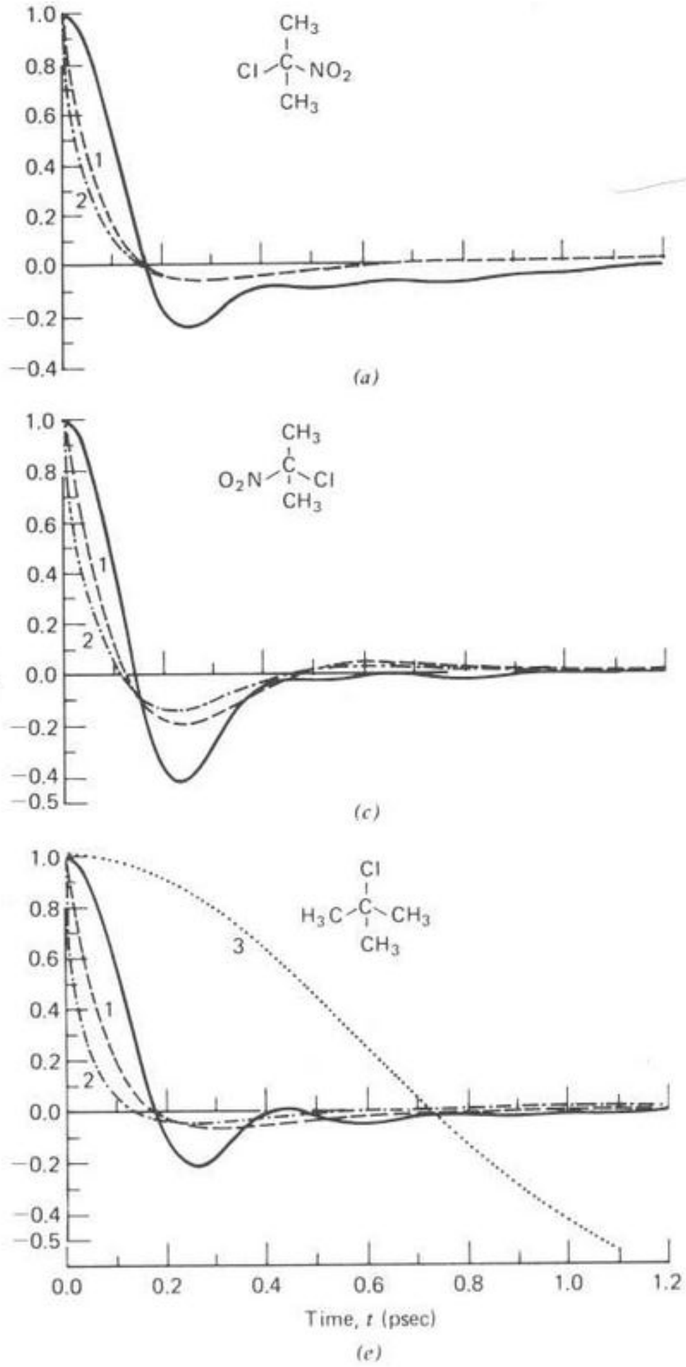

Fig. 15. Key as in Fig. 14. (*a*) Liquid at 293°K; (*b*) liquid at 253°K; (*c*) rotator phase at 233°K; (*d*) rotator phase at 209°K; (*e*) rotator phase at 238°K; (*f*) liquid at 274°K.

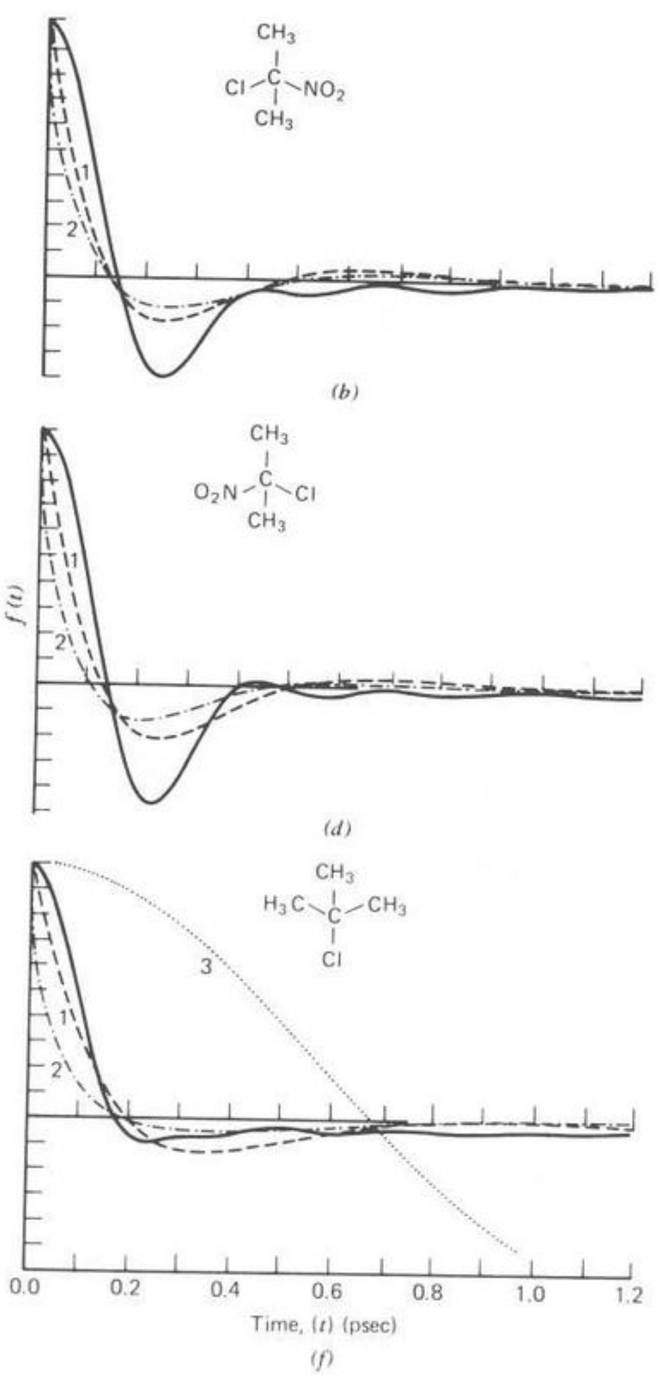

Fig. 15. Continued

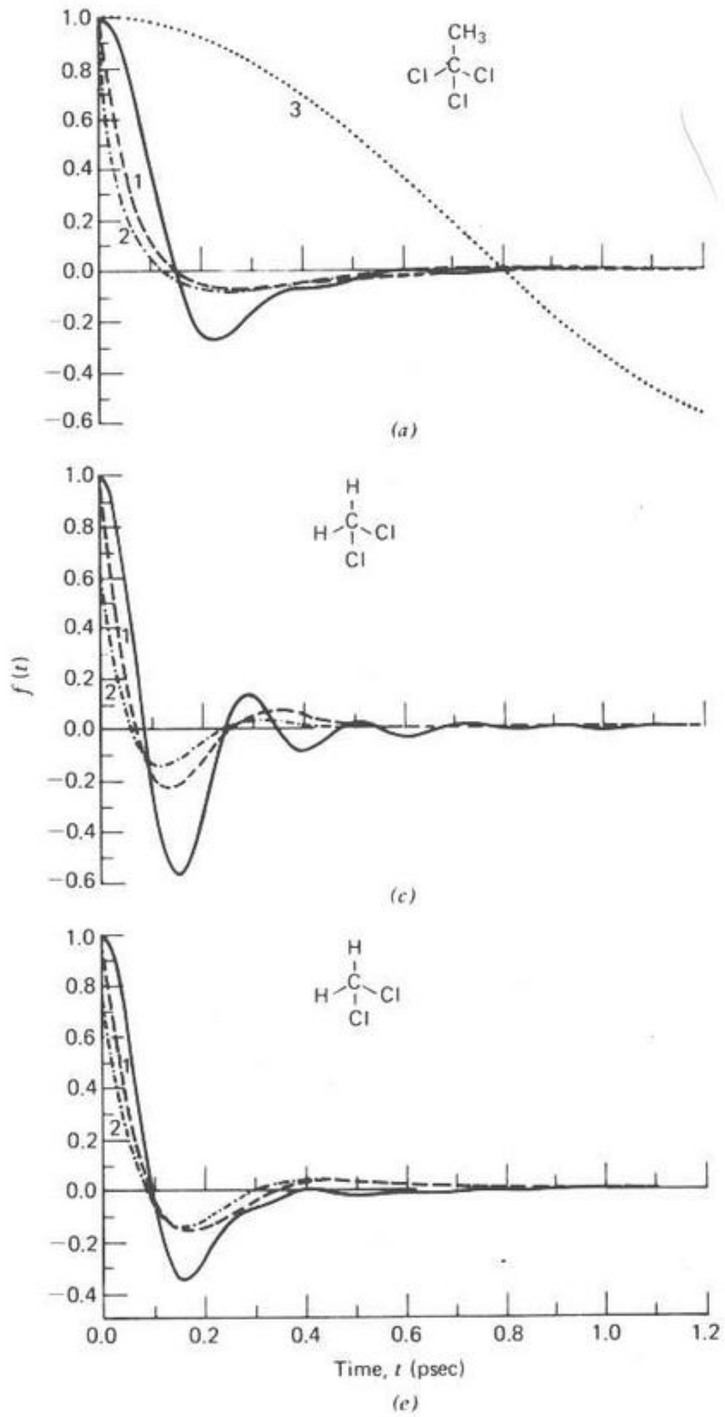

Fig. 16. Key as in Fig. 14. (*a*) Rotator phase at 233°K; (*b*) liquid at 293°K; (*c*) liquid at 188°K; (*d*) liquid at 249°K; (*e*) liquid at 298°K; (*f*) liquid at 293°K.

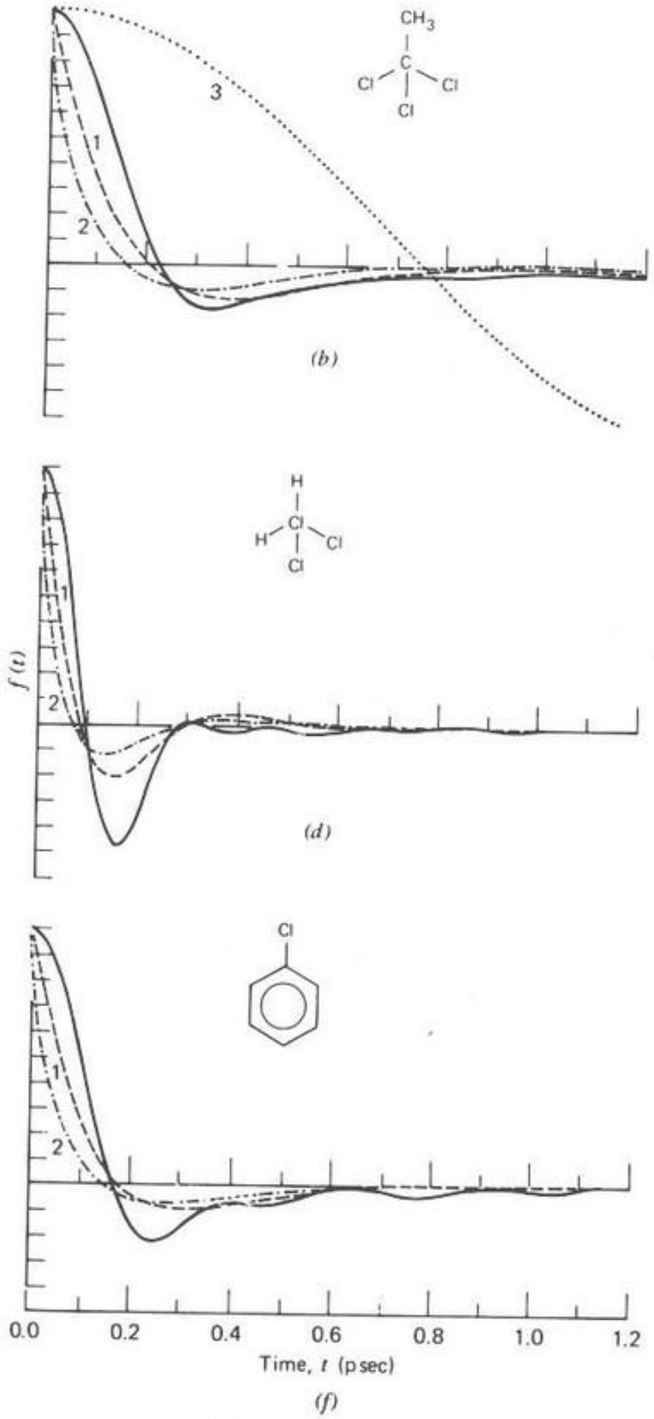

Fig. 16. Continued

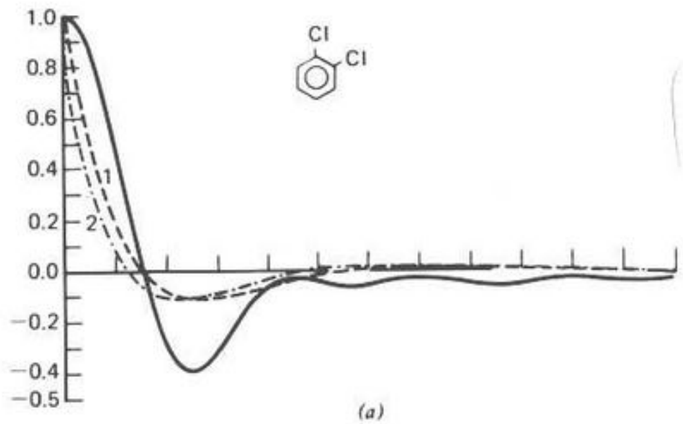

(a)

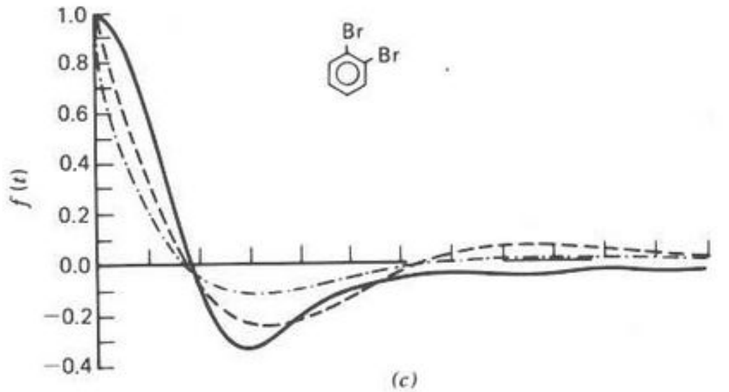

(c)

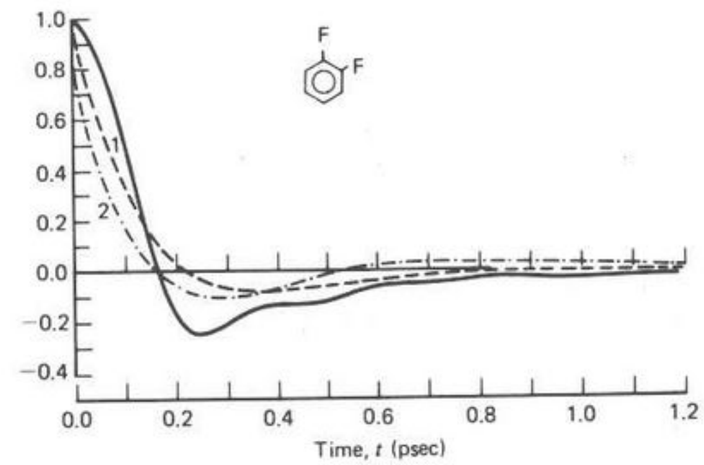

(e)

Fig. 17. Key as in Fig. 14. Liquids at 293°K.

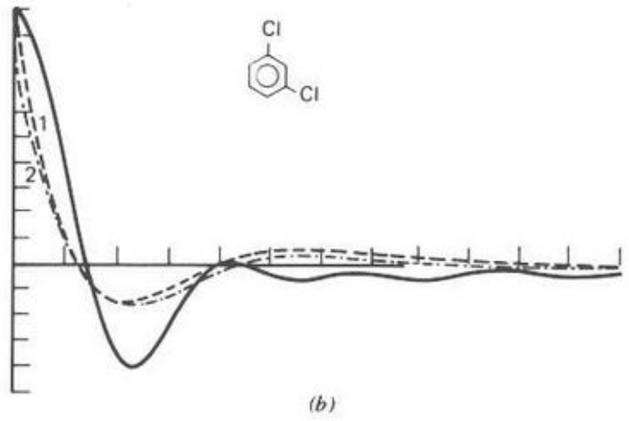

(b)

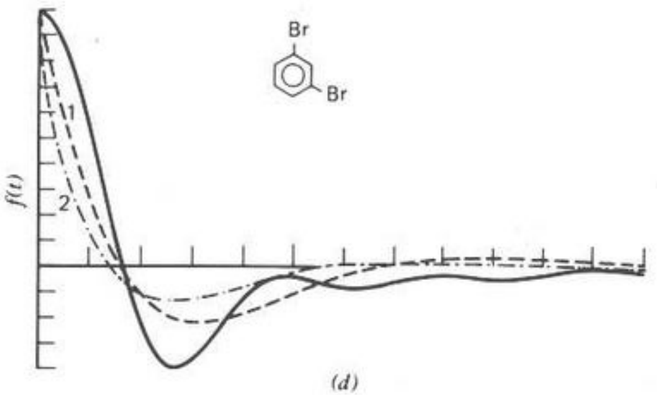

(d)

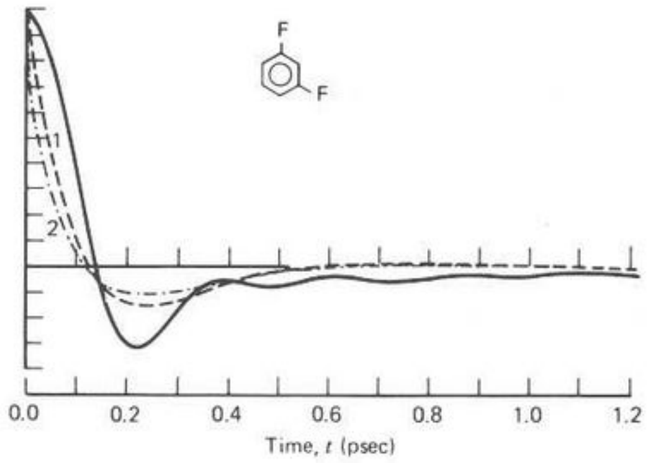

(f)

Fig. 17. Continued

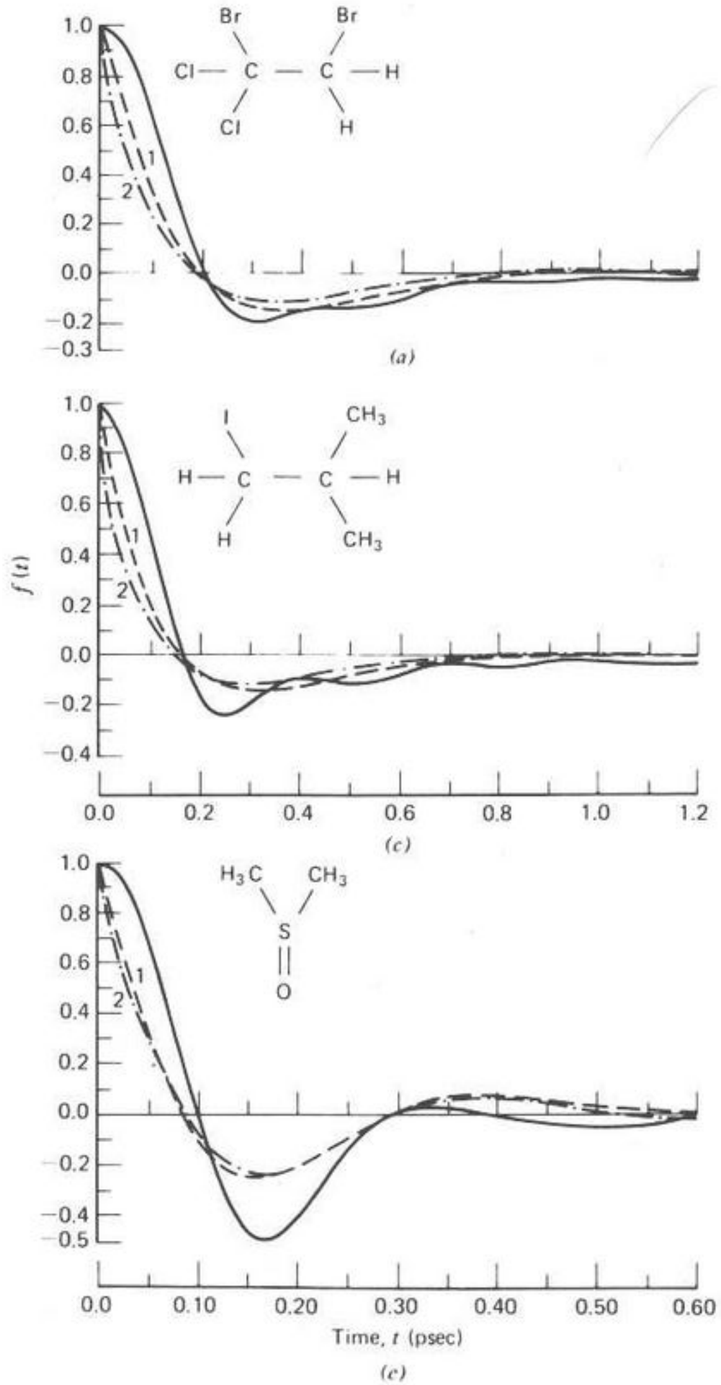

Fig. 18. Key as in Fig. 14. (*a*) to (*d*) Liquids at 295°K; (*e*) and (*f*) liquids at 293°K.

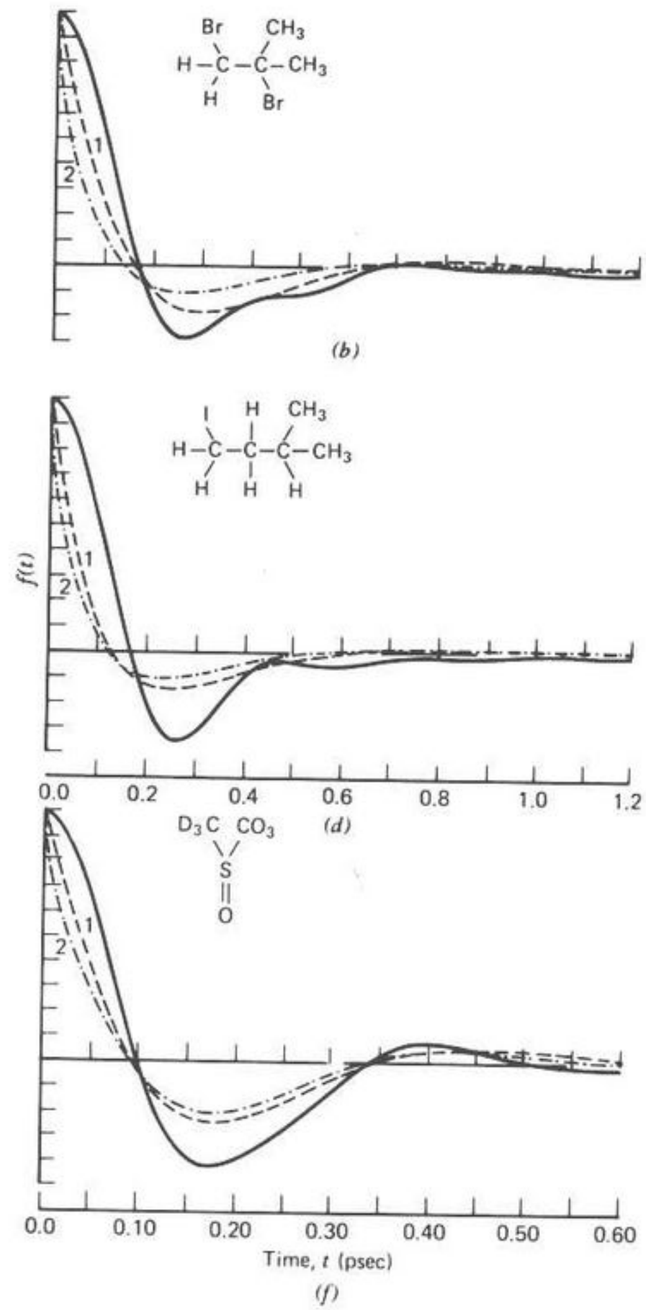

Fig. 18. Continued

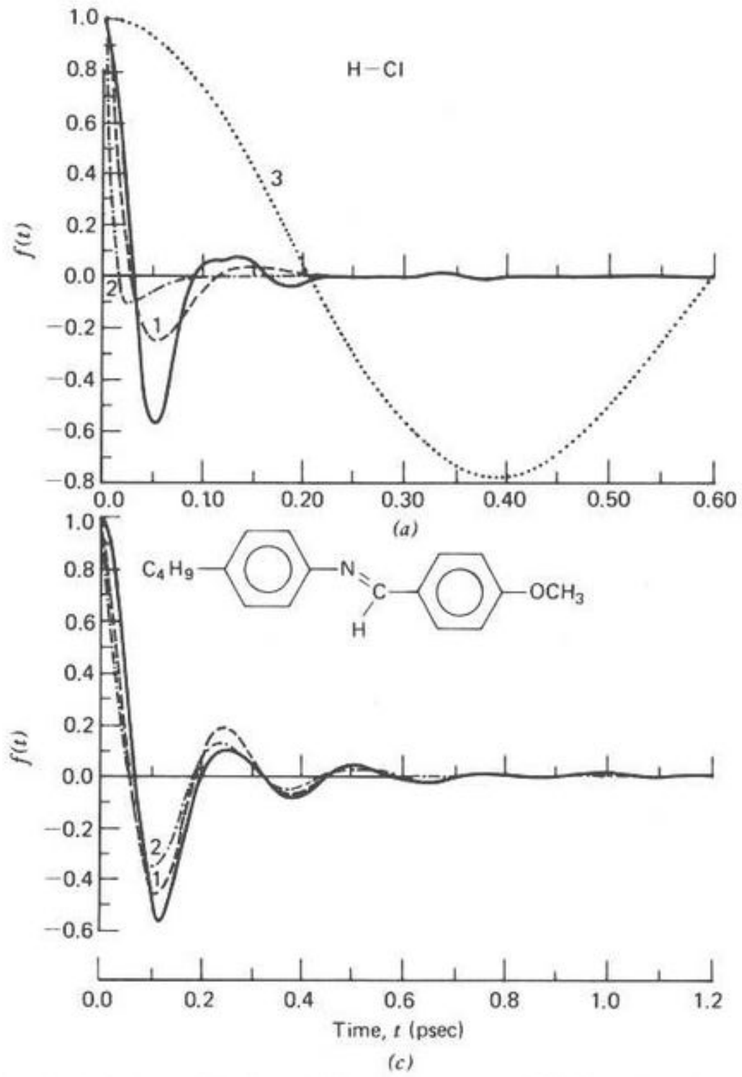

Fig. 19. (*a*) to (*c*) Key as in Fig. 14. (*a*) Rotator phase (100°K); (*b*) liquid at 293°K; (*c*) nematic phase at 296°K; (*d*) curve 1—frequency domain curve of $\alpha(\bar{\nu})$ predicted by an early form of itinerant oscillation at 238°K for the rotator phase of *t*-butyl chloride. Integration of this curve up to only 400 cm^{-1} produces the spurious oscillations of curve 2, which is the correlation function. It is necessary (because of the asymptotic ω^{-2} behavior at high frequences) to integrate up to 3000 cm^{-1} before these disappear. Abscissas: upper, time, *t* (psec); lower, $\bar{\nu}$ (cm^{-1}).

advantage of a better signal-to-noise ratio than a conventional grating instrument, whereby the spectrum is scanned element by element. A highly efficient optical system is needed because of the low emission in the far infrared of conventional sources such as the mercury discharge lamp. Although some 1500 laser lines are known in the far infrared, the need for broad-band spectroscopy ensures the continuing usefulness of the inter-

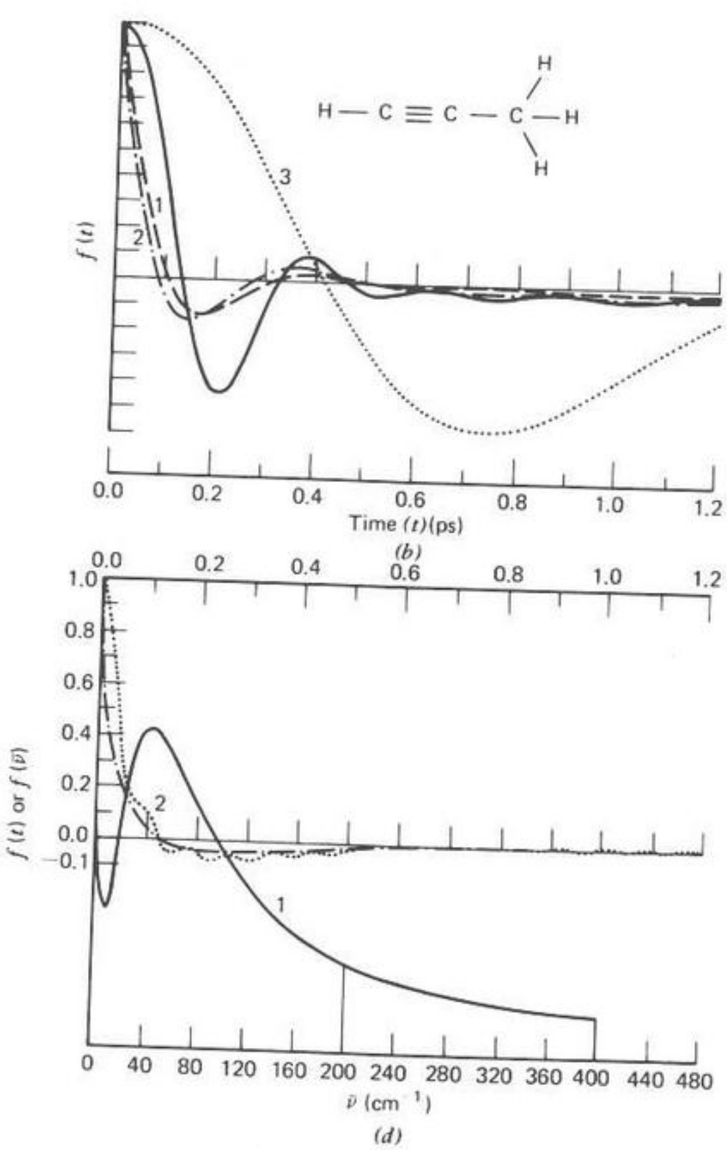

Fig. 19. Continued

ferometric system that indicated for work in compressed gases, liquids, and solids. The spectrometer consists basically of a Michelson two-beam interferometer connected, off-line, to a digital computer which selects the component frequencies from the interference record (interferogram) observed by the detector as the path difference *X* between the two partial beams of the interferometer is varied.

The power variation at the detector is recorded as a function of the path difference *X* in Fig. 22. This is twice the mirror displacement. The beam divider is a thin film of stretched dielectric, usually poly(ethylene

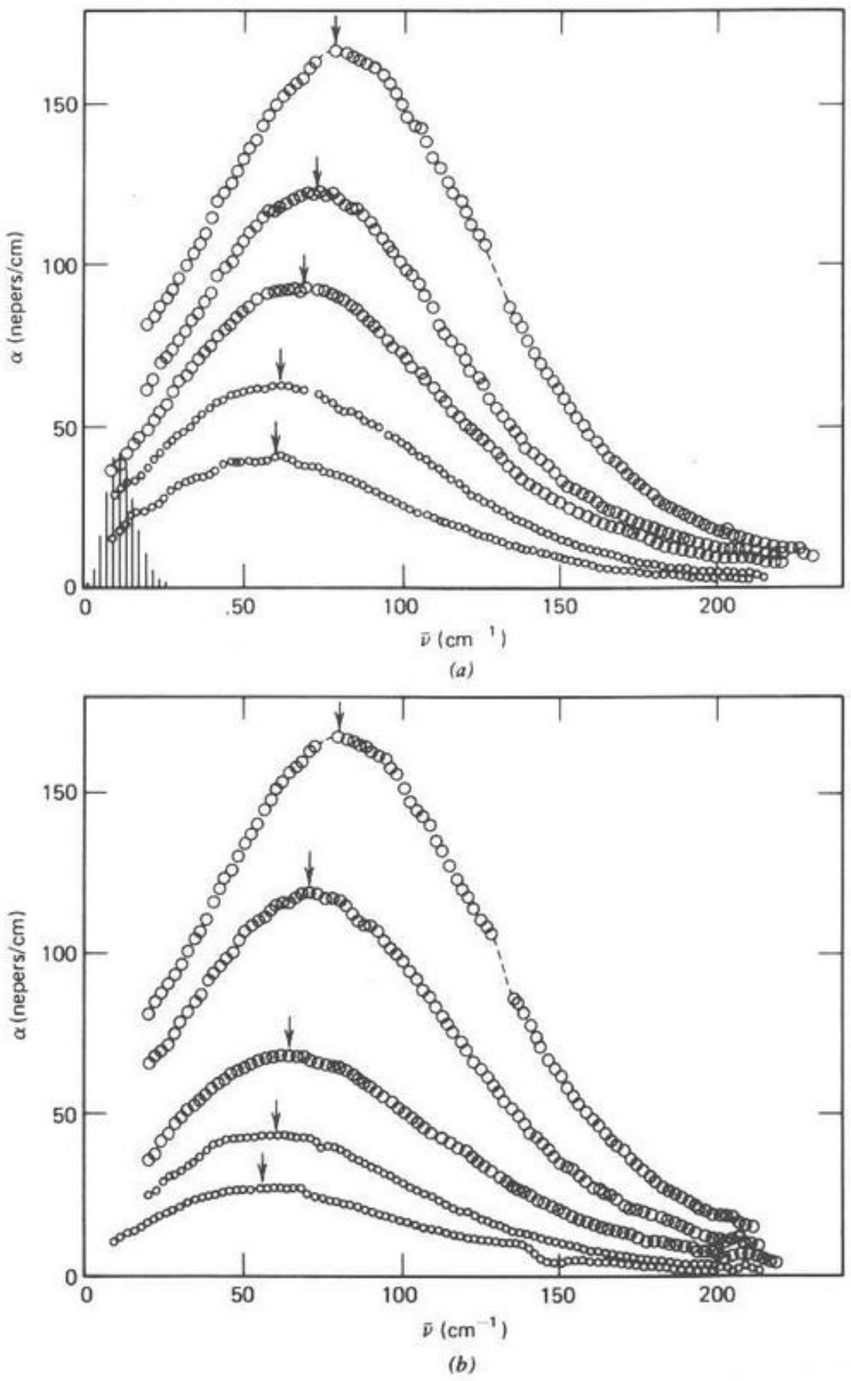

Fig. 20. (*a*) Absorption of dichloromethane in CCl_4 at 298°K, corrected for solvent absorption. From top to bottom: pure CH_2Cl_2 ($N = 9.4 \times 10^{21}$ molecules/cm^3); $N = 7.22 \times 10^{21}$ molecules/cm^3; $N = 4.93 \times 10^{21}$ molecules/cm^3; $N = 3.25 \times 10^{21}$ molecules/cm^3; $N = 1.97 \times 10^{21}$ molecules/cm^3. (*b*) The same in decalin solvent. The stick spectrum represents some $J \rightarrow J+1$ ($\Delta K = 0$) lines for quantized free rotation of CH_2Cl_2, regarded as an approximate symmetric top. [Reproduced by permission from *J. Chem. Soc. Faraday Trans. 2*, **74**, 343 (1978).]

TABLE III

Information Available from Far-Infrared Broad Bands of Rotational and Intermolecular Origin

Measurement	Physical significance
$A_0/N = \frac{1}{N}\int \alpha(\bar{\nu})\, d\bar{\nu}$ band	For a dilute dipolar gas, may be used to estimate the dipole moment μ, given an accurate sum rule. For a compressed nondipolar gas, may be used to estimate its first multipole moment subject to theoretical constraints (e.g., bimolecular collisions) and molecular symmetry. In nondipolar liquids and plastic crystals, A_0/N may be compared with its equivalent in the compressed gas and an estimate made of the cancellation of dipole inductions due to intermolecular potential symmetry. The constancy or otherwise of A_0/N with dilution of a dipolar solute in a nondipolar solvent is a useful method of investigating molecular association and complex formation and of probing liquid crystalline environments.
$\bar{\nu}_{max}$, the maximum power absorption frequency	As a dilute dipolar gas is compressed, $\bar{\nu}_{max}$ shifts gradually to higher frequency as the overall $\alpha(\bar{\nu})$ contour broadens (Fig. 1). At liquid densities $\bar{\nu}_{max}$ is removed a long way from its value in the gas phase (by as much as $100\,cm^{-1}$). It is therefore strongly dependent on intermolecular potential energy. Successive approximants of the Mori continued fraction may be used to model $\bar{\nu}_{max}$ and the contour $\alpha(\bar{\nu})$. Equation (I.30) is such that the mean-square torque is well defined and measurable from $\bar{\nu}_{max}$. Higher approximants would relate $\bar{\nu}_{max}$ to this and its derivatives.
$\alpha(\bar{\nu})$, the zero-THz power absorption coefficients	This is a probability distribution of wavenumber (i.e., a spectral function). Its Fourier transform is thus a correlation function, relating random reorientations of dipoles taken in a temporal sequence. The correlation function obtained by Fourier transformation of $\alpha(\omega)$ is $-\ddot{C}_m(t) \equiv \langle \dot{\mu}(0) \cdot \sum_{i \neq j} \dot{\mu}_j(t) \rangle$ where μ is the permanent molecular dipole moment. In its ability to yield $-\ddot{C}_m(t)$ directly, accurately, and in detail, the zero-THz $\alpha(\bar{\nu})$ profile is uniquely placed as a probe into the short-time details of molecular dynamics. Any model of the fluid state must match up with $C(t)$ satisfactorily as well reproduce $C_m(t) = \langle \mu_i(0) \cdot \sum_{i \neq j} \mu_j(t) \rangle$, measurable from the dielectric loss.

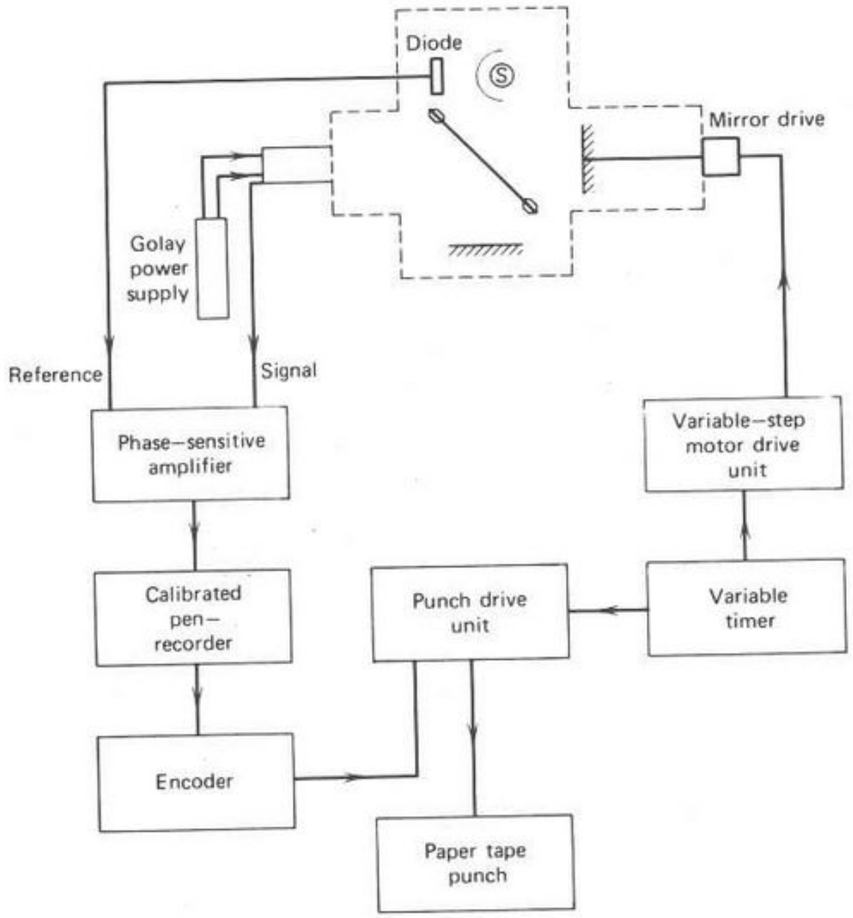

Fig. 21. Schematic of the Grubb–Parsons/N.P.L. interferometer.

terephthalate). Internal reflections in this beam divider determine the transmissivity of the interferometer and cause it to be strongly frequency-dependent, so that different beam dividers are needed for different frequency regions.

Submillimeter detector technology is rapidly advancing, but the Golay pneumatic cell is conveniently operable at ambient temperatures. The faster and more sensitive Rollin detector is helium-cooled and extends the spectral range to overlap with the microwave klystron frequencies. Two types of interferogram are usually used (Fig. 23), resulting from amplitude and phase modulation of the detected signal. Phase modulation discriminates in favor of the interferogram range, resulting in a higher signal-to-noise ratio in the detected signal. The modulation is achieved by aperiodic displacement of one of the mirrors through a distance of the

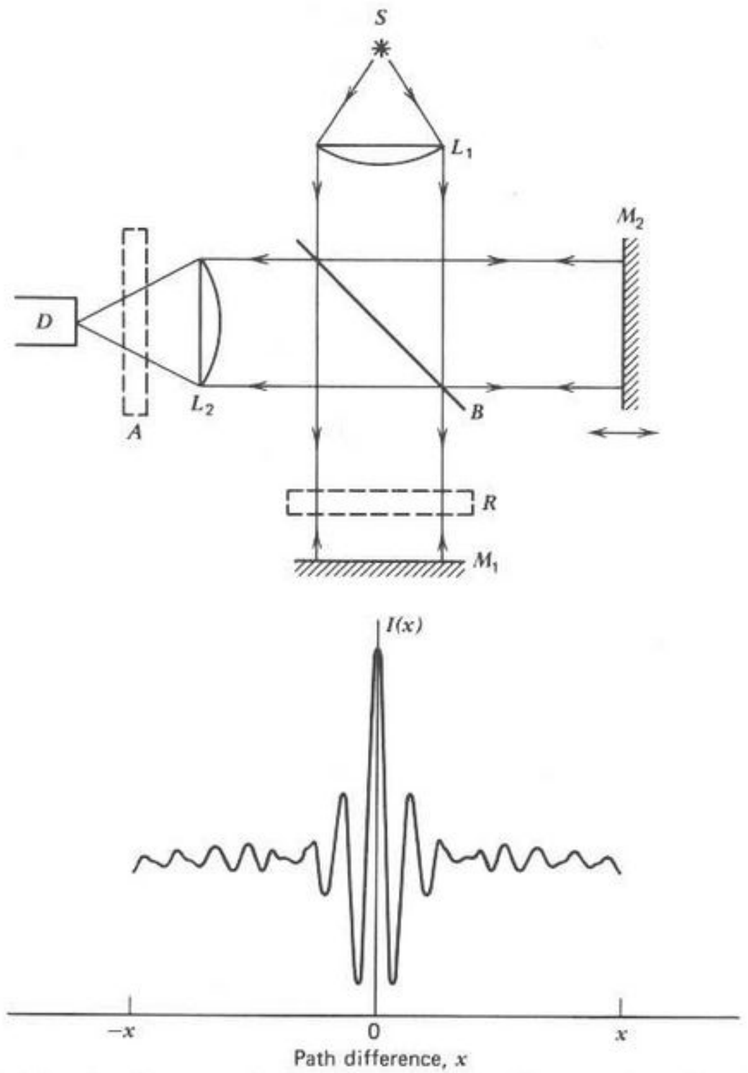

Fig. 22. Michelson interferometer (top) and interferogram (bottom): B, melinex beam divider; L, planoconvex TPX lens; D, detector; M_2, moving (step) mirror; M_1, fixed mirror; R, sample in asymmetric mode (for measurement of power absorption and refractive index); a sample in absorption mode.

order of a mean wavelength. This then provides an antisymmetrical interference record (Fig. 23). At far-infrared frequencies the magnitude of the oscillations and tolerances in the quality of the motion are such that a relatively simple vibrator may be used to sinusoidally drive the mirror on a loudspeaker coil. This development by Chamberlain[57] removes the following disadvantages of amplitude modulation of the detected signal.

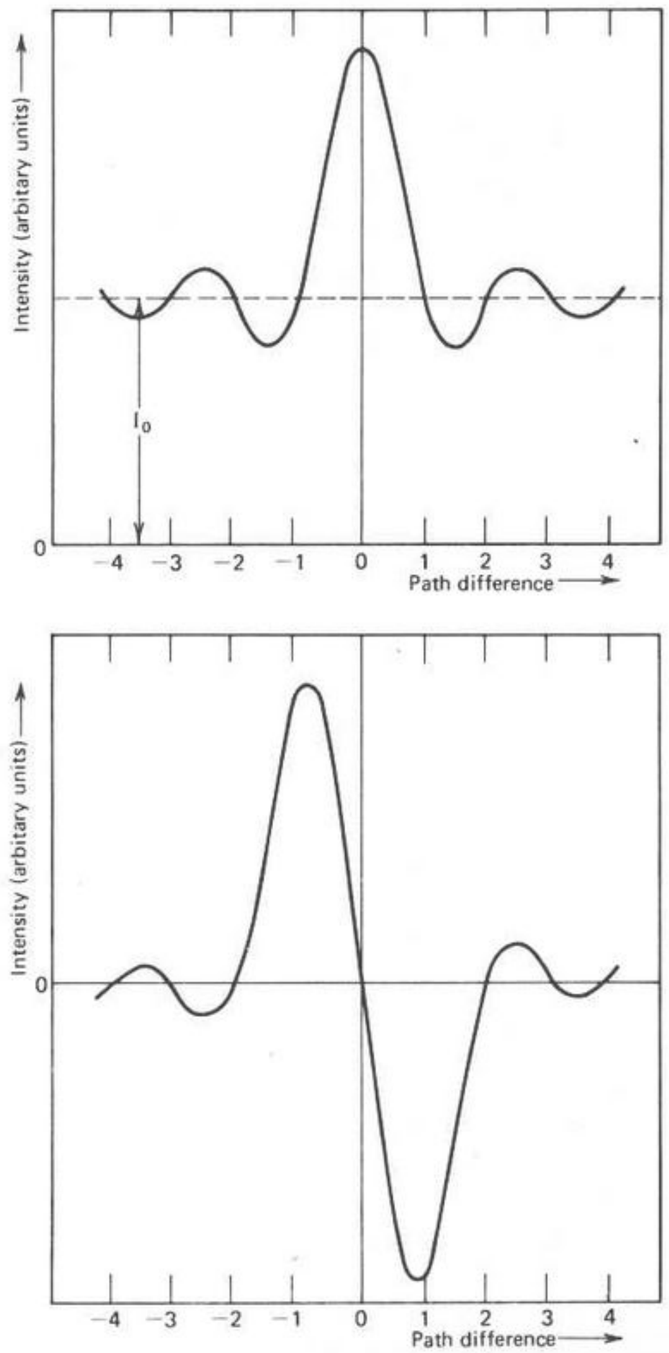

Fig. 23. Schematic of amplitude (top) and phase (bottom) modulated interferograms. I_o as defined in the text.

1. The beam dividers cause the interferometer to have a transmissivity that is strongly frequency-dependent. In the polarizing interferometer, devised by Martin and Pupplett[58] and discussed later, the transmissivity is constant up to a cutoff frequency which is inversely proportional to the grid spacings of the polarizers and beam divider through which the incident and emergent beam passes. Features of the transmissivity are improved by phase modulation in both types of interferometer.
2. Considering the grand maximum [point I(0) in Fig. 22] of a typical amplitude-modulated interferogram, the maximum of the interference fluctuations is a little more than half the total signal, but the detector is required to record all of the signal. Phase modulation allows the detector to record only that part which is varying with path difference and eliminates the background. Thus lower amplification gains are required, electronic noise is reduced, and source noise is removed. Stray rays emitted by the interferometer are discarded.
3. A rotating chopper, as used in amplitude modulation, cuts off half the available radiation. In the Martin–Pupplett instrument the signal is modulated by rotating the beam divider, and this square-function modulation gives a superior spectrum to both the sinusoidal amplitude modulation and sinusoidal phase modulation.

Computation of the Spectrum from the Interferogram. If the interferometer is irradiated with monochromatic radiation of luminance $B_0(\bar{\nu}_0)$ at a wavenumber $\bar{\nu}_0$, and if the reflectivity and transmission of the beam divider are 50% the energy detected will be $B_0(\bar{\nu}_0)/2$. However, whatever the reflectivity of the beam divider, the average intensity in the two beams is always equal, since each beam undergoes one reflection and one transmission before reaching the detector. It follows in general that

$$I_0(x) = \tfrac{1}{2} B_0(\bar{\nu}_0) + \tfrac{1}{2} B_0(\bar{\nu}_0) \cos(2\pi\bar{\nu}x) \tag{I.82}$$

where x is the path difference between the beams and equals twice the distance traveled by the movable mirror. Cosine fringes are therefore observed. For a polychromatic source of luminous density $B(\bar{\nu})$,

$$I(x) = \tfrac{1}{2}\int_0^\infty B(\bar{\nu})\, d\bar{\nu} + \tfrac{1}{2}\int_0^\infty B(\bar{\nu}) \cos(2\pi\bar{\nu}x)\, d\bar{\nu} \tag{I.83}$$

We define the interferograms as

$$F(x) = \tfrac{1}{2}\int_0^\infty B(\bar{\nu}) \cos 2\pi\bar{\nu}x\, d\bar{\nu} \tag{I.84}$$

and note in passing that $I(x) - F(x)$ is eliminated with phase modulation.

$F(0)$ is the amplituded-modulated grand maximum where all frequencies interfere constructively. The detected spectral power $B(\bar{\nu})$ and the interferogram are a Fourier transform pair whence

$$B(\bar{\nu}) = \int_{-\infty}^{\infty} \cos 2\pi\bar{\nu}x \, dx \tag{I.85}$$

By digitally recording $F(x)$, $B(\bar{\nu})$ is calculated numerically. Equations (I.84) and (I.85) apply to the ideal case when the interferogram is perfectly symmetrical about $x=0$ [i.e., $F(tx)$ is an even function of x]. With imperfect alignment the following equations are used:

$$\begin{aligned} F(x) &= \int_{-\infty}^{\infty} B(\bar{\nu}) \exp(2\pi i\bar{\nu}x) \, d\bar{\nu} \\ B(\bar{\nu}) &= \int_{-\infty}^{\infty} F(x) \exp(-2\pi i\bar{\nu}x) \, dx \end{aligned} \tag{I.86}$$

Assuming that $F(x)$ is real implies that $\tilde{B}(\bar{\nu})$ is Hermitian; that is, if $B(\bar{\nu}) = p(\bar{\nu}) - iq(\bar{\nu})$, then p is an even function of $\bar{\nu}$ and q is an odd function of $\bar{\nu}$. Phase modulation implies that

$$I(x) = \int_{-\infty}^{\infty} B(\bar{\nu}) \, d\bar{\nu} + \int_{-\infty}^{\infty} B(\bar{\nu}) \cos[2\pi\bar{\nu}x - \phi(\bar{\nu})] \, d\bar{\nu} \tag{I.87}$$

where $\phi(\bar{\nu})$ is the phase difference due to any residual asymmetry. On placing an isotropic specimen in front of the detector, the expression for the center power becomes

$$I_0(x) = I_0 + F_0(x)$$

where

$$\begin{aligned} I_0 &= \int_{-\infty}^{\infty} B_0(\bar{\nu}) \, d\bar{\nu} \\ F_0(x) &= \int_{-\infty}^{\infty} B_0(\bar{\nu}) \cos[2\pi\bar{\nu}x - \phi(\bar{\nu})] \, d\bar{\nu} \end{aligned} \tag{I.88}$$

and

$$B_0(\bar{\nu}) = \tau(\bar{\nu}) B(\bar{\nu})$$

Here $\tau(\bar{\nu})$ is the transmissivity of the specimen. Fourier-transforming (I.88) yields

$$\begin{aligned} \tilde{S}(\bar{\nu}) &= B_0(\bar{\nu}) \exp[-i\phi(\bar{\nu})] \\ &= \int_{-\infty}^{\infty} F_0(x) \exp(-2\pi i\bar{\nu}x) \, dx \end{aligned} \tag{I.89}$$

from which the transmission spectrum $\tau(\bar{\nu})$ may be recovered for the sample.

Truncation and Sampling of the Interferogram. For the purposes of numerical Fourier transformation, we must truncate the limits of the integrals in (I.83) to (I.89) and must also record the interferogram digitally, using a stepping motor to drive the mirror. The integration limits cannot be infinite when the independent variable is path difference derived from the displacement of the mirror. If the maximum path difference is X, the spectral resolution is then determined by $\Delta\bar{\nu} = 1/X$. If we truncate the integral in the range $-X$ to X, the interferogram function $F(x)$ is effectively multiplied by a rectangle function $\pi(x/2X)$, where

$$\begin{aligned} \pi(x/2X) &= 1 \qquad |x| < X \\ &= 0 \qquad |x| > X \end{aligned} \tag{I.90}$$

The transform of $F(x)\pi(x/2X)$ is the convolutuion

$$g(\bar{\nu}) * 2X \sin(2\pi x\bar{\nu})/(2\pi x\bar{\nu}) \tag{I.91}$$

which results in a physically meaningless negative region in the final spectrum. To overcome this problem a weighted rectangular function is used which causes a loss of resolution. This is $\pi(x/2X)W(x)$, where $W(x) = \cos^2(\pi x/2X)$.

If a finite number $(2N)$ of ordinates of the interferogram are sampled, the sampling theorem of information theory shows that the spectrum will be meaningfully divisible into N frequency elements. The maximum spacing (Δx) at which the ordinates of the interferogram need to be measured is then given by

$$\Delta x = 1/(2|\bar{\nu}_1 - \bar{\nu}_2|) \tag{I.92}$$

a relation which also defines the cutoff frequency of the instrument, past which the spectrum will be distorted by folding (periodicity in the Fourier series used to calculate the Fourier transform).

Synchronous Detection. The real interferogram $F(x)$ is aperiodically scanned at a constant speed and recorded using phase modulation followed by synchronous amplification in which the periodic detector output is amplified, filtered, and mixed with a reference signal derived from the modulation process. This leads to a dc output that is directly related to the peak-to-peak detector output. The process is outlined below. A schematic representation of the electronics is displayed in Fig. 21.

STEP 1

Suppose that the radiation of power $J(y)$ is modulated at a frequency f to give at any instant t a signal $J(y,ft)$ which can be expressed as a Fourier

series:

$$J(y,ft)=\tfrac{1}{2}K^0(y)+\sum_{l=1}^{\infty}\left[K^{(l)}(y)\cos 2\pi lft+Z^{(l)}(y)\sin 2\pi lft\right] \quad \text{(I.93)}$$

where $K^{(l)}(y)$ and $Z^{(l)}(y)$ are the Fourier coefficients. In the case of phase modulation we take the time origin so that $J(y,ft)$ is odd with respect to t. The detected signal is then given by

$$J(y,ft)=\sum_{l=1}^{\infty}Z^{(l)}(y)\sin 2\pi lft \quad \text{(I.94)}$$

STEP 2

The output from the detector is $uJ(y,ft)$, where u is the responsivity (signal delivered per unit power input).

STEP 3

The detector signal is amplified with a gain of g.

STEP 4

It is passed through a filter tuned to the frequency f to give

$$D(y,ft)=guZ^{(1)}(y)\sin 2\pi ft \quad \text{(I.95)}$$

STEP 5

In a synchronous recording this is multiplied and phase-linked with a reference signal, also of frequency f. This results in a slowly varying recorded signal:

$$V(y)=(2/\pi)guZ^{(1)}(y) \quad \text{(I.96)}$$

and a series of time-dependent terms of frequency multiples of f.

STEP 6

A series of low-pass filters removes the time-dependent terms to give $V(y)$ as the output signal. $Z_1(y)$ is the coefficient of the fundamental term in the series expansion of $J(y,ft)$. In amplitude modulation the recorded signal is proportional to the total power $J(y)$ that would reach the detector in the absence of modulation. With phase modulation this is not so.

The path difference at any instant t is not y but $y+j(ft)$, where j is the jitter amplitude function. The corresponding power at the detector is then

$$J(y,ft)=J+G(y,ft) \quad \text{(I.97)}$$

where $$G(y,ft)=\int_{-\infty}^{\infty}B_0(\bar{\nu})\cos\left[2\pi\bar{\nu}y-\phi(\bar{\nu})+2\pi\bar{\nu}j(ft)\right]d\bar{\nu}$$

Expanding the cosine, we obtain

$$\cos(2\pi\bar{\nu}j(ft))=\tfrac{1}{2}\mu^0(p\bar{\nu})+\sum_{l=1}^{\infty}\mu^{(l)}(p\bar{\nu})\cos 2\pi lft$$

$$\sin(2\pi\bar{\nu}j(ft))=\sum_{l=1}^{\infty}\alpha^{(l)}(p\bar{\nu})\sin 2\pi lft \quad \text{(I.98)}$$

where p is the jitter amplitude. Comparison with (I.93) yields

$$Z_1(y)=-\int_{-\infty}^{\infty}\alpha^{(1)}(p\bar{\nu})B_0(\bar{\nu})\sin\left[2\pi\bar{\nu}y-\phi(\bar{\nu})\right]d\bar{\nu}$$
$$=G\phi(y) \quad \text{(I.99)}$$

The recorded signal $V(y)=(2/\pi)guZ^{(1)}(y)$ now contains no y-independent terms and is the phase-modulated interferogram. The effect of phase modulation is to modify the transmitted power spectrum by the wave-number-dependent factor

$$|\alpha^{(1)}(p\bar{\nu})|$$

For sinusoidal modulation,

$$j(ft)=p\sin 2\pi ft \quad \text{(I.100)}$$

and

$$\alpha^{(1)}(p\bar{\nu})=2J_1(2\pi\bar{\nu}p) \quad \text{(I.101)}$$

where J_1 is the first-order Bessel function of the first kind. Limitations in the final spectrum due to variations in this factor can be minimized by matching $\alpha^1(p\bar{\nu})$ with the transmission characteristic of the interferometer, governed largely by beam-divider effects. Square function modulation produces a spectrum superior to sinusoidal modulation. Such a square function is possible with a rotating chopper as used in a polarizing interferometer.

The Polarizing Interferometer.[58] To measure absorptions in the very far infrared range 2 to 40 cm^{-1}, we have access to the apparatus designed originally by Martin and Pupplett. This uses a wire-mesh beam divider and similar meshes as polarizer and analyzer. Figure 24 is a schematic. The polarizer (P_1) is a circular grid with reflection and transmission coefficients close to 100% from frequencies approaching zero up to $1/(2d)$ cm^{-1}. It is

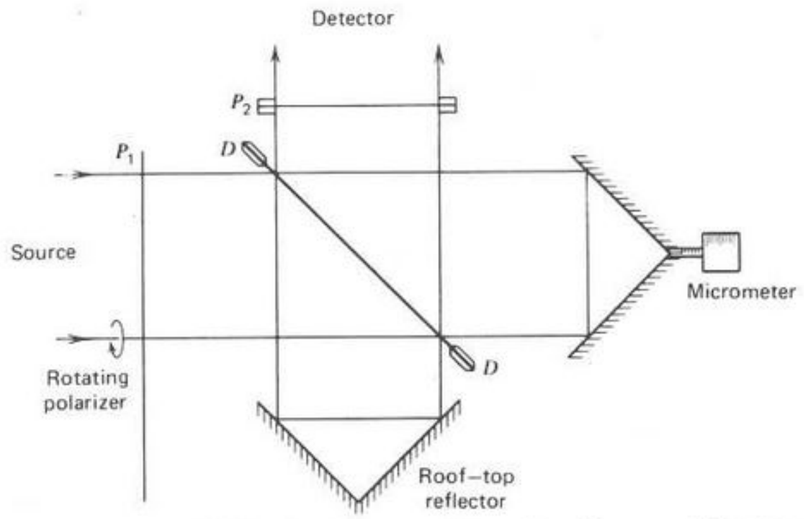

Fig. 24. Schematic of a polarizing interferometer. [Reproduced by permission from *J. Chem. Soc. Faraday Trans. 2*, **74**, 59 (1978).]

spun about its center point acting as a polarizing chopper blade and producing square function modulation. A second polarizer (P_2) is held fixed. The beam divider windings are at 45° to those of P_2. Roof-top reflectors replace the Michelson plane mirrors.

A collimated beam is plane-polarized at P_1 and then divided by the flat wire-grid polarizer D into a beam A, polarized with its *E*-vector at 90° to the second beam B. Then A and B are recombined at the wire grid D and finally pass through the polarizing analyzer P_2, which has its axis parallel to or at 90° to P. The reflectors M_1 and M_2 act as polarization rotators. For a monochromatic source, the beam is elliptically polarized after recombination at D with an ellipticity varying periodically with increasing path difference between beams A and B. For the *E*-vector leaving the beam divider,

$$\mathbf{E}_j = \frac{a}{\sqrt{2}}\mathbf{n}\cos(\omega t + \Delta_A) + \frac{a}{\sqrt{2}}\mathbf{t}\cos(\omega t + \Delta_B) \tag{I.102}$$

where $\boldsymbol{n}$ is the unit vector normal to the plane of the paper (Fig. 24), and t that in the plane and transverse to the direction of propagation. Δ_A and Δ_B are phase shifts for beams A and B. For the *E*-vector leaving the polarizer P_2,

$$\begin{aligned} |E_0| = \mathbf{E}_j \cdot \mathbf{p} &= (a/2)[\cos(\omega t + \Delta_A) + \cos(\omega t + \Delta_B)] \\ &= a\cos(\omega t + \bar{\Delta})\cos(\Delta/2) \end{aligned} \tag{I.103}$$

where $\bar{\Delta}$ is the mean of Δ_A and Δ_B and

$$\Delta = \Delta_A - \Delta_B = (2\pi/\lambda)x \tag{I.104}$$

where x is the path difference in the interferometer. Here $\boldsymbol{p}$ is a unit vector in the direction of the optical axes of P_1 and of P_2. After leaving P_2, the beam is plane-polarized with an amplitude that varies periodically with path difference in the same way as in a Michelson interferometer. From (I.103) the emergent intensity is given by

$$I_p = \langle |E_0^2| \rangle = \frac{a^2}{2}\cos^2\left(\frac{\Delta}{2}\right) = \frac{a^2}{4}(1 + \cos\Delta) \tag{I.105}$$

Alternatively, if the axis of P_2 were rotated by $\pi/2$:

$$|E_0| = \mathbf{E}_j \cdot \mathbf{p}^1 \qquad \text{where} \qquad \mathbf{p} \cdot \mathbf{p}' = 0$$

and hence

$$I_t = \frac{a^2}{4}(1 - \cos\Delta) \tag{I.106}$$

The transmissivity of the instrument is constant up to a cutoff frequency which is inversely proportional to the grid spacing. The resolution is not limited by departures from the flatness of the grid or by any phase retardation in the polarizing grid.

2. *Significance of the Experimental Results*[59]

Spectra are always of the absorption type, so that the sample whose absorption coefficient is to be measured is placed between the interferometer and the detector. By comparing sample thicknesses d_2 and d, we obtain

$$\alpha(\bar{\nu}) = (d_2 - d_1)^{-1}\log_e(I_0(\bar{\nu})/I(\bar{\nu})) \tag{I.107}$$

where $I_0(\bar{\nu})$ is the background power spectrum and $I(\bar{\nu})$ is that for an increase in sample thickness $(d_2 - d_1)$. In this section we discuss briefly the sources of uncertainty in $\alpha(\bar{\nu})$ arising from the experimental setup. The quality and reproducibility of the spectra are optimum when the product $(d_2 - d_1)\alpha_{max}$ lies between 0.5 and 1.5, which amounts to an overall absorption by the specimen of about 60 to 85% of the incident radiation. Under these conditions phase-modulated spectra (e.g., those of Fig. 20) are repeatable to within 2% and reproducible between different laboratories. Figure 25 shows the far-infrared absorptions of chloroform under amplitude- and phase-modulation conditions.

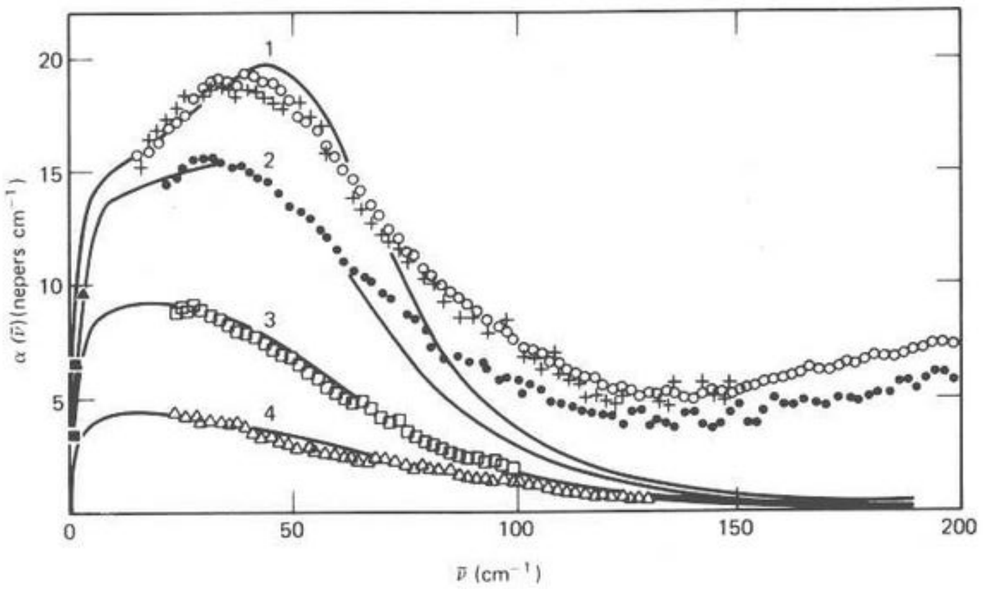

Fig. 25. Far infrared spectrum of liquid chloroform. ○, Phase modulation: +, amplitude modulation; ▲, klystron (112 GHz); ■, microwave measurements. Ordinate: $\alpha(\bar{\nu})$ (nepers/cm)[1]; abscissa: $\bar{\nu}$ (cm^{-1}).

The systematic uncertainties that arise from a particular instrument and set of conditions are typically small (Fig. 25). As Fig. 12 shows, however, $\pm 2\%$ uncertainty is small enough to be insignificant when making comparisons with the theoretical models available. The data in Fig. 26 were taken with different window materials and different detectors (Golay and Rollin types). Further good agreement is usually obtainable, with skill, between different types of beam splitter in the Michelson interferometer.

A source of systematic uncertainty in the "cube" design is the highly convergent beam through the sample, effective collimation being difficult to reconcile with the all-important need for maintaining maximum flux throughput via sometimes highly absorbing pressure windows. These convergence effects have been discussed by Fleming[60] but are small when the difference $(d_2 - d_1)$ is small, which is always the case for intense absorbers such as dipolar liquids. With longer sample paths the data may be checked against those obtained with accurately collimated laser radiation. When $(d_2 - d_1)$ is of the order of the wavelength of the incoming radiation, spurious peaks sometimes arise as a sine wave superimposed on the computed spectrum due to multiple internal reflections occurring within the sample cell. These have been recognized in the work of Baise[114] on compressed nitrous oxide. Experience has shown that the cell window material is important in determining the extent of this effect. Z-cut crystalline quartz

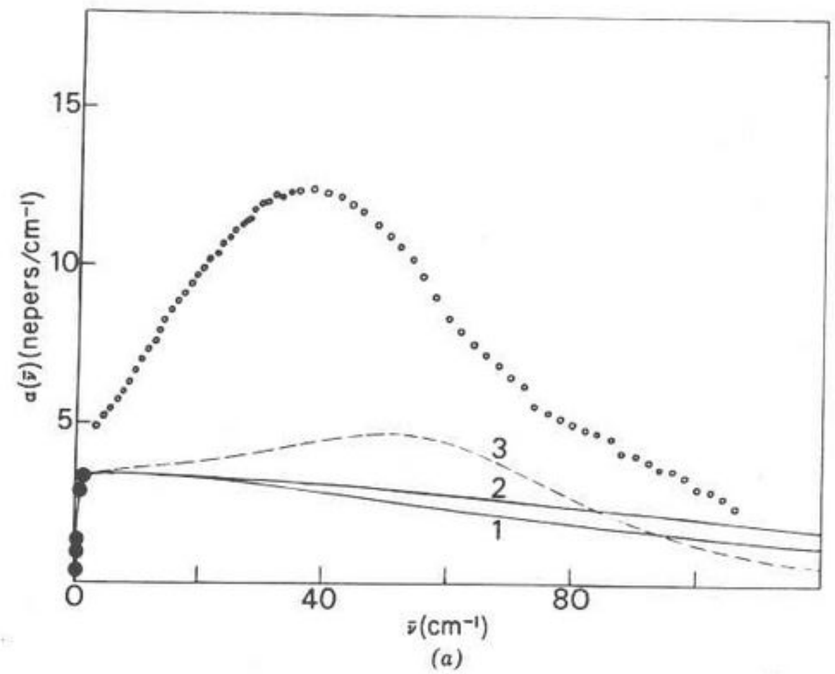

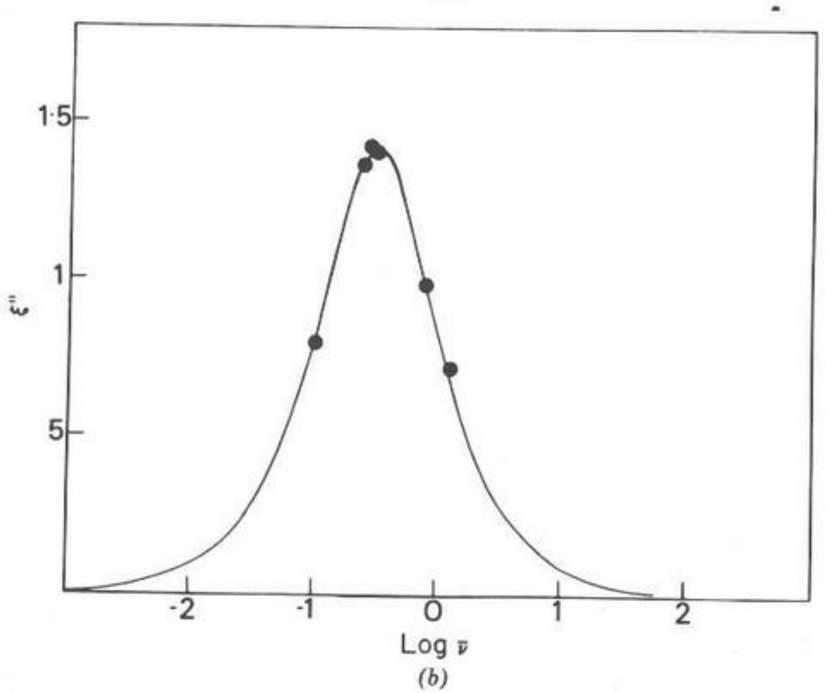

Fig. 26. (*a*) Agreement between various experimental sources for liquid bromobenzene. ●, Microwave (klystron) spot frequencies; ○, polarizing interferometer; ⊕, Grubb–Parsons/N.P.L. "cube" interferometer. (1), (2), (3) Various theoretical models (see original reference). (*b*) — Calculated loss curve for liquid bromobenzene using Langevin's equations for an asymmetric and a symmetric top molecule. The theoretical curve from Mori three-variable theory is also coincident. ● Experimental loss data. [Reproduced by permission from *J. Chem. Soc. Faraday Trans. 2*, 73, 1074 (1977).]

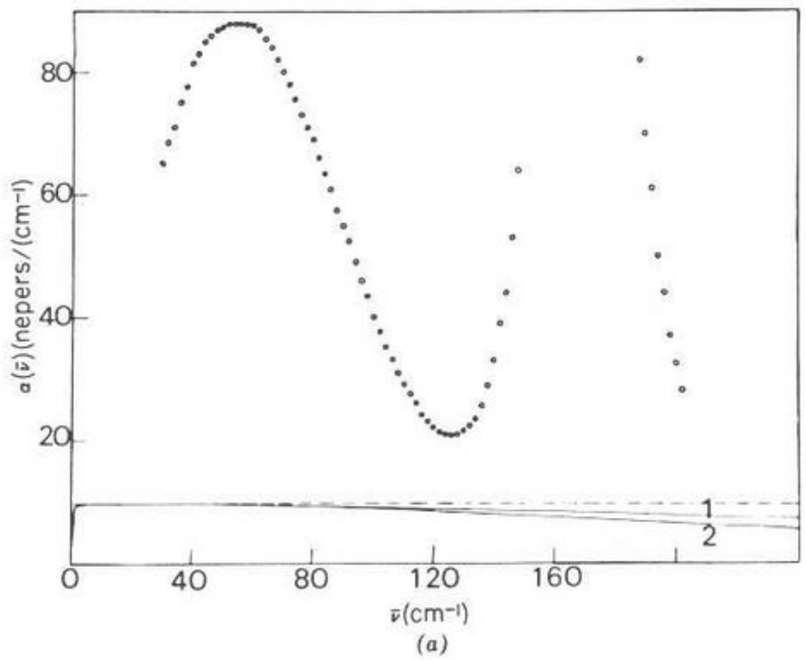

Fig. 27. (*a*) Far infrared spectrum of benzonitrile liquid at 296°K. Ordinate: $\alpha(\bar{\nu})$ neper cm^{-1}; abscissa: $\bar{\nu}$ (cm^{-1}). The low-frequency peak is the Poley absorption, the other an intramolecular proper mode. The dotted line is the Debye plateau and the solid lines (1) the Langevin equation as applied to a spherical top with the mean moment of inertia of the true asymmetric top (2). It is clear that neither version produces the Poley absorption when fitted to the low-frequency (microwave) loss. (*b*) ● Experimental loss data for benzonitrile. (—), Theoretical, as for Fig. 26*b*.

windows, when optically parallel, enhance the effect, which is eliminated by wedging very slightly. There is usually less of an effect with polymeric window material, so that these are used wherever practicable. These effects may be recognized from the relation

$$\Delta\bar{\nu} = \frac{1}{2n(d_2 - d_1)}$$

which defines the frequency spacing of the spurious peaks in terms of the sample refractive index n.

One further cause of experimental uncertainty arises from the intense higher-frequency proper modes of absorption as illustrated in Fig. 27. These are intramolecular in origin (vibrational, difference modes, etc.), but their intensity with respect to the Poley absorption is sometimes enough to block off almost the whole of the flux throughput. The interpretative difficulty is one of extrapolation and resolution of the Poley band from the proper mode. For the purposes of theoretical analysis we chose our spectra carefully to avoid these complications.

Sample-Cell Technology. The design of sample cells is beyond the scope of this chapter, but it has an essential bearing on the quality of the final spectra because of the need to maximize flux throughput. The reader is referred to original articles for examples of designs for use with dilute and compressed gases, nondipolar liquids, dipolar liquids, mesophases, and solids. Specialized designs are available[50] for studies of liquid water, an enormously intense absorber in the far infrared,[1] and for ultra-accurate standards measurements. One concern common to all designs is the preferability of evacuating the whole system (interferometer, sample cell, and detector) to eliminate water vapor, which absorbs strongly in the far infrared. For the same reason special care ought to be taken to eliminate moisture from the samples being investigated.

II. EVALUATION OF MODELS OF FLUID-STATE MOLECULAR DYNAMICS*

In Section I we have been concerned with rationalizing the growth of modeling techniques for the fluid-state molecular dynamics in terms of a continued-fraction expansion of the Liouville equation, for which all such models are approximate solutions. In this we compare the theoretical and experimental data for selected dipolar systems, ranging from the moderately compressed gas (Section II.B.2), through to the glassy condition where the zero-THz profile is a continuum loss peaking at frequencies

*In this section note that $K_n(t) \equiv \phi_{n+1}(t)$ for the memory functions.

sometimes separated by many decades on the log scale (Section II.F). Features of this progression have been illustrated in terms of one particular model, the itinerant oscillator/librator, in Fig. 9. In Section III, a further dimension is added by the use of machine simulations of a structured (diatomic) molecule based on the algorithm developed recently by Tildesley and Streett.[61]

At the outset, in Section II.A some fundamental points are discussed which remain at issue and will probably be best tackled not by the invention of more models but by the use of molecular dynamics and Monte Carlo simulations.[61] The most intractable problems—that of the internal field and the related one of electrodynamic coupling (dipole-dipole being the longest in range)—have already been introduced. However, we have taken the line that these should not distract us from our major tasks of relating, whenever possible, theories of statistical autocorrelations of dipole vectors to zero-THz absorption profiles. We have also defined the liquid state as that where rotation–translation coupling is the most pronounced characteristic. This is, however, with the hindsight of only a few months, when the results of Section I.B first suggested themselves to us. Before that no clear-cut mathematical formulation of the effect of linear velocity on $\langle \omega(t) \cdot \omega(0) \rangle$ has been included in the purely rotational models of Table I. The new theory of translation–rotation coupling being yet in its infancy, we proceed on the understanding that the use of purely reorientational formalism for the liquid-phase molecular dynamics is a widespread approximation, similar to the use of (I.39) in neutron scattering. In stating this we might be doing an injustice to Wolynes and Deutch and to others who may have considered such effects from a hydrodynamic point of view.

A. The Dipolar Autocorrelation Function and Dielectric Loss—The Fluctuation/Dissipation Theorem[62]

The mean observed value of $A_j(t)$ in (I.2) is given by

$$\langle A(t) \rangle = \int_\Gamma A(p,q)\, {}^1f_A(p,q,t)\, dp\, dq \tag{II.1}$$

where Γ denotes the phase space (of p and q) and ${}^1f_A$ is the first-order space distribution function akin to the probability density functions of Section I.A. In (II.1) and the following, we drop the subscript j for convenience. For an isolated system,

$$\frac{d\,{}^1f_A}{dt} = 0 = \frac{\partial\, {}^1f_A}{\partial t} + \mathfrak{L}\, {}^1f_A \tag{II.2}$$

By considering the change H' brought about in the equilibrium Hamiltonian H_0 by an external perturbation $E(t)$, we have

$$H' = -X(p_r, q_r)E(t) \tag{II.3}$$

where X is a property of the system (canonical ensemble of r molecules) deemed responsible for the increase in the Hamiltonian. If $E(t)$ is an electric force field, then X will have the units of the electric dipole moment. The new distribution function is now

$$f = f_0 + f'(t) \tag{II.4}$$

where $f \equiv {}^1f_A$ and

$$\frac{\partial f'}{\partial t} = -\mathfrak{L}_0 f' - \mathfrak{L}' f_0 - \mathfrak{L}' f' \tag{II.5}$$

in the same notation. The term $\mathfrak{L}'f'$ is the product of operator and functional increments, and since the perturbation is weak is considered as negligible. Equation (II.5) thus becomes

$$\frac{\partial f'}{\partial t} = -\mathfrak{L}_0 f' + E(t)\mathfrak{L}_X f_0 \tag{II.6}$$

where the operator $\mathfrak{L}_X$ is defined by

$$\mathfrak{L}_X = \sum_r \left[\frac{\partial X}{\partial p_r}\frac{\partial}{\partial q_r} - \frac{\partial X}{\partial q_r}\frac{\partial}{\partial p_r} \right] \tag{II.7}$$

Integrating (II.6) yields

$$f'(t) = \int_{-\infty}^{t} \exp(-\mathfrak{L}_0(t-t'))E(t')\mathfrak{L}_X f_0\, dt' \tag{II.8}$$

If it is assumed now that the system can be observed by a study of the property Y (related to X), then from (II.1) and (II.8) for Y we may write

$$\langle Y(t) \rangle = Y_{eq} + \int_{-\infty}^{t} E(t')\, dt' \int_\Gamma Y(t') \exp(-(t-t')\mathfrak{L}_0) \times \mathfrak{L}_X f_0(t')\, dp\, dq \tag{II.9}$$

$$\equiv Y_{eq} + \int_{-\infty}^{t} E(t)\Psi_{YX}(t,t')\, dt' \tag{II.10}$$

In (II.10) we may deduce that

$$\Psi_{YX}(t,t') = \int_\Gamma Y(t-t')\Omega_X f_0(0)\,dp\,dq \tag{II.11}$$

from the fact that $\Omega_X f_0$ is stationary in time, since the operator is taken at equilibrium. Similarly, Y is stationary, since it depends only on coordinates and momenta. Ψ_{YX} depends only on the change $\delta t = t - t'$ and is the response of Y to a unit impulse of E. It is thereby known as the response function, or, because of the change δt, as the after-effect function. Equations (II.1) to (II.11) limit the relation of molecular statistical mechanics to macroscopic zero-THz bandshapes to the regions of linear response where the probe force field $E(t)$ is small. We shall not stray outside this region in this section. In the canonical ensemble

$$f_0 \propto \exp(-H_0/kT)$$

so that

$$\Omega_X f_0 = f_0 \dot{X}/kT \tag{II.12}$$

Denoting means over p, q, and t by $\langle \cdot \rangle$, (II.11) becomes

$$\begin{aligned}\Psi_{YX}(t) &= \frac{1}{kT}\langle \dot{X}(0)\,Y(t)\rangle \\ &= \frac{1}{kT}\langle X(0)\,\dot{Y}(t)\rangle \\ &= -\frac{1}{kT}\frac{d}{dt}\langle X(0)\,Y(t)\rangle\end{aligned} \tag{II.13}$$

Therefore,

$$\langle Y(t)\rangle = Y_{eq} - \frac{1}{kT}\int_{-\infty}^{t} E(t')\dot{\psi}(t-t')\,dt' \tag{II.14}$$

where $\psi(t) = \langle X(0)\,Y(t)\rangle$ is a multiparticle correlation function. Equation (II.14) allows calculation of the forced response of the system from the correlation functions of the spontaneous fluctuations at equilibrium of the properties X and Y. It is of general validity for linear response, where without loss of generality $E(t)$ may be represented by a single sinusoidal component:

$$E(t) = E_0 \mathrm{Re}[\exp(i\omega t)]$$
$$Y(t) = \mathrm{Re}[\exp(i\omega t)]$$

Taking $Y_{eq} = 0$, we have then the fluctuation–dissipation theorem in the form

$$\langle Y(t)\rangle = E_0 \mathrm{Re}\left[\exp(i\omega t)\int_0^\infty \exp(-i\omega t_0)\Psi_{XY}(t_0)\,dt_0\right] \tag{II.15}$$

1. *Application to Dielectric Susceptibility*

The complex dielectric susceptibility ($X^*(\omega)$) is related to the complex permittivity ($\epsilon^*(\omega)$) by

$$X^*(\omega) = \frac{\epsilon^*(\omega)-1}{4\pi} = \frac{\langle m_z(t)\rangle}{VE_0\exp(i\omega t)} \tag{II.16}$$

where $\langle m_z(t)\rangle$ is the resultant dipole moment in the direction (z) of the probe field E. V is the volume of the system and $\langle m_z(t)\rangle / V$ is the polarization.

From (II.15),

$$X^*(\omega) = \int_0^\infty \exp(-i\omega t)\Psi_z(t)\,dt \tag{II.17}$$

where

$$\Psi_z(t) = -\frac{1}{kT}\langle \mathbf{M}_z(0)\cdot\dot{\mathbf{M}}_z(t)\rangle$$

Since in an isotropic fluid

$$\langle \mathbf{M}_z(0)\cdot\mathbf{M}_z(t)\rangle = \tfrac{1}{3}\langle \mathbf{M}(0)\cdot\mathbf{M}(t)\rangle$$

we have finally

$$\frac{\epsilon^*(\omega)-1}{\epsilon^*(\omega)+2} = -\frac{4\pi}{9kTV}\int_0^\infty \exp(-i\omega t)\dot{\psi}(t)\,dt \tag{II.18}$$

where we have used the internal field relation

$$E_0^*(\omega)/E^*(\omega) = \frac{\epsilon^*(\omega)+2}{3}$$

to relate the external applied field E_0 to the field E which figures in the Maxwell equations for the system (regarded as a macroscopic sphere *in vacuo*). Equation (II.18) is generally valid in this case, whatever the origin

of the resultant dipole moment **M** (atomic polarization, ionic, orientational, etc.), $\psi(t)$ reduces to an autocorrelation only:

1. For a fluid where the molecular fluctuations are uncorrelated.
2. Where the molecules are only slightly polarizable so that $\epsilon^*(\omega)-1$ is small.
3. Where deformation polarization is negligible.

Under these conditions:

$$C_{\mathbf{M}}(t)=\langle \mathbf{M}(0)\cdot\mathbf{M}(t)\rangle=\sum_{ij}\langle \boldsymbol{\mu}_i(0)\cdot\boldsymbol{\mu}_j(t)\rangle$$
$$=N_{\mathbf{u}}^2\langle \boldsymbol{\mu}(0)\cdot\boldsymbol{\mu}(t)\rangle \tag{II.19}$$

where $\mathbf{u}=\boldsymbol{\mu}/|\boldsymbol{\mu}|$. Thus

$$\epsilon'(\omega)-1=\frac{4\pi N\mu^2}{3kTV}\left[1-\omega\int_0^\infty C_{\mathbf{u}}(t)\sin\omega t\,dt\right]$$
$$\epsilon''(\omega)=\frac{4\pi N\mu^2}{3kTV}\int_0^\infty C_{\mathbf{u}}(t)\cos\omega t\,dt \tag{II.20}$$

where $C_{\mathbf{u}}(t)$ is the dipole autocorrelation function $\langle \mathbf{u}(t)\cdot\mathbf{u}(0)\rangle$. In (II.20),

$$4\pi\mu^2/3kTV=(\epsilon_0-1)=4\pi\chi_0$$

In a pure, strongly dipolar liquid such as CH_2Cl_2, (II.19) and (II.20) are still approximately valid, but dilution has an appreciable effect on the position of $\bar{\nu}_{\max}$ (Fig. 20). The micro–macro correlation theorem implies that the decay of $\langle \mathbf{M}(t)\cdot\mathbf{M}(0)\rangle/\langle \mathbf{M}(0)\cdot\mathbf{M}(0)\rangle$ should still be identical with but faster or slower than that of $\langle \mathbf{u}(t)\cdot\mathbf{u}(0)\rangle/\langle \mathbf{u}(0)\cdot\mathbf{u}(0)\rangle$. However, the relations among $\epsilon''(\omega)$, $\epsilon'(\omega)$, and $C_{\mathbf{u}}(t)$ are altered from those of (II.20). The physical origin is that each molecular dipole polarizes its neighbors, which in turn react upon it as discussed in Section I. Scaife[8] has explained why the solution to this problem can only be approximate, but Kivelson and Madden[17] have developed formal relationships and provided a systematic framework, based on the Mori continued fraction, for introducing successive approximants relating $C_{\mathbf{u}}(t)$ to $C_{\mathbf{M}}(t)$. The ratio of relaxation times of $C_{\mathbf{M}}(t)$ and $C_{\mathbf{u}}(t)$ is, in this theory,

$$\frac{\tau_{\mathbf{M}}}{\tau_{\mathbf{u}}}=\frac{1+Nf}{1+N\dot{f}} \tag{II.21}$$

Here $1+Nf$ is a factor akin to Kirkwood correlation g which measures the correlation between neighboring dipoles, and $\dot{f}$ is a dynamic orientation time correlation function for the factor $[d(\cos C_{\mathbf{m}}(t))/dt]$ of two different dipoles. The difficulty is that $\dot{f}$ is determined formally only in terms of a projected Liouville operator. Furthermore, the factor $[1+Nf]$ is sample-shape-dependent and must always be identified with a particular geometry (e.g., the sphere *in vacuo* used above). Perhaps the treatment of the internal field most in the spirit of this review is that of Sullivan and Deutch,[63] who have introduced the projection operator: $\hat{P}G=\mathbf{M}\cdot\langle\mathbf{MM}\rangle^{-1}\cdot\langle\mathbf{M}G\rangle$ independent of geometrical factors. Formally, then,

$$\frac{\epsilon^*(\omega)-1}{\epsilon(0)-1}=\mathfrak{L}_a\left(-\dot{C}_p(t)\right)$$
$$\equiv\left[1+i\omega\tau_p(\omega)\right]^{-1} \tag{II.22}$$

where

$$\tau_p^{-1}(\omega)\propto\int_0^\infty\exp(-i\omega t)k(t)\,dt$$
$$k(t)=\mu^{-2}\langle\mu_Z(1)\exp\left[i(1-\hat{P})\mathfrak{L}t\right]\dot{M}_Z\rangle$$

While $k(t)$ is a multiparticle correlation function, it is a local quantity that does not depend on sample and surroundings. The projector $\hat{P}$ removes the correlation over long ranges arising from dipole–dipole coupling or hydrodynamically.

Nevertheless, the formal nature of (II.22) remains, although a number of approximations can be incorporated within its framework (rather like Table I). We do not propose to review these numerous equations here, but proceed strategically on the basis that for moderately dipolar fluids the problem in numerical terms is considerably deflated, as demonstrated by Brot[52] and by, Greffe, Goulon, Brondeau, and Rivail.[64] Brot has considered the internal-field problem in a group of intercorrelated molecules constrained in a cavity just large enough for correlations to be negligible outside. Using the Lorentz field, he obtains

$$C_{\mathbf{u}}(t)=\frac{27kT}{4\pi^3N\mu^2}\int_0^\infty\frac{\alpha(\bar{\nu})n(\bar{\nu})\cos(2\pi\bar{\nu}ct)d\bar{\nu}}{\bar{\nu}^2\left(\left[\epsilon'(\bar{\nu})+2\right]^2+\epsilon''(\bar{\nu})^2\right)} \tag{II.23}$$

and with the Onsager field,

$$C_{\mathbf{u}}(t)=\frac{27kT(2\epsilon_0+\epsilon_\infty)^2}{4\pi^3N_\mu^2(\epsilon_\infty+2)^2}\int_0^\infty\frac{\alpha(\bar{\nu})n(\bar{\nu})\cos(2\pi\bar{\nu}ct)d\bar{\nu}}{\bar{\nu}^2\left(\left[\epsilon'(\bar{\nu})+2\epsilon_0\right]^2+\epsilon''(\bar{\nu})^2\right)} \tag{II.24}$$